PREDICTING VEHICULAR COLLISIONS IN VEHICLE-TO-VEHICLE NETWORKS USING PHYSICAL LAYER TECHNIQUES

A Dissertation
Presented to
The Academic Faculty

By

Billy Kihei

In Partial Fulfillment
of the Requirements for the Degree
Doctor of Philosophy in the
School of Electrical and Computer Engineering

Georgia Institute of Technology

December 2017

PREDICTING VEHICULAR COLLISIONS IN VEHICLE-TO-VEHICLE NETWORKS USING PHYSICAL LAYER TECHNIQUES

Approved by:

Dr. John A. Copeland, Advisor
School of Electrical and Computer Engineering
Georgia Institute of Technology

Dr. Yusun Chang, Co-Advisor
School of Electrical and Computer Engineering
Kennesaw State University

Dr. Gregory Durgin
School of Electrical and Computer Engineering
Georgia Institute of Technology

Dr. George Riley
School of Electrical and Computer Engineering
Georgia Institute of Technology

Dr. Raheem Beyah
School of Electrical and Computer Engineering
Georgia Institute of Technology

Dr. Ellen Zegura
School of Computer Science
Georgia Institute of Technology

Date Approved: August 14, 2017

Come unto me, all ye that labour and are heavy laden, and I will give you rest. Take my yoke upon you, and learn of me; for I am meek and lowly in heart: and ye shall find rest unto your souls. For my yoke is easy, and my burden is light.

Jesus Christ

To

my totally awesome wife Liz :), my family,

and

my shield and exceedingly great reward: Jesus Christ.

ACKNOWLEDGEMENTS

All thanks to the LORD and Savior Jesus Christ! I literally almost walked away from entering the doctorate program, and then He literally directed my steps right into it.

Liz, thank you so much for doing this with me, and helping me explain to others what all those squiggles mean :), I love you. Thank you, Jesus, for overflowing financial favor. Thank you Father God for not one, but three advisors: Dr. Chang, Dr. Copeland for consistently demonstrating your support for me and my work, and Dr. Wan Choi for hosting me in the WSCL lab. My lab mates Hamza, Cris (and Amanda), Deuk, Brian, and who helped in experiments (Jason, Joseph, James, Jennifer, Henry, Jacob, Achevi): this thesis work was enabled due to your selflessness. The outstanding professors at GT: Dr. Ayanna-Howard, Dr. McClellan, Dr. Zajic, and Dr. Durgin. My lab mates in the WSCL at KASIT: Hojin, Ayoob, Jaeyoung, Youngbim, and Kyungrak: that summer was so much fun! Our dog Bowser has been a great dog through this time too. To my TI:GER team: DeWitt, Jeff, Adam, Horace, and mentors Christian and Bobby. To my project sponsors GDOT and NSF. To my colleagues at CETL and STEM for letting me build their website to pay for school. To the Giglio family for sponsoring my TI:GER project. Thank you, God, so much for the family that raised me. To my mom and dad: for all your love and support. To my brothers and their families: Ben, Sterling, Buh, and Kourtney. To my wife's family: Marilyn, Sydney, Joseph, and William. Thank you to my GT family: Patrick, Jill and Julie in ORS, my ORS students, Dr. May, S. Gordon, Dr. Esogbue, Ms. Jackie, Dr. Benton-Johnson, Etta Pittman, Mrs. Trappier, Mrs. Elleby, Mrs. Torrence, Chris M., Dr. Laughter, and Cedric. All my friends who encouraged me during this time. To my Lockheed family Jerry, James, Denise, Nate, and Will Payne for being my radar guru. To my church family: Mount Paran faithful mens Bible study, the Flores, the Bells, the Cardosos (brother Adilson thank you), and the Burches. This work has, is, and always will be for Jesus because everything I have, has been given to me! Thank you my Heavenly Father so much for:

Jesus Christ.

TABLE OF CONTENTS

LIST OF TABLES

LIST OF FIGURES

SUMMARY

The wireless communication technology known as Vehicle-to-Vehicle (V2V) operating at the 5.9GHz Dedicated Short Range Communications (DSRC) band is set to enter the world stage. This dissertation presents novel physical layer (PHY) techniques for providing collision avoidance services to drivers and future autonomous systems participating in V2V networks. To date, predicting car collisions by observing PHY characteristics of DSRC radios in V2V networks is not well investigated nor validated. V2V networks rely heavily on safety message (SM) passing; hence collision avoidance services are enabled by the contents contained within the SM. Based on the existing V2V protocol standards, the foundational research presented could contribute additional safety benefits for V2V networks if any V2V device is misbehaving. The periodic broadcast of either SM or non-safety network traffic could be leveraged to identify events indicative of a collision. The advancements presented in this work will allow future investigators the opportunity to design new collision avoidance methods and to develop additional services for both drivers and autonomous systems. With this body of work, car accidents could be reduced and V2V enhanced to provide collision avoidance not just at the application layer, but directly from the PHY. By enabling V2V devices to sense the whereabouts of other transmitters regardless of the authenticity or accuracy of the critical safety data within SMs, then the reliability of V2V networks can be assured for making connected transportation safer.

CHAPTER 1
INTRODUCTION AND BACKGROUND

The United States averages over 5.6 million car accidents per year, of which, over 1.6 million result in injuries and over 30,000 end fatally. To improve the lives of motorists, the United States is preparing to mandate all domestically sold vehicles to be equipped with a new technology called: Vehicle-to-Vehicle (V2V) communication [1]. Vehicles equipped with V2V are proven to be able to establish an ad hoc network by exchanging safety messages (SM) with each other to determine if a vehicular collision will occur [2]. V2V has emerged from the study of Mobile Ad Hoc Networks (MANET) [3] which focused on the networking of information through unfixed links between nodes with power constraints. From MANETs, Vehicular Ad Hoc Networks (VANET) [4] focus on the routing of information and collision prevention services in which the nodes move at terrestrial speeds with unlimited power sources. VANETs and V2V have become synonymous, though recently V2V has received more popularity due to the immediate deployment set to happen before the end of the decade. V2V devices communicate in the allocated 5.9GHz Dedicated Short Range Communication (DSRC) spectrum [5]. The DSRC spectrum is divided into seven 10MHz channels (plus 5MHz lower spectrum guard band to the adjacent 5GHz industrial, scientific, and medical band) across 75MHz of frequency space including one control channel (CCH) and up to six service channels (SCH). The main operating mode of a Single-Input-Single-Output (SISO) V2V transceiver is the periodic exchange of a SM in the CCH containing information about the transmitting vehicle such as speed, steering wheel angle, and Global Positioning Coordinates (GPS). If a transceiver is Multiple-Input-Multiple-Output (MIMO) with more than two radio frequency (RF) front-ends, then one RF port may be continuously tuned to the safety channel, Ch. 172, for exchanging SMs exclusively while the other ports may be configured in either channel switching between CCH

or in diversity mode [6]. In MIMO systems, SMs could also be allowed to transmit within the CCH and Ch. 172. MIMO architectures are currently suggested to boost performance by leveraging the spatial diversity between multiple antenna elements and collaboration of multiple receivers locally. V2V will be the largest deployment of an ad hoc safety related communication system, however, the system relies on two critical requirements: 1) the sender must be trustworthy and 2) the data received must be accurate. Because data contained within the message is necessary for providing safety benefits, the collision avoidance strategy is *data-centric*, in that other vehicles within a 270-375m[1] broadcast range must be equipped with V2V to determine if drivers should be warned of an impending collision or if an autonomous system should be actuated. This is contrasted with this dissertation objectives which present techniques that could enable a *data-decoupled* collision avoidance system operating as a parallel integrate mode leveraging the two existing V2V standards: Wireless Access in Vehicular Environments 1609.1-4 (WAVE) [7] and IEEE 802.11p [8], hereafter referred together as WAVE-802.11p.

1.1 WAVE-1609 Architecture

The WAVE-802.11p architecture is illustrated in Figure 1.1. The standards cover all layers of the protocol stack and distinguishes between exchanging safety data and non-safety data. For non-safety data, the Internet Protocol (IP) / Transmission Control Protocol (TCP) stack allows for routing of infotainment network traffic among vehicles or roadside units (RSU). Services that use non-safety data usually require sessions to be maintained, which allows for the exchange of delay-tolerant network traffic (e.g. email, weather, traffic updates). For safety data, the WAVE protocol suite describes secure, low-latency transmission, and processing of SM and WAVE service announcements between vehicles and infrastructure. Following WAVE 1609.1, a SM application generates SMs per the SAE J2735 [9] format. A supporting standard SAE J2945 [10] recommends a SM be transmitted at a frequent beacon

[1]Maximum transmit distance at any moment can vary depending upon the environment and vehicle positions.

interval of 10Hz for other V2V devices to use the data received in collision avoidance applications. A SM is a 39 byte one-hop message that can be sized up to 100 or 800 bytes depending on the amount of security encryption applied by the mechanism that follows the WAVE 1609.2 standard. For initial deployment, encryption will be maintained by Private Key Infrastructure (PKI) security management system, where it is expected that private certificate authorities (CA) will handle all key and certificate generation/revocation. DSRC radios may come bootstrapped with 3 to 5 years worth of certificates, and new certs may be delivered "Over-The-Air" (OTA), or upon scheduled update by the dealership. For V2V transceivers with a SISO/MIMO architecture, the WAVE 1609.4 medium access control (MAC) extension describes the rules for channel switching. A single V2V device follows universal coordination time to alternate between the CCH for SM packets and a SCH for non-safety (Ch. 172 is dedicated safety for MIMO systems).

1.2 IEEE 802.11p

An 802.11p transceiver physical layer closely follows that of IEEE 802.11a implementing an orthogonal frequency division multiplexing (OFDM) [11] process as seen in Figure 1.2 which generates the frame structure depicted in Figure 1.3 where data bits are encoded using typical digital modulation schemes (e.g. Binary Phase Shift Keying (BPSK), Quadrature Phase Shift Keying (QPSK), Quadrature Amplitude Modulation-16 (QAM), and QAM-64) and then represented in the frequency domain as data symbols. A frame is composed of a preamble of ten short training symbols, two long training symbols, followed by a signal field, and finally a train of data symbols.

Differences between 802.11a and 802.11p: IEEE 802.11p doubles the symbol duration of IEEE 802.11a because of the smaller 10MHz bandwidth channels which effectively provides long symbol durations to help improve the reliability of reception within a dynamic mobile environment. Unlike 802.11a, the 802.11p MAC does not require the establishment of a basic service set among nodes before communicating. A V2V device

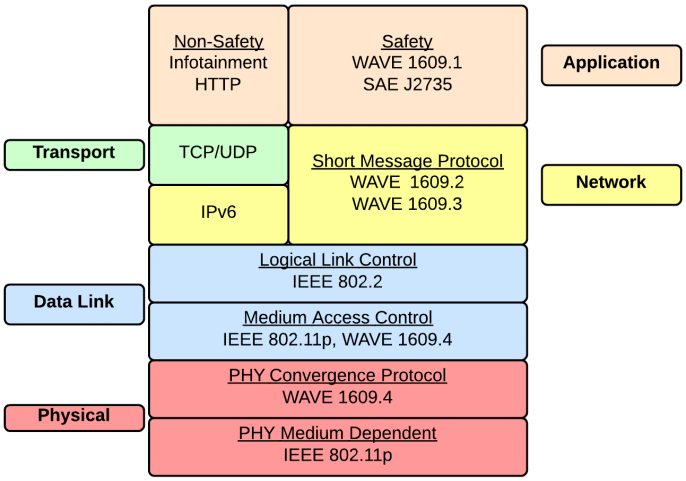

Figure 1.1: WAVE-802.11p protocol stack.

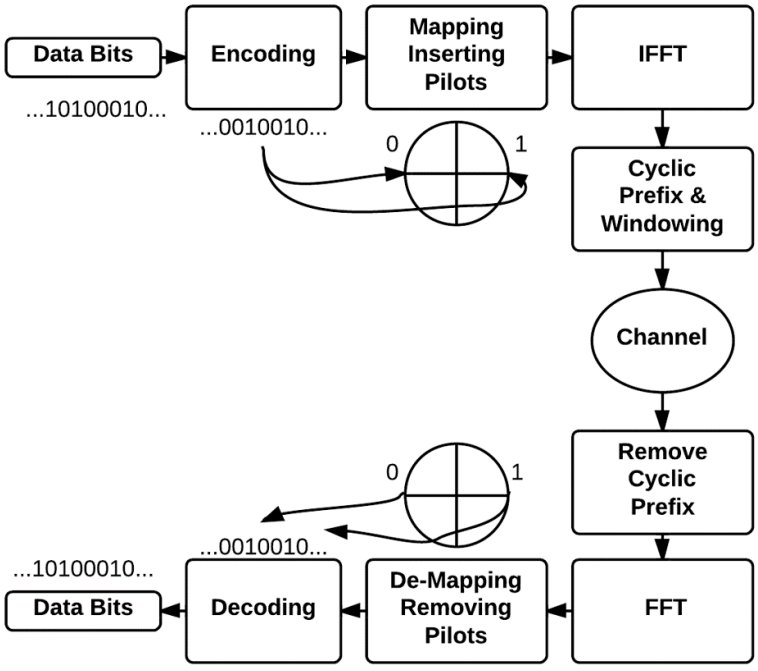

Figure 1.2: IEEE 802.11a/p transceiver architecture.

is free to transmit in the channel at any moment following 802.11 carrier sense multiple access with collision avoidance[2] (CSMA/CA) rules using enhanced distributed channel access. When other applications need to transmit, some V2V upper layer standards employ a form of IEEE 802.11e access control (AC) queues which guarantees that SMs have priority access to the channel over other network traffic. However, for V2V to maintain a low single-hop delay the *packet* related collision avoidance mitigation overhead mechanisms such as Request-to-Send, Clear-to-Send, and ACKnowledgement mechanisms found in 802.11a are not included in the 802.11p standard for SMs. This ensures that SMs can expect a timely delivery and a lower probability of frame collision compared to larger non-safety frames. Non-safety network traffic can leverage full CSMA/CA mechanisms to ensure reception, but comes at a cost of longer channel dwell time which can impact the local network throughput between vehicles.

Ensuring that V2V remains a reliable system for collision avoidance is a significant engineering challenge considering the many security threats and environmental limitations that can negatively affect the network performance. The state-of-the-art provides many ways to provide collision avoidance for drivers and autonomous vehicles, however, many of the approaches towards collision avoidance propose distributed systems that rely on active sensors, cooperative systems that rely on other V2V vehicles, or methods that erroneously assume the sending and receiving vehicle are always trustworthy.

[2]Frame collision avoidance at the physical layer, *not* vehicular collision avoidance.

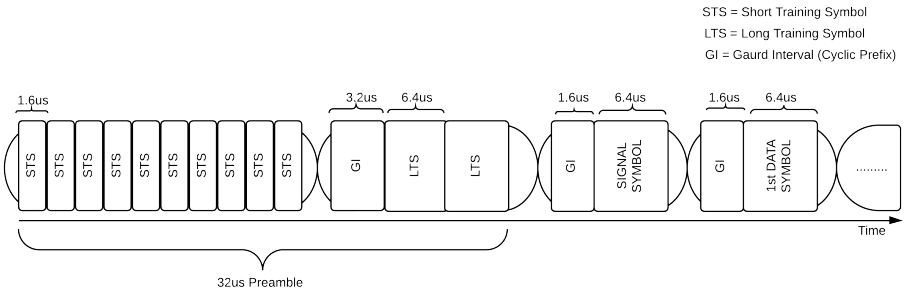

Figure 1.3: Transmitted 802.11p frame structure.

1.3 Methods for Collision Avoidance without V2V

Automobile manufacturers have taken up the task of providing many of the functions that V2V will provide by offering integrated systems of different sensors on the vehicles in the form of an active driver assistance system (ADAS). A vehicle ADAS can be comprised of sensor technologies such as LIDAR, ultrasonic, millimeter wave radar, and computer vision [12]. Yet these technologies are not without their limitations, since all active sensors rely on short-range unobstructed line-of-sight (LOS) they tend to perform poorly under intense glare, rain/snow, and with opaque object obstruction as documented in a recent autonomous car competition [13].

A future ADAS for both autonomous and driver-in-the-loop vehicles could include V2V. In that type of ADAS, active safety sensors are integrated with V2V devices to provide 360° coverage of the vehicle in LOS or non-line-of-sight (NLOS) situations. Several industry patents [14][15] have been awarded describing on-vehicle systems that use V2V and sensing devices to effectively identify other road users and correct or identify their locations using sensor fusion techniques. Camera based techniques have also been investigated by Obst et al. [16] using multi-object vision tracking systems for validating V2V detected entities if the sender SM data is incorrect. In NLOS scenarios, Vlastaras et al. [17] suggested installing radars along with RSUs to facilitate the detection and notification of vehicles approaching intersections that do not have V2V installed. Though forward facing cameras, radars, ultrasonic, and LIDAR sensors have already been deployed, these active sensors are not expected to be mandatory.

Existing ADAS systems can also affect the end-user in ways that are counterintuitive. Reliance on LOS sensors require integration of sensors with different fields-of-view (FOV) and performances across different vendors. Thus, maintenance issues related to forward facing radars and ultrasonic sensors can add over $616 to an already expensive bumper replacement [18]. Vision systems also suffer from obstructed views on the windshield due to

bugs, weather, or even cracks due to road debris, which can render an entire collision avoidance system useless until the window is either cleaned or inclusion repaired. Furthermore, human machine interaction (HMI) of ADAS systems may lead to an increase in distracted driving related accidents. New alerts and collision avoidance interfaces may annoy drivers, leading them to turn warnings off, if false alarm rates are too high or simply make the operators nervous. Nevertheless, ADAS systems with active sensors may eventually become standard due to economies of scale. Back-up cameras are now required on every new light weight vehicle sold domestically to reduce the number of small children accidentally hit [19]. The reduction in cost for camera components were due in large part to the proliferation of the smartphone. The automotive industry has historically pushed against mandated safety technologies (e.g. seatbelts [20]), arguing that they won't be able to meet their bottom line, however, when a new technology reaches scale the marginal cost can be recouped with minimal effect to the price tag. It is expected that V2V, if mandated, would also benefit from economies of scales while providing 360° awareness even in NLOS conditions.

1.4 Current V2V Collision Avoidance Approaches

V2V has received the most attention from public stakeholders due to its capability to scale in manufacturing. In the most basic hardware implementation, 802.11p is a firmware reconfiguration of existing Wi-Fi chipsets, paired with additional middleware that includes the WAVE protocol stack. Furthermore, V2V by itself is an attractive technology for its ability to provide collision avoidance in NLOS situations and detect other V2V equipped vehicles in more scenarios than active sensors. Thus, there are many use cases that V2V can provide reliable collision avoidance if other nodes are trustworthy and truthful.

Current methods for V2V-based collision avoidance focus primarily on the communication link between two or more vehicles; relying heavily on received SM data being reliable. As vehicles exchange SMs a collision likelihood can be determined either locally by the DSRC radio safety application or by an on-board ADAS system which receives the SM

BSM Data	Size (bytes)	BSM Data	Size (bytes)
Message ID	1	Speed	2
Message count	1	Heading	2
Temporary ID	4	Acceleration	7
Timestamp	2	Brake System status	2
Position (lat/long/elev)	4/4/2	Steering wheel angle	1
Positional accuracy	4	Vehicle size	3

Figure 1.4: SAE J2735 required safety message data (total size: 39 bytes).

data from the DSRC radio (the latter more likely for production vehicles).

Huang et al. [21] described a vector based approach to providing collision avoidance alerts using received SM data through a DSRC radio using the WAVE protocol stack. The algorithm showed 100% success for two vehicles over different LOS intersection topologies, but the collision algorithm suffered up to 3% failure rate for vehicle densities over 200 stations. Also, erroneous warning messages were generated at least once over many different speeds. Ahrems [22] demonstrated with real vehicles that a kinematic-based collision avoidance algorithm using SM data through V2V would be able to alert drivers at LOS intersections. Biswas et al. [23] presented an overview of the V2V system in predicting simulated crash experiments which showed that V2V could save up to 14 more vehicles from colliding in a highway pile up, but as the packet delivery rate drops to below 50% (due to SM congestion in the CCH) then the likelihood of drivers being notified of collisions becomes lower.

1.4.1 V2V Susceptibility to Failures

V2V is architected as a large distributed system which relies heavily on the authenticity and integrity of the SM data to be reliable for collision avoidance. Observing Figure 1.4, the data sent in a SM is acquired from the DSRC radio, internal/external GPS radio, or the in-vehicle network bus polled directly from digital sensors or the vehicle computer.

Device Level and Upper Level Security Issues

An on-going topic for V2V is ensuring anonymous SM integrity across several layers of reliability. The first reliability layer is to secure the hosts raw motion information provided to a DSRC radio generated by on-board sensors and securing position information generated by a GPS device. Safety critical on-board sensor data sent to the DSRC radio is assumed to be on a safety-critical bus separate from a non-safety data bus that uses a Controller Area Network (CAN) bus, but CAN data is typically bridged with safety critical data such as the auto-unlock mechanisms bridged with the crash detection system. Bridging non-safety systems with safety critical systems is a vulnerability which could provide an adversary access to the safety-critical bus to alter sensor data as demonstrated by Koscher et al. [24]. On-board GPS receivers are susceptible to spoofing attacks, but can mitigate attacks using several approaches presented by Jafarnia-Jahromi et al. [25] or using a common approach that sends registration credentials before acquiring GPS coordinates from satellites and Differential GPS (DGPS) stations. However, once GPS data is validated the GPS data must be routed to end-points within the in-vehicle CAN network including in-dash navigation systems, telematics services, electronic recording units, and within the safety-critical bus network to the DSRC radio. This leaves GPS data susceptible to similar data alteration attacks as on-board sensor data, unless a dedicated GPS unit is used strictly for V2V co-located on the V2V on-board unit (OBU).

Assuming on-board sensor data and GPS data are polled securely, the second reliability layer focuses on encrypting the contents for delivery to near-by vehicles. Network layer security techniques ensure trustworthiness of anonymous SM transmissions using the WAVE 1609.2 standards, but anonymizing the data while still meeting time-sensitive delivery requirements for a SM (suggested single-hop delay is less than 100ms) is still an active research area as outlined by Zhao et al. [26]. As new security processes are developed and proved successful, the next layer of reliability must ensure that the safety critical data received is accurate.

Regardless of the encryption method used in V2V, misbehaving nodes could broadcast erroneous SM data either intentionally or unintentionally. Unintentional misbehavior could be the result of equipment malfunction or loss of GPS service. Intentional misbehavior could be caused by malicious software altering SM data either before transmission or after reception. However, if a worm attack spreads through a V2V network as simulated by Jian et al. [27], encryption mechanisms applied at the network layer can ensure authenticity of SM data before being sent, but encrypting erroneous data will still result in misinformation being delivered. Data integrity is essential for collision avoidance, but ensuring data integrity among misbehaving nodes is still a challenge.

A misbehavior detection scheme (MDS) can be employed to detect or correct misinformation, but an MDS alone may not be sufficient for driver safety. Yan et al. [28] proposed an MDS with active sensors in LOS conditions to correct SM data, but the driver is left vulnerable in NLOS conditions where accident prevention is needed most. A cooperative MDS has been proposed by previous works compiled by Erritali and El Ouahidi [29], but cooperative approaches perform poorly among multiple misbehaving nodes. Barnwal and Ghosh [30] presented a decentralized MDS which sized virtual zones of separation distance relative to the receiver to detect misbehavior, but if the receiver is unknowingly misbehaving (i.e. receiver GPS is compromised), then the zones may be sized incorrectly.

GPS and Motion Data Accuracy Issues

The highest reliability layer currently seeks to correct errors in a received SM using localization techniques. These techniques are also useful for places where GPS signals suffer extreme attenuation such as overpasses or tunnels. Depending on the amount of satellites in view of the GPS receiver, Boukerche et al. [31] described that GPS data can often exhibit slow update rates and inaccuracies that range from $\pm$10m to $\pm$30m (some OBU devices advertise $\pm$1m accuracy, but this is not guaranteed). For a high-speed driving scenario, this could be a dangerous error. GPS accuracy can be improved significantly by using on-

ground DGPS stations, but DGPS services may not always be available. In those situations, GPS-free localization and cooperative vehicle localization techniques may be employed to resolve inaccuracies. Sun et al. [32] proposes using RSU and dead-reckoning algorithms to resolve vehicle position. If both RSU infrastructure and GPS is unavailable, cooperative positioning techniques highlighted by Alam and Dempster [33] use Kalman filters to process received position information among neighboring vehicles to obtain more accurate relative positions. Like RSU techniques, Ashok et al. [34] proposed that cellular base stations can supply localization services for vehicles using the cellular network by triangulation. Passing SMs through the on-board cellular interface could be possible with 5G technologies, but cellular infrastructure may not be available such as on mountain highways. Furthermore, it is not clear if cellular carriers would take on the liability for routing SMs through their base stations if loss of services lead to accidents. While cooperative methods work well among available and trustworthy neighbors, collision avoidance services could be unavailable when needed most, such as remote areas lacking infrastructure or late nights where traffic density is lower and speeds tend to be higher [35].

1.5 Alternatives to Data-Centric Collision Avoidance

While each of the approaches contribute towards either securing or correcting the contents of a SM, each approach is either cooperative data-centric or relies on infrastructure. This dissertation demonstrates that by performing collision avoidance at the physical layer, the safety benefits of V2V could be decoupled from the data contained in a SM. Current V2V literature neglects physical layer (PHY) based collision avoidance applications for drivers, rather the emphasis has been on LOS active sensors integration or cooperative V2V for resolving errors. The DSRC radio RF front end is currently not used for real-time collision prediction, though recently, some investigations have proposed analyzing the incoming signal from a misbehaving node to determine a physical characteristic about the sender.

PHY observations can be made by observing radio characteristics such as channel state

estimations, direction-of-arrival, signal strength, carrier frequency offset, and Doppler shift. Most investigations which will be identified in their relevant chapters have only observed PHY metrics for providing *secondary* observations for resolving GPS errors or correcting speed errors. This is contrasted with this dissertation work which proposes using PHY metrics to provide collision avoidance services to drivers and autonomous systems, specifically using: signal strength, direction-of-arrival (DOA), and Doppler shift observations. It is assumed that the observations could be reliably extracted from a received signal (either SM or non-SM packet) to assist in providing a collision avoidance service. This dissertation demonstrates that unique physical characteristics correlate with threatening behavior, regardless if the SM critical data payload contents are accurate. The main advantage of the techniques presented is that PHY-based collision avoidance need only rely on a SM being received.

1.5.1 Dissertation Contribution

The objectives of this dissertation are to provide collision avoidance to drivers through foundational physical layer collision avoidance techniques. These techniques could be applied towards OBUs to warn drivers or autonomous systems in V2V networks. It is shown that deviations from normal driving which lead to accidents are detectable by observing large-scale characteristics of a received V2V signal. Current V2V literature neglects physical layer collision avoidance applications for automotive safety. The research presented suggests that DSRC radios could be the enabling technology to provide a robust 360° sensor for collision avoidance. The specific contributions of this dissertation are as follows:

- A new understanding of how the DSRC wireless channel is affected by vehicle lane placement and orientation.
- A method for a single-channel DSRC radio to determine a collision by observing the received signal strength indication.

- A method for enabling single-channel DSRC radios to receive measurements of direction-of-arrival estimation (DOAE) in real-time per frame.
- The Doppler shift collision avoidance theory for terrestrial V2V networks.
- A method for a single-channel DSRC radio to determine its environment by observing the Doppler phenomenon using omnidirectional antennas.
- The first ever use of a new sensor view: the Doppler profile, to enable collision prediction in V2V networks, validated using real-world data.

In addition to the major contributions, together, these techniques could provide PHY-based collision avoidance in V2V without requiring changes to existing WAVE-802.11p protocols. Future work would integrate these techniques for providing reliable and stable collision avoidance services to vehicles.

The existing V2V standards leave the reliability of the ad-hoc network susceptible to both primitive and intelligent RF attacks [36][37]. In a primitive attack vector, the communication channel is injected with high energy noise/autocorrelation content. In an intelligent attack vector, physical attributes about the signal are spoofed with the intent to throw off the collision avoidance techniques to be discussed. Other wireless systems such as cellular and Wi-Fi do not have anti-jamming mechanisms, however, these networks are not built for critical safety applications. Since the primary purpose of V2V is to provide safety critical applications, a primitive RF jamming attack would bring down the wireless system in a local area. This dissertation work assumes that no RF jamming attacks are used during the operation of the PHY-based collision avoidance techniques to be discussed. Mitigating this attack-vector is outside the scope of this work, but could be addressed in future investigations by leveraging anti-jamming techniques for V2V communications [38].

1.5.2 Overview

This dissertation is arranged into several chapters covering unconventional channel measurements, collision prediction, and new technologies derived from the physical layer observations. Chapter 2 provides a foundational understanding of the V2V channel by presenting insights into the effects of vehicle orientation and lane spacing on the LOS channel response common to terrestrial V2V networks. Chapter 3 describes a received signal strength technique for collision avoidance. Chapter 4 describes in detail a method towards providing DOAE to single-channel DSRC radios. Chapter 5 describes a theoretical background on Doppler domain collision avoidance. Chapter 6 describes the Doppler profile and its applications towards providing collision avoidance and environment identification through machine learning to achieve exceptional results. Chapter 7 describes future work which would provide the integration of the complete theoretical architecture and performance considering all aspects of the methods presented.

CHAPTER 2
THE EFFECT OF VEHICLE ORIENTATION AND LANE SEPARATION ON LOS SIGNAL STRENGTH

Understanding the LOS V2V channel response on signal strength is foundational for gaining insight into the PHY layer observations used by the received signal strength and Doppler shift techniques presented in the following chapters. For example, unique changes in the V2V channel due to vehicle road configuration can provide valuable context for collision avoidance such as how vehicles facing opposite directions in the same lane is indicative of a head-on collision. The vehicle road configuration can be described by two aspects: lateral lane separation between two V2V equipped vehicles and the relative orientation of the vehicles with respect to the front bumper. The V2V wireless channel imposes large-scale and small-scale fading effects, that primarily affect the data recovery performance of the underlying WAVE-802.11p radio. In channel modelling, characterizing large-scale fading effects can provide valuable insight into how lane separation and vehicle orientation can contribute towards the PHY layer observations for providing collision avoidance services. The contents of this chapter relate the results first identified in [39] which developed an improved LOS channel model for DSRC derived from the vehicle road configuration (i.e. lane separation and relative orientation). By developing a new path loss model that considers vehicle road configuration, it is possible to quantifiably understand how the placement and vehicle bodies play a role in the channel response at a DSRC radio front end.

2.1 Introduction

Understanding large-scale fading effects in V2V at the 5.9GHz DSRC band has received broad coverage in related literature over the last 15 years. Most V2V channel measurement campaigns describe the expected path loss of the V2V channel through empirical models.

The path loss is a channel metric which describes how fast the received signal strength decays with distance. It is well known that the path loss exponent and reference path loss (y-intercept on a log-log scale) varies for different environments, but it is not well understood how the channel changes in each environment relative to lane separation or vehicle orientation. An improved path loss model valid for LOS V2V communications at distances less than 100m is presented to help quantify the channel response related to vehicle placement and form. The path loss model developed removes the Gaussian random variable component, typically used to model shadowing in classic power law path loss models, and instead makes the y-intercept and path loss exponent Gaussian random variables. Derived from extensive empirical measurement campaigns in which vehicle orientation and lane separation are varied, the new channel model is compared to experimental data in which the vehicles move at different speeds. The improved path loss model performs a better fit to experimental data than existing path loss models, including two-ray ground reflection, dual-slope piecewise linear, and classic power law; suggesting that vehicle orientation and lane separation play an important role in how the received signal responds at the DSRC front end. Understanding how the vehicle road configuration affects large-scale effects like path loss, can contribute directly towards understanding the underlying principles that the PHY-based collision avoidance system exploits.

As vehicles maneuver, the wireless channel can change unpredictably. The received signal strength (RSS) of a SM can experience significant swings in signal power due to a variety of channel characteristics. The path loss is an important channel characteristic used to model the RSS for a given separation distance between two transceivers. A popular model is the classic power law, in which the path loss exponent γ dictates the rate at which the path loss changes as a function of separation distance. A variant of the classic power law model considers a breakpoint in which the path loss exponent changes from γ_1 to γ_2 after a certain distance. Another popular model is the two-ray ground reflection which considers the main LOS path and dominant ground reflection causing constructive and destructive

interference at a receiver.

For the classic power law model, $\gamma = 2$ is traditionally accepted as the decay rate of signal power in LOS free-space; yet most V2V path loss studies report in LOS, $\gamma < 2$, across many different environments. One reason for this apparent decrease in path loss, is that the road environment features more scatters which diffuse the signal in more directions, thereby adding more energy at the receiver [40]. Furthermore, the path loss reported varies considerably from 1.4 up to 1.77 for LOS. A statistical component which accounts for fluctuations in the RSS due to random shadowing is traditionally incorporated into path loss models to account for these unexpected inconsistencies, but generalizing with an added "noise" term could be unsuitable for accurately understanding the V2V channel.

The following reports on various path loss exponents across an extensive measurement campaign where vehicle orientation and lane separation are varied. The observed distribution of channel characteristics is then developed to suggest a modification of the classic power law model to better capture vehicle configurations, while being agnostic to the specific type of vehicle body. The motivation for this new development is in response to the existing literature reporting different path loss measurements depending on approaching vs. leaving trajectories [41][42], suggesting that vehicle orientation and lane separation could affect the way path loss is measured, which consequentially affects how large-scale PHY-based collision avoidance metrics like received signal strength indication (RSSI) could be perceived.

2.2 Background: LOS Large-Scale Fading in V2V

In the background literature, measurement campaigns have developed empirical path loss models for rural, highway, urban, and suburban environments. A new understanding about how vehicle lane spacing and orientation affects the path loss is captured by a newly developed model and compared to the three most popular path loss models used for simulating V2V networks: classic power law, dual-slope piecewise linear, and two-ray ground reflec-

tion.

2.2.1 Classic Power Law Model

The classic power law is derived from

$$P_r = \frac{G_t G_r P_t \lambda^2}{16\pi^2 d^\gamma} \tag{2.1}$$

where G_t, G_r are the antenna gains, P_t is the transmit power, λ is the carrier wavelength, d is the distance between transmitter and receiver, and γ is the path loss exponent. For path loss modeling, equation (2.1) is more commonly represented on a log-distance scale, in which a maximum likelihood linear fit line can be written as

$$P_L(d) = \alpha + 10\gamma \log_{10}(d) + X_\sigma \tag{2.2}$$

where α is a y-intercept, γ is now represented as the slope of the fit line, and $X_\sigma \sim \mathcal{N}(0, \sigma^2)$ where σ describes the standard deviation off of the fit line.

One of the earliest V2V measurement campaigns by Karedal et al. [41] reported that at 5.2GHz a classic power law model was appropriate for urban, suburban, and highway environments in which each landscape exhibited $\gamma < 2$. However, the classic power law model had to be modified due to gain discrepancies depending on how the vehicles were approaching each other as [41, eq. (5)]

$$P_L(d) = P_0 + 10\gamma \log_{10}(d/d_0) + X_\sigma + \zeta P_c, d > d_0 \tag{2.3}$$

where P_0 is a known path loss at a reference separation distance d_0 (typically 10m for V2V), ζ accounts for forward, reverse, or convoy approach trajectories where $\zeta \in -1, 1, 0$, respectively, and P_c corrects forward or reverse gain differences.

Kunisch & Pamp [43] reported similar path loss findings, but did not observe any gain

discrepancies between vehicle approach direction as reported in [41]. More recent studies by Fernández et al. [44][45] considered traffic densities in obstructed-LOS at 5.9GHz in which $\gamma = 1.67$ for low traffic densities and $\gamma = 1.77$ for high traffic densities. Additionally, from [45], rural, suburban, and highway γ were 1.61, 1.76, and 1.66, respectively.

2.2.2 Dual-Slope Piecewise Linear Model

Some studies have observed the path loss changes after some distance, suggesting breakpoint models like the dual-slope piecewise linear model. Cheng et al. [42] measured path loss at 5.9GHz and presented a dual-slope piecewise linear model as [42, eq. (2)]

$$PL(d) = \begin{cases} P(d_0) - 10\gamma_1 \log_{10}(\frac{d}{d_0}) + X_{\sigma_1} & d_0 \leq d \leq d_c \\ P(d_0) - 10\gamma_1 \log_{10}(\frac{d_c}{d_0}) - & d > d_c \\ \quad 10\gamma_2 \log_{10}(\frac{d}{d_c}) + X_{\sigma_2} & \end{cases} \tag{2.4}$$

where d_c is the critical distance where slopes γ_1 and γ_2 exchange (typically $d_c = 100m$). One interesting observation was that forward and reverse approach gains were not mismatched as reported by [41]. Ito et al. [46] further characterized a LOS dual-slope piecewise linear model with a root mean square error of 3.8dB in an urban canyon environment at 5GHz which discovered no dependence on road width up to 60m, suggesting that waveguide properties exist for most narrow driving corridors.

2.2.3 Two-Ray Ground Reflection Model

The two-ray ground reflection model has received attention in the background literature for the ability to estimate dips in the RSS [40][41, eq. (3)]. The important components of the two-ray ground reflection model can be described with

$$\theta_i = atan(\frac{h_t h_r}{d}), \Gamma_{||} = \frac{\epsilon_r \sin\theta_i - \sqrt{\epsilon_r - \cos\theta_i{}^2}}{\epsilon_r \sin\theta_i + \sqrt{\epsilon_r - \cos\theta_i{}^2}} \tag{2.5}$$

where ϵ_r is the relative permittivity, h_t, h_r are the heights of the antennas, and $\Gamma_{||}$ is the reflection coefficient of the ground reflected power.

The two-ray ground model has been reported to fit rural environments better than other environments. Shagdar et al. [47] showed that varying speeds do not affect the two-ray path loss model fit at 5.9GHz. The two-ray model was also verified by Miucic et al. [48] and Boban et al. [49] to match RSS dips from 10m to 200m in rural settings. In other settings, the two-ray path loss model does not fit well for distances less than 70m-100m.

The reported path loss measurements in the existing literature are based on one set of experiments, yet are expected to generalize the expected RSS using a constant γ and σ term for X_σ. Absent is the aggregate effect of vehicle orientation and lane positioning on γ. Experiments and simulations were performed to garner new insights into the effects of vehicle configuration on the path loss and therefore signal strength is better understood in the V2V context.

2.3 Channel Measurements

Traditionally, V2V channel measurement campaigns use GPS receivers synched with channel sounding equipment performing direct pulse-based, spread spectrum-based, or frequency domain-based channel impulse response measurement techniques. But in this work an unconventional technique was employed to focus on the large-scale LOS fading effects for SMs at the packet level using real devices, instead of small-scale fading effects at the bit level.

2.3.1 Measurement Setup

The setup illustrated in Figure 2.1 was used for experimentation. Two vehicles were equipped with a 9dBi omnidirectional vertically polarized whip antenna positioned in the center of the roofs and mounted such that their height was 1.5m from the ground. A commercially available 5.9GHz DSRC radio adhering to WAVE-802.11p standards was config-

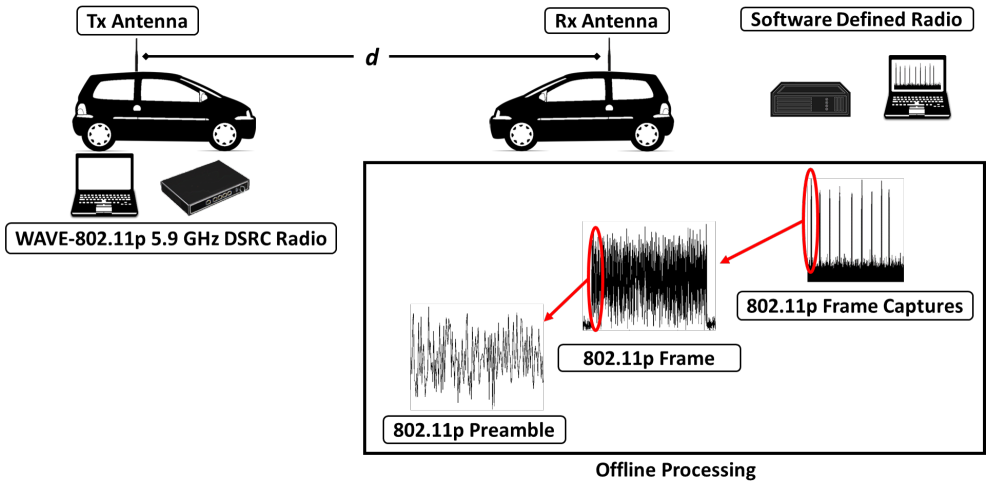

Figure 2.1: Set-up used for measurement campaign.

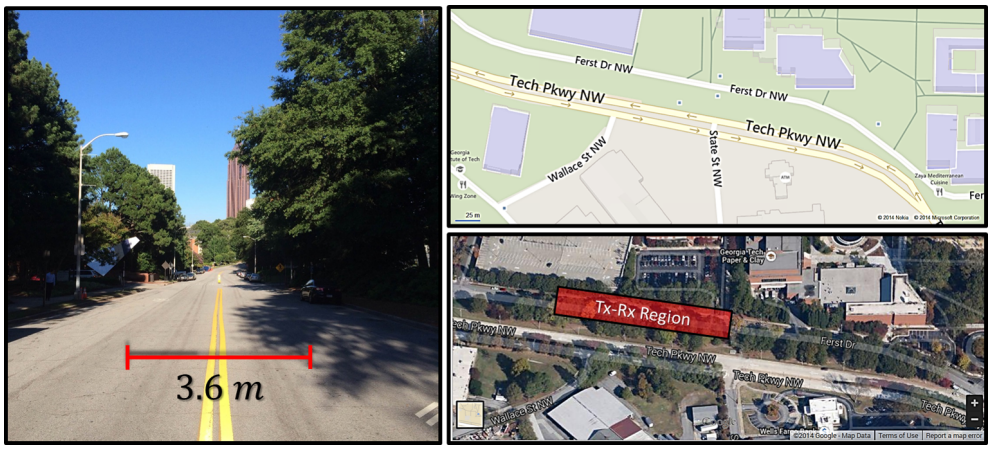

Figure 2.2: Location of measurement campaign in Atlanta, GA.

ured to broadcast SMs with a 1ms delay for a one second duration at 5.86GHz with 20dBm of transmit power. The packet waveforms were captured by a software defined radio for post-processing using custom MATLAB scripts to locate SM frames in the signal capture and calculate the RSS of the preamble per the 802.11 standard.

The measurement setup allowed for realistic offline RSS measurements following the 802.11 standard. The RSSI provided by the radio was not used, because dropped packets at the radio (due to incorrect demodulation at the receiver) do not provide an RSSI value, even though the signal power may be well above the channel noise. Thus, post-processing included RSS measurements on all SM packets above the noise floor, regardless if the data contained was recoverable.

The measurements were taken along a 100m stretch of road pictured in Figure 2.2. The environment resembled a suburban landscape featuring trees, parked cars, street signage, and two-story buildings. The road was surveyed and marked off in 10m increments so that the vehicle separation distance at each measurement point would be known.

2.3.2 Measurement Scenarios

At each measurement point, the vehicles were positioned and orientated in various configurations to stage driving scenarios expected to occur on the roadways. For these static measurements, effort was made to ensure no additional traffic/pedestrian activity was present which could have biased the experiment outcomes. The vehicles remained parked at each measurement point for the duration of the transmission. For each scenario, the vehicles could be positioned in the same lane (SL), adjacent lane (AL), or two lanes away (TL). Within a lane, the vehicles could be oriented in either the same direction (SD) or opposite direction (OD). The trajectory of the transmitter (Tx) can be described as approaching (A) the receiver (Rx) or leaving (L) the Rx. A description of each measurement scenario can be viewed in Table 2.1.

2.3.3 Measurement Results

The results of the measurements can be viewed in Figure 2.3, and tabulated in Table 2.2. The findings are in agreement with the existing literature [41][43][44][45], which validates the unconventional measurement technique. The findings also agree strongly with the adapted model, equation (2.3), as leaving trajectories (Tx rear is facing Rx) can exhibit higher path loss exponents compared to approaching trajectories. This indicates that γ could change based on the diffraction caused by the structure of the vehicles as their relative orientation changes during motion. The same lane positions depict a tighter correlation between approaching and leaving trajectories, indicating that the front and rear of the vehicles could possibly create a waveguide. As expected, for the adjacent and two lane

Table 2.1: Channel Measurement Scenarios (Vehicle Road Configurations)

Scenario	Description	
SL-OD-A*	Positioned in the same lane and facing each other, Tx approaches Rx from the front.	
SL-SD-A	Positioned in the same lane, oriented in the same direction, Tx approaches Rx from behind.	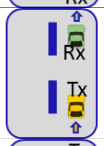
SL-SD-L	Positioned in the same lane, oriented in the same direction, Tx leaves Rx from the front.	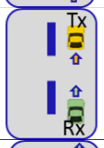
AL-SD-A	Positioned in adjacent lanes, oriented in the same direction, Tx approaches Rx from behind.	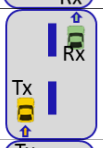
AL-SD-L	Positioned in adjacent lanes, oriented in the same direction, Tx leaves Rx from the front.	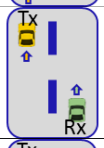
AL-OD-A	Positioned in adjacent lanes, oriented in the opposite direction, Tx approaches Rx from the front.	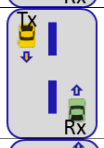
AL-OD-L	Positioned in adjacent lanes, oriented in the opposite direction, Tx leaves Rx from behind.	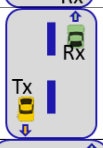
TL-SD-A	Positioned two lanes away, oriented in the same direction, Tx approaches Rx from behind.	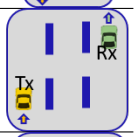
TL-SD-L	Positioned two lanes away, oriented in the same direction, Tx leaves Rx from the front.	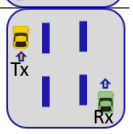
TL-OD-A	Positioned two lanes away, oriented in the opposite direction, Tx approaches Rx from the front.	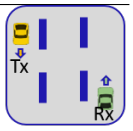
TL-OD-L	Positioned two lanes away, oriented in the opposite direction, Tx leaves Rx from behind.	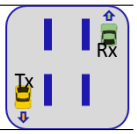

**This only occurs during a head-on collision.*

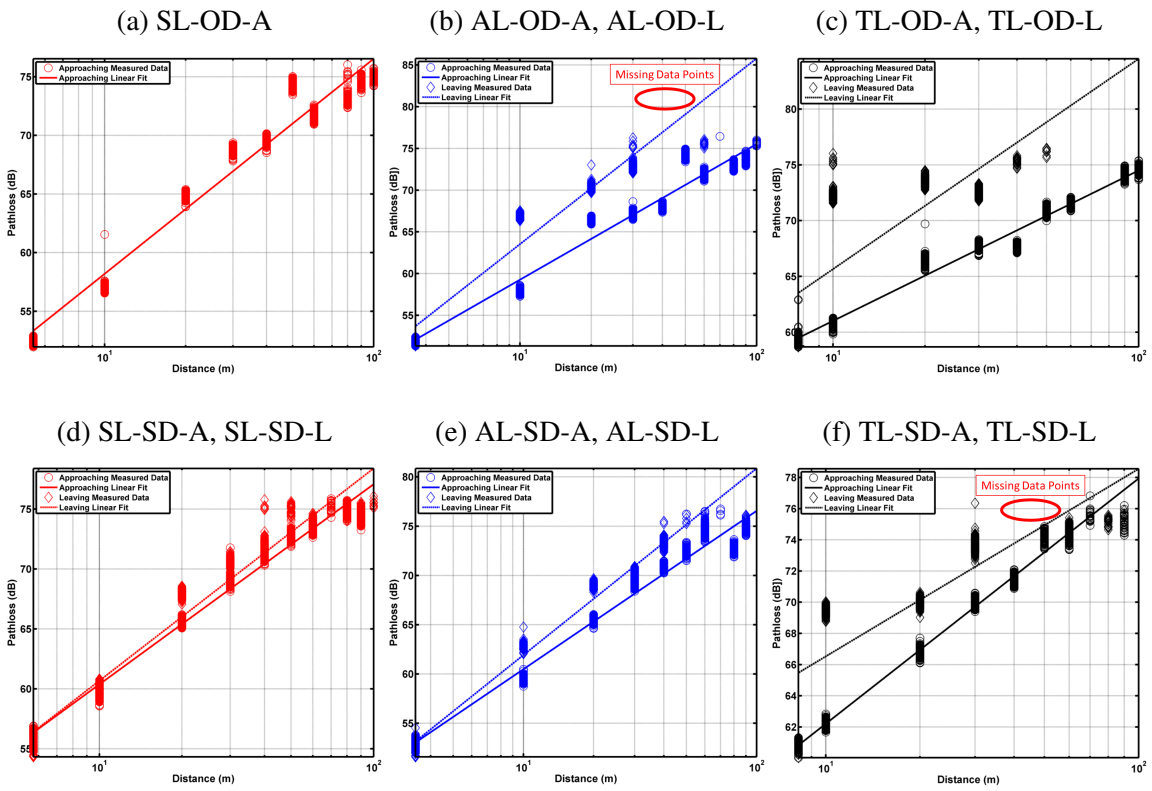

Figure 2.3: Results of static path loss measurements for various vehicle orientations and lane separations: (a) Same Lane, Opposite Direction; (b) Adjacent Lane, Opposite Direction; (c) Two Lanes Away, Opposite Direction; (d) Same Lane, Same Direction; (e) Adjacent Lane, Same Direction; (f) Two Lanes Away, Same Direction

away positions, as the vehicles are spaced further away by lane separation then the higher the expected path loss becomes.

The rear of the vehicle bodies can possibly attenuate or amplify the signal as the vehicles approach each other until the sides of the vehicles align. This holds true for either lane position, however, it is difficult to fully understand why γ exhibits large variability during stable measurement conditions. Some measurement points at 40m and 50m separation distance were missing as indicated by Figure 2.3b and Figure 2.3f for the leaving trajectory due to parked vehicles within the traveling lane. More data points are expected to result in corrected path loss values.

Though the measurements were conducted at static distances with no additional moving traffic, it is interesting to observe the range of values that γ can take on even when there

Table 2.2: Path Loss Summary

Opposite Direction				
Scenario	α	γ	σ	Position
SL-OD-A	39.86	1.83	1.59	Same Lane
AL-OD-A	43.0	1.62	1.51	Adjacent Lane
*AL-OD-L	41.30	2.22	2.21	
TL-OD-A	47.53	1.35	.78	Two Lanes Away
TL-OD-L	46.82	1.88	3.92	
Same Direction				
Scenario	α	γ	σ	Position
SL-SD-A	43.70	1.67	.92	Same Lane
SL-SD-L	42.98	1.77	1.53	
AL-SD-A	44.41	1.61	1.16	Adjacent Lane
AL-SD-L	42.98	1.89	.98	
TL-SD-A	46.48	1.57	.55	Two Lanes Away
*TL-SD-L	54.50	1.20	2.63	

**Some data points missing.*

is a strong unobstructed LOS path. The experimentation reveals a critical observation that has been left out of the existing literature, which provides insight into how the path loss in V2V environments behaves even more unpredictably than previously thought. This leaves to question the accuracy of existing power law based channel models. Especially since the reported parametric values are based solely on the observations of a few experiments in varying shadowing conditions while the vehicles were moving. Considering that V2V channel simulators may use a classic power law for simulating the RSS of SMs, the values reported by this work under ideal conditions indicates that the classic power law path loss model for short distances where accidents may occur (less than 100m) could be improved.

Observing the small sample size of obtained values in Table 2.2, it is difficult to extract any meaningful relationship between the vehicle orientation and the path loss. The same conclusion could be said for lane positioning. The only explanation for these phenomena is that the vehicle structures at certain relative positions alter the gain in the path loss, but

it is still unclear specifically how the vehicle structures contribute to these discrepancies.

2.4 Improved Path Loss Model Derivation

To illustrate how vehicle orientation and lane positions affect the LOS channel, Figure 2.4 shows each parametrized path loss model from Table 2.2, plotted individually up to 100m using the classic power law model from equation (2.2). The variability in the individual channel models reveal a standard deviation of 3.19dB, which is higher than most the individual shadowing terms, σ, reported in Table 2.2. This suggests that the existing power law models which are based on a constant γ are not suitable for generalization of the expected path loss for driving scenarios. Furthermore, the shadowing term, X_σ, in traditional channel models does not effectively capture enough random fluctuations in RSS to be considered as a generalized approach, even in clear LOS.

While it is not clear how the path loss changes based on *specific* vehicle structures, it is assumed that most vehicles equipped with V2V will feature similar vehicle forms (though hood/trunk/roof styles may be different), and similar antenna placements (due to regulation or industry best practices). Thus, a Gaussian distribution of path loss channel characteristics is assumed.

To develop the improved path loss model the X_σ shadowing term is removed and it is assumed that for clear LOS separation distances at less than 100m, that γ and α can be modelled as Gaussian random variables: $X_\gamma \sim \mathcal{N}(\mu_\gamma, \sigma_\gamma^2)$ and $X_\alpha \sim \mathcal{N}(\mu_\alpha, \sigma_\alpha^2)$. The new path loss model becomes

$$P_L(d) = X_\alpha + 10X_\gamma \log_{10}(d) - S_{offset} \tag{2.6}$$

Observing (2.6), the X_σ term from (2.2) is removed, and replaced by non-zero mean Gaussian random numbers representing the y-intercept and slope of the path loss. Also added is an offset term, S_{offset}, to shift the expected path loss depending on the amount of scatters

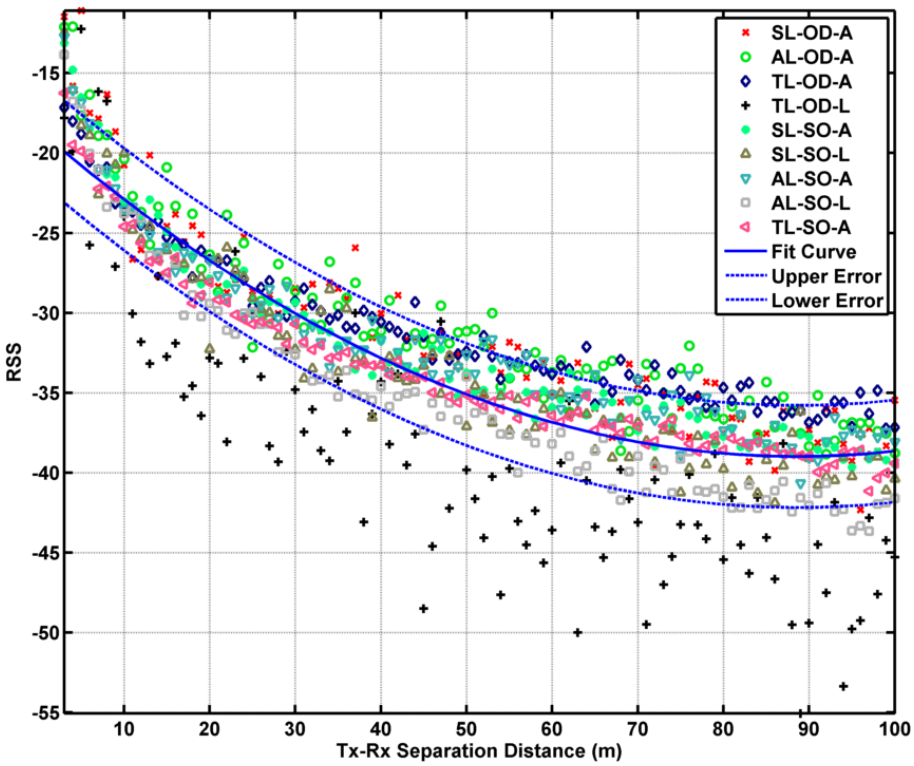

Figure 2.4: Discrepancies in individual path loss models for the same separation distance reveals that vehicle orientation and lane spacing can affect the signal strength in V2V networks (AL-OD-L and TL-SD-L omitted).

in the environment which add extra energy to the receiver.

A Gaussian distribution for X_γ and X_α could be an overly simplistic assumption, however, this is motivated by the low sample size from the static channel measurements. Repeating the path loss measurements considering multiple vehicle forms may reveal a more accurate distribution for X_γ and X_α. It should also be noted that the model is flexible enough to replace X_γ and X_α with a different distribution other than Gaussian. The new model simply adds an additional degree of freedom to the previous shadowing term X_σ, so that the improved channel model can account for possible variabilities due to vehicle structure, direction, lane position, and trajectory while the vehicles move relative to each other. Specifically, the lane separation alone can be modelled with different distributions, rather than lumping all lane separations into one model. This is because the vehicle orientations will change the RF characteristics of the channel depending on the lateral lane separation

that vehicles are expected to travel in. As the vehicles maneuver, channel characteristics for a given separation distance are selected from a distribution of possible channel parameters, any of which could be valid at the time. The appropriate distributions must be determined through experimental trials to provide the most accurate model. The LOS short distance range is leveraged to remove the need to characterize deep fades in the RSS due to constructive and destructive interference, typically observed at distances greater than 70m or 100m, though slight dips may occur within less than 70m. As mentioned earlier, a two-ray ground reflection model is better for larger separation distances, especially in rural settings.

2.5 Model Validation

To validate the model, additional experiments (using the same setup from Figure 2.1) were conducted while the vehicles were in motion. The experiments were conducted in lane orientation groups: same lane, adjacent lane, and two-lanes over. The lane scenarios were executed at four trial speeds: 16kmh, 32kmh, 48kmh, and 64kmh; the vehicles approached each other traveling the same speed for each trial (this was necessary for alignment in post-processing). A total of 12 scenarios were captured for the model validation.

2.5.1 Dynamic Experiment Methodology

Each vehicle attempted to maintain the same speed during each trial run within the 100m testing range, but at higher speeds the SM packets were transmitted and received during unknown acceleration/deceleration durations. Upon crossing (or avoiding) each other, the vehicles attempted to maintain the desired cruising speed, but often decelerated after passing each other due to unexpected traffic and pedestrian activity at the time. The RSS measured after the crossing point was disregarded in the analysis of the model validation because of this discrepancy in the estimated distances after the RSS peak. Though the leaving trajectories were not captured because of these environment issues, this does not invalidate the methodology since the new model is decoupled from a specific vehicle trajectory due to

the new statistical terms, unlike the adapted power law model from equation (2.3) which explicitly includes vehicle trajectory.

Another source of slight misalignment was caused by a Tx latency which added a delay of about 3560μs per SM transmission, even though the DSRC radio was programmed to broadcast at a set interval. The GPS positions of Tx and Rx were not logged during the capture, instead the distances were estimated in post-processing by aligning the highest RSS peak to be the closest known separation distance. The transmitter latency was multiplied by the expected experiment relative speed in post-processing to estimate the separation distances.

2.5.2 Settings for Model Validation

Typically, when using a path loss model within a simulation of wireless networks, either the parameters for a path loss model from a published measurement campaign are used, or investigators may make their own static/dynamic measurements and then select a model that best fits the measured data with the lowest root-mean-square error (RMSE). However, once a model is chosen the parameters typically remain constant for all simulations.

To mimic this process, the classic power law, proposed model, and two-ray ground model parameters were acquired from a single fit of only one dynamic scenario measurement: adjacent lane with approaching trajectories at 16kmh. This scenario was chosen because most V2V measurement campaigns use data acquired from a two-lane highway with opposite directions of travel. Furthermore, 16kmh is a slow speed which captures the most data points for an accurate fitting across different scenarios. Speed is typically not a factor in the performance of a path loss model, but the V2V environment is known to be unpredictable. Thus, the proposed model performance will be considered at different speeds.

For the proposed model, the values used for μ_γ, σ_γ and μ_α, σ_α were acquired from the static measurement campaign in Table 2.2. Groups of γ by lane scenario then allowed the

Table 2.3: Path Loss Model Parameters

Classic Power Law Model			
γ	α	σ	offset
1.85 $\frac{dB}{m}$	40.22dB	1.51dB	0dB
Proposed Model			
Grouping	X_γ	X_α	S_{offset}
Same Lane	$N(1.76, .08)$	$N(42.18, 2.04)$	2.5dB
Adjacent Lane	$N(1.71, .16)$	$N(43.47, .81)$	2dB
Two Lanes Away	$N(1.60, .27)$	$N(46.94, .54)$	1.75dB
Two-Ray Ground Reflection Model			
f_c	h_t, h_r	ϵ_r	offset
5.86GHz	1.5m, 1.5m	*3.75	10.2dB

**Average value from [50][51].*

μ_γ and σ_γ statistics to be obtained. This procedure was also performed on the reported α measurements to obtain the μ_α and σ_α statistics. The S_{offset} value was determined by acquiring the value which provides the best fit over multiple realizations of the proposed channel model. For the two-ray model, an offset term had to be determined by finding the value that best fit the two-ray model to the measured data set. For each model, the parameters for the simulation are tabulated in Table 2.3. The dual-slope model was not included in the analysis because for less than 100m, the dual-slope model becomes a classic power law. The classic power law model provided the best single instance fit of the data with and RMSE=1.51dB, which was lower than that of the proposed model and the two-ray ground reflection model.

2.5.3 New Model Validation Results

For each of the 12 scenarios the classic power law model from equation (2.2), the proposed model from equation (2.6), and the two-ray ground reflection model from (2.5) are compared across all 12 scenarios for the best RMSE fit. Because the classic power law model and the proposed model have statistical components, a Monte Carlo simulation was

executed to simulate 100,000 realizations of fits. For each realization, the RMSE from all models were compared in each of the 12 scenarios, and for each scenario the model with the lowest RMSE was declared the winner.

The raw output of the channel models is very noisy and these fluctuations are typically adjusted before applying the models in a network simulator. A better comparison is to compare the trends of the models and measured data sets by applying a 25pt moving average filter, and calculating the RMSE of the trends. The reasoning behind this is that the more accurate the trend of a path loss model is to the measured data trend (disregarding noise variation), then the more reliable the path loss model could be at predicting the RSS. Separation distances up to 85m were recorded during the measurement campaign; after 85m the noise floor was sometimes too high to obtain RSS values (like some of the outcomes for the static measurements). Also, due to some driver error, about 20m of measurement data had to be removed from the adjacent lane-32kmh and same lane-48kmh data set. The results of the Monte Carlo simulation are tabulated in Table 2.4.

The proposed model provides a better fit than the other models for two out of the three lane groupings across all speeds, but is significantly weaker in comparison to the classic power law in the adjacent lane scenario. This is expected since the classic power law model provided an initial best fit of the one adjacent lane-16kmh data set from which its parameters were derived. Further insight can be obtained by observing the RMSE averages and standard deviations for all the realizations. The proposed model outperforms the classic power law in the same lane scenario by .06dB, and the standard deviation is lower by .02dB. However, a lower RMSE is not indicative of better performance as seen in the classic power law for the two-lane scenario, where it performed on average with .03dB less of a best fit compared to the proposed model. The improved model includes the lane spacing and statistical variations due to vehicle movement which makes the model more versatile. Also of interest is that even though the classic power law performed better in the adjacent lane scenario, the mean was .28dB less than the proposed model. The two-ray ground reflection

Table 2.4: Simulation Results

Win Outcomes			
Scenario	Power Law	Proposed	Two-Ray
Single Lane	45.48%	54.52%	0%
Adjacent Lane	93.55%	6.45%	0%
Two-Lanes Over	47.84%	52.16%	0%
All	62.29%	37.71%	0%
RMSE Mean			
Scenario	Power Law	Proposed	Two-Ray
Single Lane	2.15dB	2.09dB	3.06dB
Adjacent Lane	1.32dB	1.60dB	2.39dB
Two-Lanes Over	1.45dB	1.48dB	3.19dB
RMSE Standard Deviation			
Scenario	Power Law	Proposed	Two-Ray
Single Lane	0.33dB	0.31dB	0.75dB
Adjacent Lane	0.13dB	0.14dB	0.27dB
Two-Lanes Over	0.06dB	0.22dB	0.28dB

model does not perform well in comparison to the other models.

2.5.4 Discussion

The dynamic experiment methodology could be improved to ensure that the correct distances are known at the time of SM packet reception. Both driver and equipment errors were present in this validation, due to drivers not being able to maintain a constant velocity during the entire capture and spurious delays between packet transmissions. These misalignments may have introduced an error into the performance analysis, especially since the difference between the classic power law and the proposed model is so small. However, upon closer inspection additional observations not dependent on the alignment accuracy can help show how the proposed model could be a better approach to channel modeling over the classic power law model.

To illustrate the differences between the models, Figure 2.5 plots one realization of

fitting for the 48kmh speed trial for each lane scenario. Up to 63m of separation distance is chosen for the plot for visual clarity. The two-ray ground reflection model performs poorly at predicting the data for separation distances greater than 15m. The two-ray model attempts to guess the RSS following undulating gains as the ground and LOS component add together at the receiver while the vehicles move, but the two-ray model does not capture additional gains/losses caused by diffraction over the structure of the vehicles as they move relative to each other. Furthermore, the two-ray model may not provide the best fit for separation distances less than 100m if the effective permittivity, ϵ_r, is not known. This is because within 100m of separation the reflection angle becomes steeper until the ground ray disappears from the receiver.

Observing the classic power law model, the RSS is predicted to follow the general trend of the received power, but lacks in tracking the peaks and valleys like the two-ray model. As an improvement, the proposed model be a mixture of the two models.

The proposed model attempts to capture undulating RSS gains, like the two-ray model, but maintains a general trend like the classic power law model. What is interesting about the proposed model is that though it has no physical input about the vehicles road configuration like the two-ray model, the proposed model can apparently capture the electromagnetic effects of constructive/deconstructive interference, and apparently at the correct dips and peaks like the two-ray model. What can be deduced from the outcomes of the Monte Carlo simulation, is that though the classic power law and proposed model are similar, on average the proposed model could predict the RSS better because of the additional degree of freedom provided by making the path loss exponent a random variable based on specific lane separations.

It is expected that the proposed model could be enhanced by also adjusting the model to perform better at the closer regions of less than 25m separation distance, where most the models often undershoot the actual outcome, except for the two-ray model. It is suspected that this boost happens when the vehicles hoods and roofs cause less diffraction of the

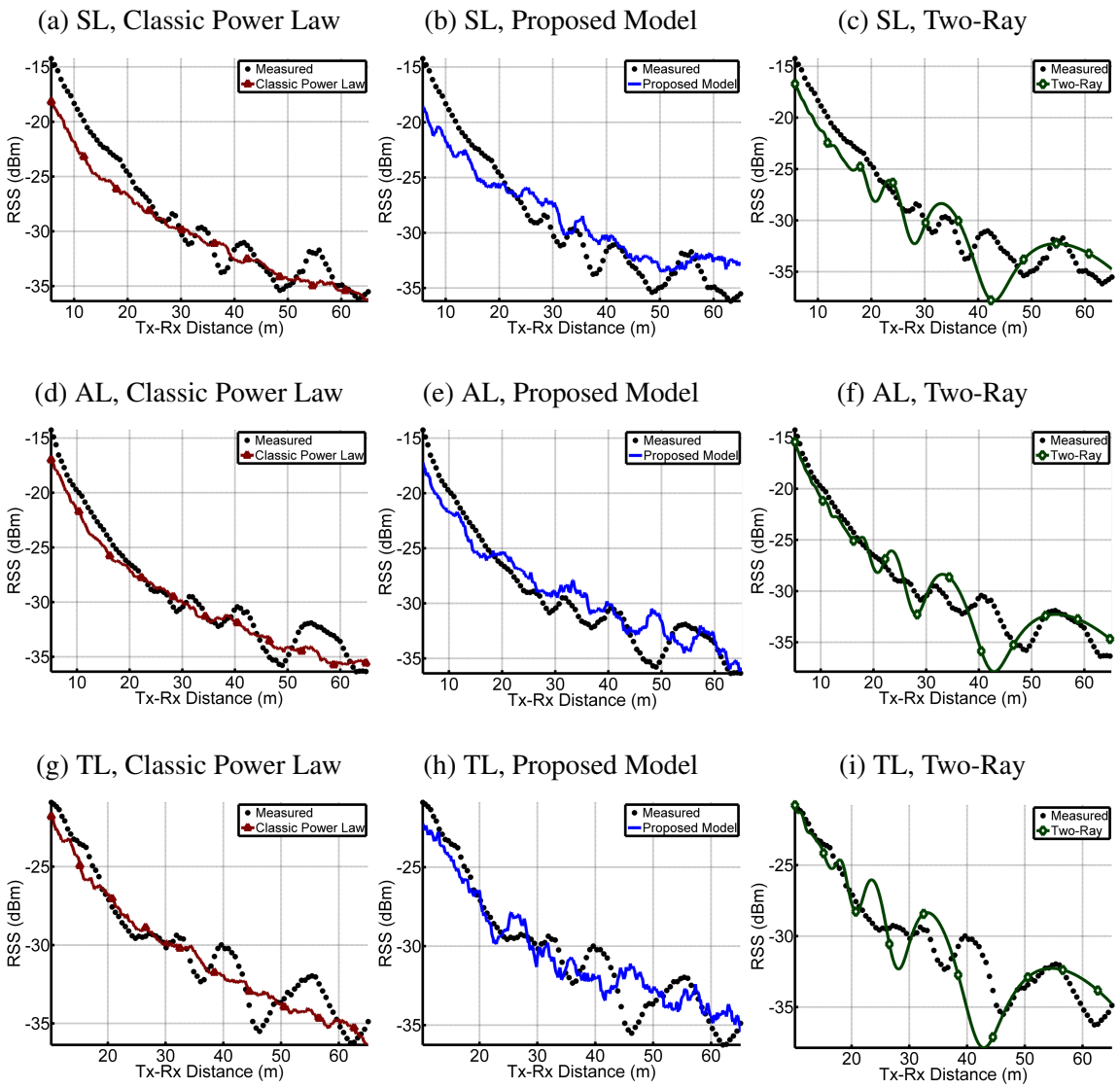

Figure 2.5: Results of dynamic measurement at 48kmh validation and comparison after applying a 25pt Moving Average Filter.

signal, as the vehicles pass each other, since the width of the roof is often much shorter than the length of the roof, thereby enabling a waveguide effect (i.e. strongest LOS) between the two vehicles.

2.6 Conclusion

The effects of lane separation and vehicle orientation (vehicle road configuration) are important for providing context to V2V collision avoidance. This chapter showed that different lane and vehicle orientations can affect how the RSS response appears at a V2V receiver. For a head-on collision, the response may be much different than that of a normal driving two-lane separation scenario. The improved model provided quantitative insight that the DSRC radio can discern vehicle road placement depending on the road configuration of the participating vehicles. This is enabled by the relative alignment of the vehicle bodies changing as vehicles travel in their respective lane trajectory. The improved channel model is only valid for LOS conditions with only two V2V equipped vehicles. It is moot in NLOS conditions to consider lane separation and orientation since it is a given that NLOS in the V2V context is typically due to the trajectory of an intersection (ignoring on-ramps, overpasses, and blind curves). For a generalized path loss model, the classic power law model is suffice though the effects of vehicle road configuration are lost. In the next chapter, a PHY-based collision avoidance technique using the RSSI trend is explored.

CHAPTER 3

AN RSSI COLLISION AVOIDANCE TECHNIQUE USING REAL V2V RADIOS

In this chapter a received signal strength indication (RSSI) collision avoidance technique is described in detail. The aspects of the method were first presented in [52] as a novel means of providing collision avoidance using smart antennas and the RSSI measurement which is a PHY metric provided by commercial off-the-shelf (COTS) V2V radios. It was the first validated use of the RSSI in V2V networks for directly predicting car collisions in both LOS and NLOS with a single omnidirectional antenna. This technique could be an *active* component in PHY-based collision avoidance, in that it could directly provide collision avoidance services by searching for trends indicative of a collision. Experimental observations of RSSI during collision and no-collision outcomes are reported to explain the prediction methodology which is rigorously tested through a simulation environment to assess the capability to perform detection. The technique does not use traditional RSS-distance estimation, fingerprinting, or cooperative methods, which depend heavily on *a priori* knowledge of path loss conditions. Instead, a decentralized approach identifies specific trends in RSSI indicative of a collision. All collision estimation can be made locally at the host vehicle receiver and detect over 35% more collisions compared to a more popular usage of RSSI, the RSS-distance method.

3.1 Background and Related Works: RSSI

This RSSI technique assumes all vehicles are equipped with a 5.9 GHz DSRC radio adhering to the WAVE-802.11p protocol stack broadcasting SMs at a beacon rate, f_{SM}. As discussed in the previous chapter, the 802.11 standard specifies that RSSI is to be measured from the preamble of received frames, but does not specify how to interpret RSSI or the maximum value. Due to this open definition, RSSI can function as a proxy to the

actual signal quality or strength. An RSSI value is typically a unit-less value on an arbitrary scale decided by the radio manufacturer. The key property of RSSI is that for both LOS and NLOS conditions, RSSI is inversely proportional to the separation distance between transmitter and receiver.

Methods using RSSI for locating wireless transmitters are extensively covered in the background literature for localizing users in static Wi-Fi sensor networks [53], but few investigations consider RSSI for providing collision avoidance in V2V. Gimnez et al. [54] explored using the RSSI of IEEE 802.15.4/ZigBee for detecting collisions between industrial equipment moving around a factory floor at slow speeds in a controlled environment. Altini et al. [55] considered using Bluetooth RSSI to help with localization of vehicles (though the awareness range was very short). Hisaka and Kamijo [56] developed a transmitter positioning algorithm for collision avoidance at intersections using the RSSI of ZigBee receivers at 2.4 GHz. The method was validated, but required four external sensors positioned around the vehicle with calibration prior to usage. The authors of [56] commented that at long distances their performance degraded. Since signals at 2.4 GHz can travel further than signals at 5.9 GHz for the same transmission power, it is not known if this method is transferrable to V2V using a SISO architecture.

For V2V collision avoidance the most accessible method using a SISO radio is to relate the RSS at the receiver to the distance from the transmitter by knowing *a priori* the channel path loss parameters [57], hereafter referred to as the: RSS-distance method. One reason why the RSS-distance method should not be considered as a collision avoidance strategy is that the V2V channel statistics are just as dynamic as the vehicle maneuvers themselves due to the constantly changing distribution of mobile and stationary scatterers across different environments. Though Chiaramonte & Branco [58] demonstrated the RSS-distance method specifically for predicting if an accident would occur in flying ad hoc networks, the path loss model was known *a priori*, which is more likely to be known in free flight between two nearby aerial vehicles. Without previous knowledge, cooperative RSS-distance

methods propose employing static infrastructure or other vehicles [59][60], but if multiple installations and vehicles are misbehaving or unavailable, then cooperative methods would be ineffective for providing collision avoidance. The RSS-distance method is typically not reliable in terrestrial V2V networks where the path loss is constantly changing as vehicles traverse different environments. SM error correcting methods based on the RSS-distance method often neglect that if the path loss is not exactly known, large errors could occur in the estimation. As presented by Alam et al. [61], a 0.2 variance in the expected path loss at a 50m separation distance could result in an estimation error of 57% or worse. Drivers with collision avoidance systems using the RSS-distance method would be susceptible to a low detection rate, especially in NLOS and at high speeds.

3.2 Experimentation

Experiments were conducted to obtain the RSSI response of COTS V2V radios while operating in the V2V context. The top three pre-crash scenarios [62] were considered for this RSSI analysis: NLOS Straight Crossing Path (no signal intersection), LOS Rear End (lead vehicle stopped), and LOS Opposite Direction. A pre-crash scenario can result in either a *collision* or *no-collision* outcome.

Two-Vehicle Study

An RSSI measurement campaign was conducted in a suburban environment while performing the pre-crash scenarios resulting in collision and no-collision outcomes. Two vehicles were equipped with a commercially available DSRC WAVE-802.11p radio and an omnidirectional whip antenna (9dBi) mounted on the center of the roofs. A collision was simulated by extending an antenna away from one vehicle using a pole[1], such that the antennas crossed each other to within 1m at full speed. Each vehicle travelled 56kmh transmitting

[1]Loss of the ground plane provided by the roof does not invalidate the RSSI capture since the RSSI technique does not rely on raw RSSI values to perform collision avoidance.

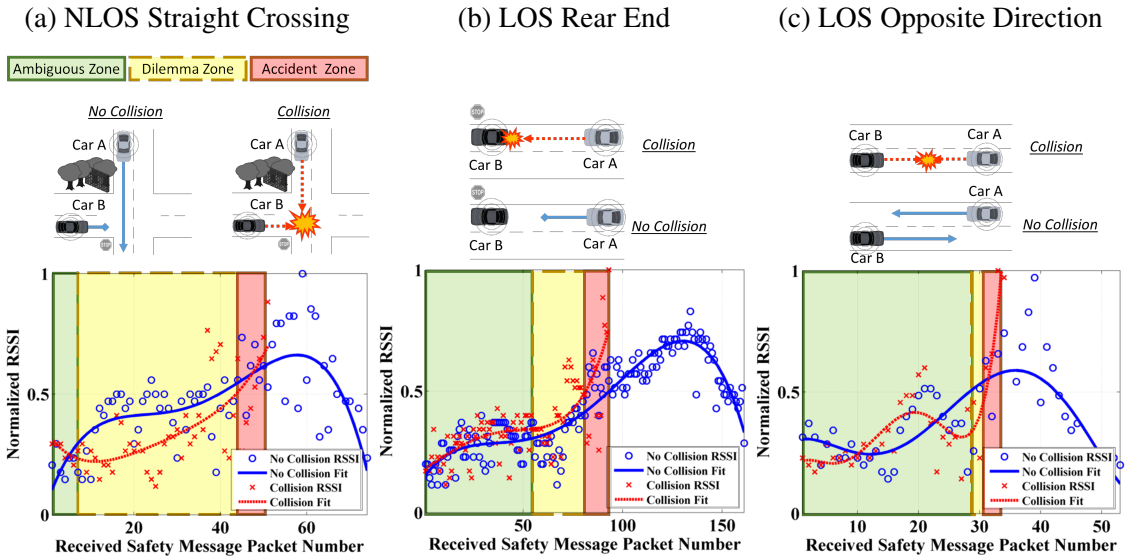

Figure 3.1: RSSI trends at Car A for collision (dashed, x's) and no-collision (solid, circles) outcomes in pre-crash scenarios.

only SMs at an f_{SM}=10 Hz while logging RSSI as packets were received. Figure 3.1 reveals the RSSI logged only by Car A[2] from both collision and no-collision outcomes. A trend line is added for clarity; the bottom x-axis indicates the received packet number.

The first observation is that using the raw RSSI value is not desirable for discerning between a collision and no-collision. The curvature/shape of the RSSI trend line reveals a more discernable characteristic across the pre-crash scenarios. Several zones of the collision trend lines are identified in Figure 3.1 as

- **Ambiguous Zone**: both collision and no-collision appear similar
- **Dilemma Zone**: collision and no-collision curves show differences
- **Accident Zone**: collision unavoidable

For each no-collision outcome, the dilemma zone captures the conservative driver behavior of Car A as a slower rate of increase towards the maximum RSSI value contrasted with the collision outcome in which the driver of Car A maintains a constant velocity, causing a

[2]Only RSSI plots for Car A are analyzed across all experiments.

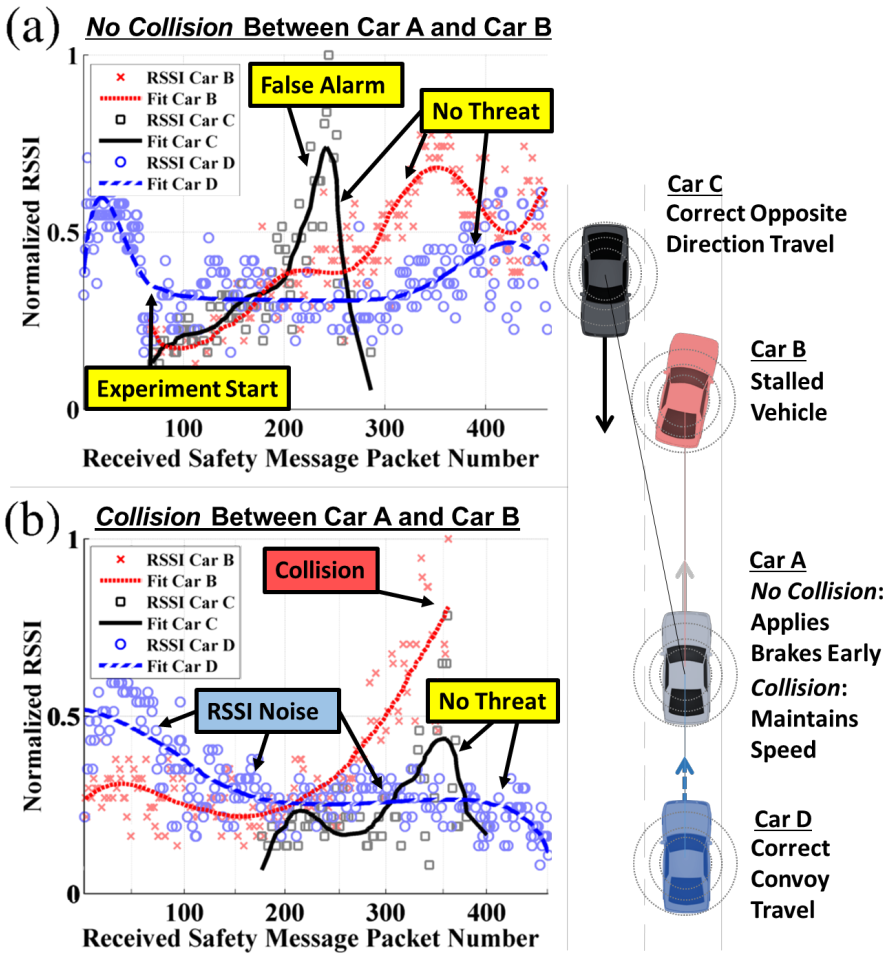

Figure 3.2: RSSI trends as recorded by Car A among multiple nodes for Rear End pre-crash scenario. If DOA is available, then RSSI values from Car C could be localized to the opposite lane to suppress a false alarm and reduce prediction complexity among multiple nodes.

faster rate of increase towards the maximum RSSI value. False alarms can arise in the ambiguous zone when Car A first begins receiving packets where a collision is unidentifiable from a no-collision outcome. A false alarm can also occur during the opposite direction travel, as seen in Figure 3.1c where the ambiguous zone is large and dilemma zone small. Because vehicles often travel in the opposite lane configuration, this source of false alarms was further investigated.

How DOA Can Reduce Passing Traffic False Alarms

The RSSI measurement campaign was expanded past the two-vehicle study to observe RSSI for multiple vehicles transmitting. Four vehicles were equipped with either a dome (6dBi) or whip (9dBi) omnidirectional antenna. Figure 3.2a depicts the experiment for no-collision and Figure 3.2b depicts the collision outcome. The Rear End pre-crash scenario between Car A and Car B is observed with one non-threating vehicle, Car D, following behind Car A in a convoy formation, while another non-threating vehicle, Car C, travels in the opposite direction in the opposite lane at a high speed.

Observing the trend line of Car B in both graphs of Figure 3.2 reveals the same collision vs. no-collision outcomes from Figure 3.1b. This is expected, but now a false alarm can be seen in Figure 3.2a caused by Car C. For the no-collision outcome, Car A applies the brakes early and slowly passes around Car B, whereas during the collision a spike between Car A and Car B is observed. Car D creates a flat/decreasing trend in the RSSI values, which can be interpreted as non-threatening. The false alarm in Figure 3.2a caused by Car C can be removed by assigning the DOA of received SM packets to each RSSI value, in which three streams of RSSI values would isolate the rear, front, and sides (opposite lane) of Car A. Using DOA to segment the region of reception reduces the prediction complexity from three to one, which would allow predicting an accident only for a specific region of Car A. Under NLOS, the packet reception could come from any angle, therefore an additional stream should consider the RSSI from all DOA regions to detect large spikes above the noise of RSSI from another non-threatening vehicle.

3.2.1 Predicting Accidents by Analyzing RSSI Trends

A novel method for predicting an automotive collision can be developed by measuring the curvature in the RSSI trend to indicate if a collision is likely. RSSI must be treated as a proxy to the received signal power, $P_r(t)$, to understand how vehicle dynamics affect what is observed in the RSSI trend.

Path Loss

RSSI values are affected primarily by large-scale fading discussed in the previous chapter, which is highly dependent on the path loss exponent (in LOS or NLOS) and channel variability. The signal strength at any given time can be written as

$$P_r(t) = P_t + G_t + G_r + PL(t) \tag{3.1}$$

where P_t is the transmit power in dBm, G_t and G_r are antenna gains in dBi, and $PL(t)$ is the time-dependent path loss in dB modeled as

$$PL(t) = PL_0 + 10\gamma log(\frac{c_0}{f_c 4\pi \frac{d(t)}{d_0}}) + X_\sigma(t), for\ \ d(t) >= d_0 \tag{3.2}$$

where c_0 is the speed of light, d_0 is a reference distance, PL_0 is the path loss at d_0, $d(t)$ is the time dependent separation distance between the receiver and transmitter, f_c is the carrier frequency, γ is the path loss exponent, and $X_\sigma(t)$ is a stationary random Gaussian process to model unpredictable shadowing effects defined as $X_\sigma(t) = X_\sigma \sim \mathcal{N}(0, \sigma^2)$, *for all* t where σ is the environment specific standard deviation. For low traffic densities, σ can be small, whereas higher traffic densities may exhibit larger variability in $P_r(t)$.

Relating RSSI to Vehicle Dynamics

As vehicles approach, a collision outcome will shape the RSSI trend with more positive curvature while a decreasing/negative curvature indicates no-collision. The vehicle dynamics affecting the curvature (i.e. RSSI trend "acceleration") is best observed by taking the 2nd derivative of (3.1) to obtain

$$\ddot{P}_r(t) = \frac{10\gamma(\dot{d}(t)^2 - d(t)\ddot{d}(t))}{d(t)^2} \tag{3.3}$$

By inspection of (3.3), the path loss exponent γ acts as a gain factor for the curvature, indicating that for high path loss environments such as NLOS, the curvature will increase

or decrease faster for the same separation distance. At large separation distances, $d(t)^2$ dominates to reduce the curvature to a small value. This is analogous to the ambiguous zones from Figure 3.1 where both collision and no-collision outcomes appear similar. In the dilemma zone where the distance between the vehicles is shorter, the sign of $\ddot{P}_r(t)$ is determined by the relative velocity between the vehicles, $\dot{d}(t)^2$, which dominates how fast the received signal power will increase to reveal either a positive curvature indicating a potential collision, or negative curvature indicating no-collision. Higher speeds will increase $\ddot{P}_r(t)$, but when vehicles brake as captured by the relative acceleration, $\ddot{d}(t)$, the curvature will decrease.

A set of criteria to predict a potential collision can now be developed. Any transmitter moving away from the receiver at a faster rate than the receiver is approaching poses no threat, indicated by $\ddot{P}_r(t) < 0$. If the curvature is observed to be $\ddot{P}_r(t) = 0$, such as when vehicles convoy at the same speed, a collision will not occur. Another observation is that $\ddot{P}_r(t) > 0$ does not always indicate that a collision will occur, such as during vehicle braking $\ddot{P}_r(t)$ will have decreasing positive values until $\dot{d}(t)^2 == d(t)\ddot{d}(t)$. Therefore, an additional condition must be placed on $\ddot{P}_r(t)$ to correctly predict a collision: if $\ddot{P}_r(t) > 0$ and is either increasing or remaining constant, a collision will occur. With this understanding of how $P_r(t)$ is affected by vehicle movements, the proposed RSSI collision avoidance algorithm can be defined.

3.2.2 RSSI Collision Prediction Method

The RSSI collision prediction is described in Figure 3.3. When a frame is received, the WAVE-802.11p communication stack measures the RSSI. It is assumed that the DOA, θ, is available for the received frame (acquired from a smart antenna or external DOA estimation system). Pictured are four virtual arrays: three for LOS processing depending on which antenna region the packet was received and one for NLOS processing which uses all RSSI values regardless of θ. With the DOA Selection operation, additional processing

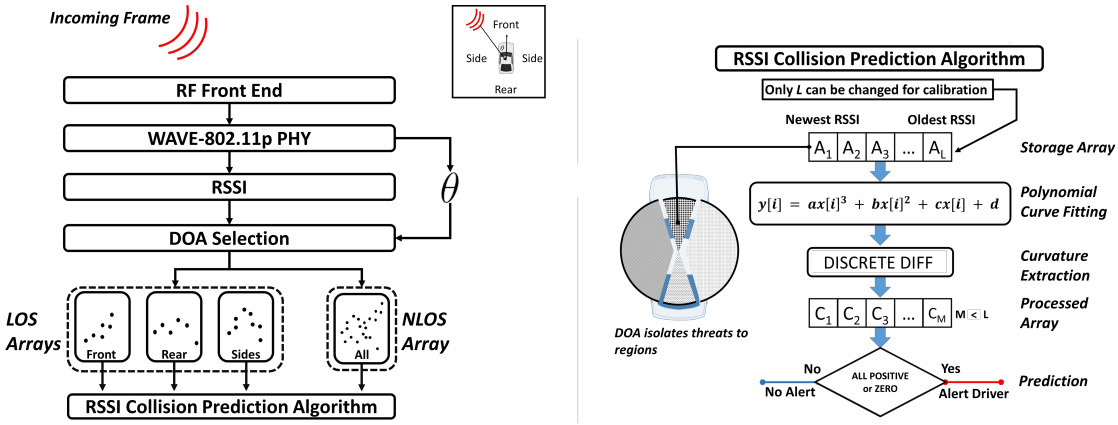

Figure 3.3: RSSI collision prediction method.

can be used to sort the RSSIs. Each array has a storage capacity of length L. If an array is full when a new frame is received, the end element is discarded and new value added to the front. Finally, the RSSI Collision Prediction Algorithm detailed in Algorithm 1 is performed on every array which receives a new RSSI value.

Algorithm 1 RSSI Collision Prediction Algorithm

if length(A) == L AND all(A)$\geq$ $RSSI_{on}$ **then**
  Fit curve, C, to RSSI values in A
  Take discrete derivative of C three times to obtain C'''
  if $C''' \geq 0$ **then**
    if $counter < DL$ **then**
      Pending alert, $counter^{++}$
    end if
  else
    No threat, $counter = 0$
  end if
  if $counter$ == DL **then**
    Alert driver
  end if
end if

All arrays for LOS and NLOS can have different $RSSI_{on}$, L, and DL for different host vehicle speeds.

When an array, A, is passed to Algorithm 1 every item in A must be greater than a threshold, $RSSI_{on}$. A curve, C, is then fit between the values of A to obtain a trend line. For implementation, a 3rd degree polynomial is chosen for fitting based on observations made from the no-collision outcomes of Figure 3.1 which show braking dynamics exhibit-

ing a 3rd degree polynomial shape. The curve C is then differentiated three times to extract measurements of curvature denoted by curvature array C'''. If every value in C''' is positive or zero, then a $counter$ variable is incremented and an alert is pending. As an alert is pending, a collision is predicted to occur if the $counter$ reaches a Detection Limit, DL.

There are three parameters which are adjustable for each array and can be adapted based on the host vehicle speed: $RSSI_{on}$ sets the RSSI value that the prediction system begins to operate, L sets the observation window length used to fit the curve C, and DL sets how many consecutive collision trends should be detected before an alert warns the driver. L primarily controls the accuracy of the detection rate, and DL controls the stability of the false alarm rate. $RSSI_{on}$, L, and DL should be set based on extensive calibration to ensure optimal performance.

3.3 Simulation

The method is evaluated for detection and false alarm rate then compared against the RSS-distance method. Using a custom MATLAB simulation environment, vehicle dynamics are simulated by a kinematic motion model with constant deceleration during braking. The separation distances between transmitter and receiver generated from the motion model are passed to a static classic power law path loss model eq. (3.1) to simulate the RSSI at the receiver. The improved channel model developed by the previous chapter was not included in the simulation because for numerous simulations trials, μ_γ and μ_α become the expected value of the channel being modelled, resulting in a classic power law model. Furthermore, the RSS-distance method depends on a constant path loss, therefore for strict comparison the improved channel model was not included. Though SM information need not be accurate, both the proposed prediction system and RSS-distance method require that a SM be received by the WAVE-802.11p communication stack to leverage the known transmit power as 20dBm [63]. To simulate real channel conditions which affect packet reception (such as multipath and mid-air frame collisions) empirical packet delivery models

for both LOS and NLOS conditions from [64][65] are utilized.

Modelling multiple vehicles within reception range is not included in the simulation because it is assumed that DOA is available to reduce complexity amongst multiple vehicles to just one vehicle. Only vehicles nearest to the host vehicle are considered. It is assumed that a SM transmitted by additional vehicles suffer from vehicle obstructions resulting in an RSSI value that does not pass the $RSSI_{on}$ parameter. Vehicle obstructions have been reported to reduce the SNR by as much as 20dB at only 10m [66], thus the performance is only tested for predicting a collision between the host vehicle and nearest LOS/NLOS threat.

The LOS Rear End and NLOS Straight Crossing Path (intersection) simulation scenarios are depicted in Figure 3.4. The Critical Decision Point, CDP, is the closest position of the receiver to the Impact Point that a driver can hard-brake without hitting the transmitter. Any RSSI value received after the CDP is unusable to the driver for avoiding a collision. The CDP is derived from the braking formula in [67], defined as $CDP = ImpactPoint - (.278sT_{react} + .039s^2/a_{hard})$ which includes the driver reaction time T_{react}, receiver speed s in kmh, and hard-deceleration rate a_{hard} in m/s^2. The dilemma zone is the range from when $RSSI_{on}$ is passed, up to the CDP. The dilemma zone varies depending on the value of T_{react} which is not the same for all drivers, therefore T_{react} is statistically modelled based on empirical studies of driver response time to braking for a yellow light [68].

To simulate a collision outcome, the receiver maintains a constant velocity up to the transmitter. To simulate a no-collision outcome the receiver brakes well in advance of the CDP with a soft-deceleration constant a_{soft}, such that the receiving vehicle slowly decelerates to stop at most 15m from the expected Impact Point. The DL could be reached at any point after $RSSI_{on}$ is passed, however, if DL is reached after the CDP then a collision is recorded as a missed alert.

A correct detection is recorded if the collision outcome is correctly predicted within the

dilemma zone. A false alarm is recorded if the algorithm incorrectly predicts a collision outcome within the dilemma zone when a collision would never occur. It is ideal to have a long dilemma zone; however, a trade-off exists where a long dilemma zone means more opportunities for false alarms. The prediction system parameters $RSSI_{on}$, L, and DL need to be selected to maximize the detection rate while minimizing the false alarm rate.

For the RSS-distance evaluation, the Crameŕ-Rao Lower Bound derived in [61] is utilized to obtain the estimation error. For RSS-distance to be reliable, the estimation error must converge before the CDP is reached. The simulation environment defines a convergence zone as the range from soft-brake CDP to hard-brake CDP, and an accident zone as the range from the hard-brake CDP to the expected Impact Point. For RSS-distance, a collision is missed if the average distance estimation within the convergence zone places the host vehicle behind the convergence zone. In a no-collision outcome, a false alarm occurs if the average distance estimation within the convergence zone places the host vehicle within the accident zone. There are no adjustable parameters for the RSS-distance method because it relies on knowing *a priori* the path loss variation.

3.4 Results

Two evaluations were executed in the simulation environment. Evaluation I determines an optimal L and DL that will achieve the highest detection rate and lowest false alarm rate for a given path loss model. With $RSSI_{on}$, LOS parameters, and NLOS parameters held constant, only σ statistically varies the RSSI values, while T_{react} also varies the length of the dilemma zone. Evaluation II uses the optimal L and DL to compare the performance of the proposed prediction system and RSS-distance method under varying path loss models. Simulation settings are highlighted in Table 3.1.

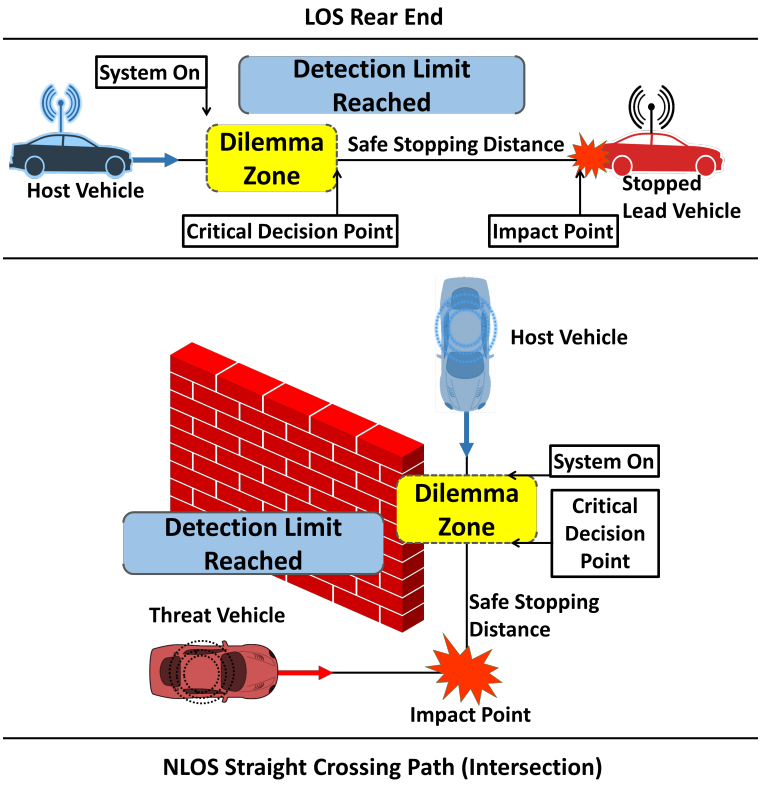

Figure 3.4: Simulation environment for LOS and NLOS scenarios

3.4.1 Obtaining the Optimal Selection of L and DL

Simulation results reveal the receiver operating characteristic (ROC) curves generated for LOS in Figure 3.5a and NLOS in Figure 3.5b. 1000 trials per combination of L and DL were tested at three different speeds. Ideally, a detection rate of 1 and false alarm rate of 0 is optimal, however, a binary decision must be made in which trade-offs between detection and false alarm rates occur primarily due to statistical variance of the channel which cannot always be known *a priori*.

The best performance for the method in LOS occurs at a speed of 64 kmh with a detection rate of 61% and false alarm rate of 30%. The slower speed has a higher false alarm rate due to a longer ambiguous zone. This suggests that for slow speeds, the prediction system should turn off since accidents at posted speeds less than 32 kmh rarely occur for LOS and NLOS [70]. This is controlled by setting $RSSI_{on}$ to a very high value at a host

Table 3.1: Simulation Settings

Evaluation I: Selecting L and DL	
Parameter	**Value**
Trials per L, DL Combination	1,000
Initial Separation Distance [63]	300m
Tested Speeds	32/64/96kmh
a_{hard}, a_{soft} [69]	7.4, $2m/s^2$
G_t, G_r, P_t [63]	9dBi, 9dBi, 20dBm
f_c, f_{SM} [63]	5.86GHz, 10Hz
LOS: γ, σ, PL_0 [44][45]	(1.77, 3.44dB, 47.53dB)
NLOS: γ, σ, PL_0 [44][45]	(2.25, 5.20dB, 46.69dB)
LOS: $RSSI_{on}$, NLOS: $RSSI_{on}$	-50dBm, -100dBm
T_{react} [68]	$\mathcal{N}$(.9723,.2569) seconds
Evaluation II: Proposed vs. RSS-Distance	
Parameter	**Value**
Simulation Runs	10
Trials per Run	10,000
$\gamma_{LOS}, \gamma_{NLOS}$ [44][45]	$\mathcal{N}$(1.77,.44), $\mathcal{N}$(2.25,.61)
$\sigma_{LOS}, \sigma_{NLOS}$ [44][45]	$\mathcal{N}$(3.44,1.11), $\mathcal{N}$(5.20,1.14)
PL_0^{LOS}, PL_0^{NLOS} [44][45]	$\mathcal{N}$(47.53,6.02), $\mathcal{N}$(46.69,8.05)

vehicle speed less than 32 kmh. The high-speed test performs similarly to the low speed test because the amount of RSSI values available are fewer, which decreases the size of the dilemma zone.

For NLOS, slow speeds have the best performance with 48% accuracy and a 37% false alarm rate. Because NLOS decreases the packet delivery probability, the prediction system must operate in a shorter dilemma zone to predict a collision. Thus, slow speeds help extend the dilemma zone and higher path loss helps detect collisions sooner, but a higher f_{SM} would obtain more RSSI samples for the same distance covered. If non-safety messages are assumed to be transmitted at 20dBm, then performance gains could be improved, but this would only be possible if the two vehicles both switched to the same SCH. With the optimal L and DL parameters selected the predicted system can now be tested in many different channel conditions.

(a) LOS Rear End (b) NLOS Straight Crossing Path (Intersection)

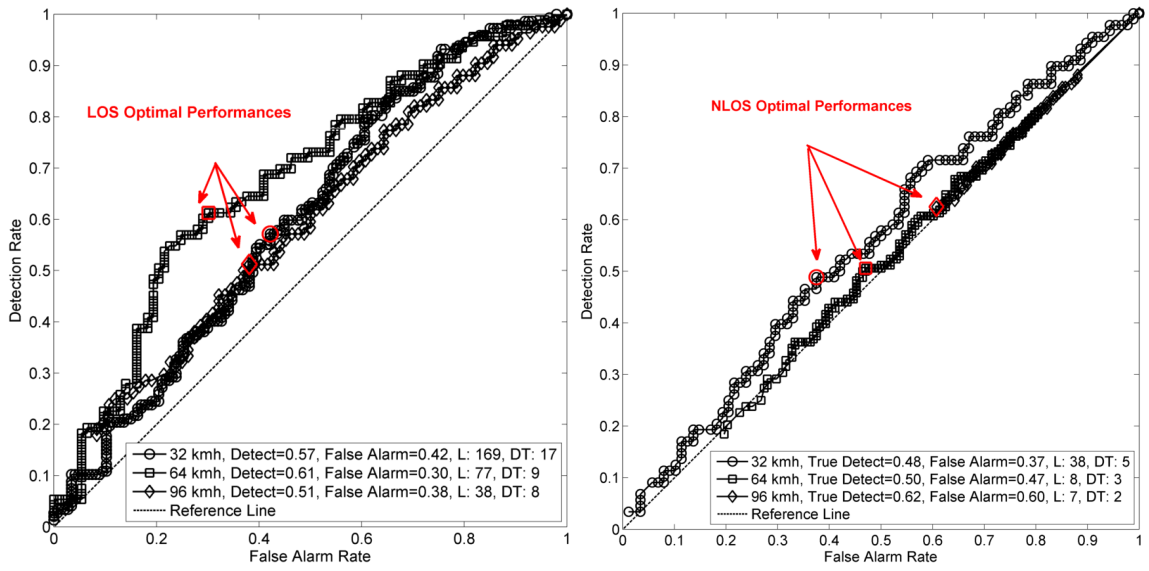

Figure 3.5: ROC curves for varying L and DL at different speeds

3.4.2 RSSI Technique vs. RSS-Distance Method

The RSSI trend method and RSS-distance method are evaluated under various channel conditions. This is accomplished by varying all path loss parameters for both LOS and NLOS based on a statistical distribution obtained from empirical studies [44][45]. The simulation executes 10 simulation runs of 10,000 channel realizations per run. The result for LOS is reported in Figure 3.6a and NLOS in Figure 3.6b.

For LOS and NLOS, the proposed prediction system sustains a detection rate above 45% across each speed test, out-performing the RSS-distance method by reliably predicting on average over 35% more collisions. However, the false alarm rate increases from the previous evaluation in which the path loss parameters only varied according the shadowing term. The RSS-distance method performs poorly in LOS with a very low detection rate. Though detection and false alarm rates are low for higher speeds, this is attributed to the f_{SM} not providing enough RSSI samples within the convergence zone, indicating again that a higher f_{SM} or better receiver architectures would be needed to provide more accurate predictions. In NLOS, the RSS-distance method suffers from very poor detection rates and

(a) LOS Rear End

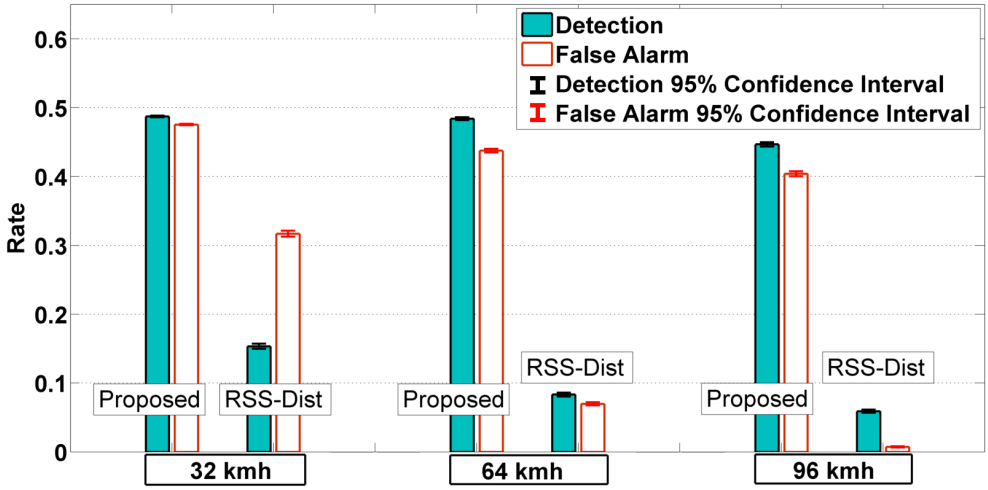

(b) NLOS Straight Crossing Path (Intersection)

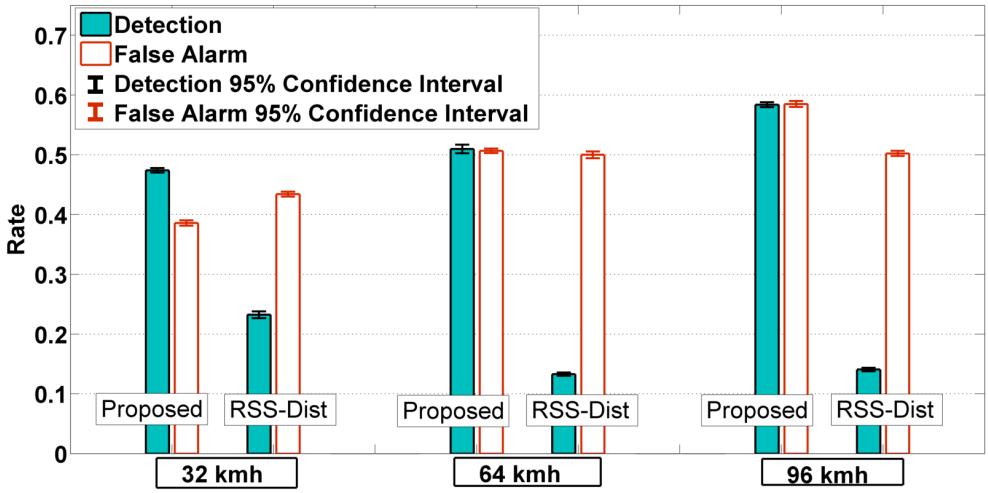

Figure 3.6: RSSI Technique vs. RSS-distance method

high false alarm rates. This is expected because the variance in the path loss exponent is higher for NLOS than for LOS, which severely affects the estimation error.

3.5 Discussion

The results suggest that the proposed prediction system needs further enhancement to reduce the false alarm rate and increase the detection rate for large variances in various channel conditions. Future investigations could apply different techniques for extracting the curvature, or vary $RSSI_{on}$ based on packet sampling once the prediction system is implemented in actual WAVE-802.11p radios. RSSI in vehicular environments is known to be noisy, but as revealed in this work and supported by empirical studies of the background literature, the inverse relationship between RSSI and separation distance is maintained even in NLOS. A high frame delivery rate could improve the performance from the results reported, which could be feasible for DSRC radios that take advantage of channel diversity through multipath. A lower f_{SM} could reduce the dilemma zone, but f_{SM} is expected to be broadcast at a rate of 10 Hz, especially during times of low vehicle density where driver speeds tend to increase. The technique performs better if the prediction system parameters $RSSI_{on}$, L, and DL are adapted based on the host vehicle speed, however, it was first claimed that the PHY-based techniques could function correctly even if the host vehicle is also misbehaving. It is assumed that GPS has a higher potential to be the source of misbehavior than the vehicle speedometer, therefore the host vehicle speed was more reliable. The detection rates reported through simulation could be replicated or improved in deployment if P_t, G_t, G_r, and γ remain constant as vehicles maneuver, these assumptions are addressed below.

- **Constant** P_t: Though WAVE 1609 standards allow for applications to vary the transmit power per packet, the proposed method only observes the RSSI of SM packets for two reasons. First, the SM is guaranteed f_{SM} transmission attempts per second, which provides RSSI values to the regardless if other network traffic is transmitted

or not. Second, due to the safety function of SMs, the broadcast level could be set at the highest transmission power allowed for the DSRC spectrum.

- **Constant G_t, G_r**: Antenna gains and placement could vary depending on the auto manufacturer. It is assumed that standardization and best practices may be adopted across the industry to ensure antenna properties fall within a common interoperability range.

- **Constant γ**: The RSSI technique in LOS assumes to predict for only a same lane collision. From the previous chapter in Table 2.4, the same lane γ distribution exhibited a small variance. Therefore, in a same lane collision scenario it is assumed the path loss exponent does not change drastically for separation distances less than the broadcast range. The path loss exponent could vary between LOS and NLOS conditions depending on the obstructions between the transmitter and receiver, but as reported in [45] the path loss exponent can be estimated as constant within some variance for distances much larger than the expected SM broadcast range. For rural settings, a two-ray path loss model is typically more appropriate to describe precise RSSI fluctuation, however, a linear trend can still be estimated for distances less than the expected SM broadcast range. The improved channel model from the previous chapter showed that for different lane separations the vehicle road configuration would change the RSS as the vehicles moved. In this sense, the channel model is an improvement, however, the classic power law model is still an overall good representation of the RSS for same lane conditions.

3.6 Conclusion

The capability of WAVE-802.11p based V2V networks to provide collision avoidance to drivers among misbehaving nodes by observing the RSSI is possible. Experimental observations demonstrated that RSSI trends during a collision can be different from RSSI trends

during a no-collision outcome. False alarms due to multiple vehicles can be reduced when paired with a DOA estimation system. The technique leverages the relationship between relative velocity and sharpness in the RSSI curvature. By checking the third derivative of C against zero, the prediction does not have to set a specific threshold to define what collision "curvature" is, which could vary for many different channel conditions. Also, the prediction does not have to track RSSI per transmitter (though the DOA selection block allows it). It only matters that a collision is being detected, not where the threat is coming from. The prediction methodology attempts to detect collision behavior in RSSI among varying channel conditions, whereas the traditional RSS-distance method attempts to guess the varying channel conditions which is more unreliable in practice for vehicular environments. This was supported in simulation as the proposed prediction system detected over 35% more collisions than the RSS-distance method. As a standalone system, the RSSI technique can provide acceptable collision avoidance, however, reliance on the DOA estimation to reduce false alarms requires a means of tracking the DOA estimation per SM. The next chapter presents a method for doing so using a SISO architecture.

CHAPTER 4
ENABLING SINGLE-CHANNEL DSRC RADIOS TO RECEIVE DOAE OBSERVATIONS FROM AN EXTERNAL OBSERVER

A PHY-based collision avoidance system must obtain the direction-of-arrival (DOA), θ, of a transmitter upon reception of a frame. This is accomplished by integrating an external DOA estimation (DOAE) system with the RF front end. Enabling per frame synchronization between DOAE and the DSRC radio could enable angular tracking of transmitters to assist in predicting collisions. Like the previous chapter, tracking θ over time for a transmitter could help the host receiver understand what the lane separation is between the two vehicles. In LOS, θ is the bearing angle between the receiving host vehicle and the transmitting vehicle, which would typically be obtained through GPS upon reception of a SM. However, if the transmitter is misbehaving then it is critical for the V2V radio have some other method of obtaining θ in azimuth and elevation to provide reliable collision avoidance services to drivers. For example, vehicles on overpasses could be mistaken as colliding with the vehicles below due to GPS inaccuracies or signal loss due to deep fades [71]. To enable a single-channel[1] DSRC radio to perform DOAE on an impinging signal is not trivial. The radio must estimate θ reliably amongst multipath impairments and recover the data within the signal. No related works have validated through experimentation a reliable DOAE method that can simultaneously perform data recovery in a doubly selective wireless channel using real devices. Multi-channel DSRC radios may be engineered to perform the DOAE operation if additional hardware and processing is integrated into the data recovery architecture, but this is impractical for the initial V2V deployment. Most first generation V2V radios must be deployed at an affordable price point using existing 802.11a chipsets which do not inherently contain DOAE functionality. Changing the underlying hardware

[1]Single-channel radios are synonymous with SISO architectures. Multi-channel radios are synonymous with MIMO architectures

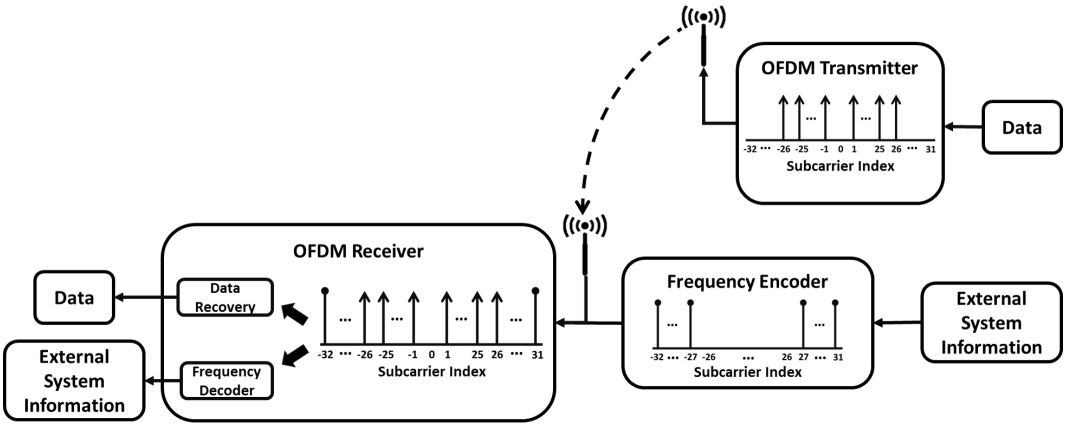

Figure 4.1: Frequency injection interfacing block diagram.

architecture could increase price, delay deployment, and cause unforeseen interoperability issues between radio manufacturers.

One realistic implementation of simultaneous data recovery and DOAE could be a dedicated DOAE system integrated with a V2V radio. In this configuration, the DOAE system measures θ on the arriving frame while the V2V radio recovers the data, but there is a major implementation hurdle: the estimate of θ must be passed to the V2V radio safety application reliably. A separate application programming interface (API) would need to be developed and maintained across multiple vendors and legacy vehicles, which could prove to be very difficult in practice. Second and third generation V2V radios may enter the market to add more functionality through software defined radio (SDR) technology.

With SDRs, additional flexibility can be integrated into the DSRC radio by a software update. Assuming a single-channel DSRC radio with software defined functionality, it may be possible to add a form of single-channel DOAE functionality that can simultaneously perform data recovery. Furthermore, this could be maintainable and accomplished securely using a new analogue interface first presented in [72] called frequency injection interfacing (FII). FII can be implemented with any OFDM communication system. This chapter implements FII into the PHY-based collision avoidance system by highlighting key aspects of DOAE in the V2V context.

4.1 Introduction

FII is described in Figure 4.1 where an external system or observer can communicate to an OFDM receiver through a frequency encoder by injecting additional frequency content into the received signal. Specifically, the null subcarriers at the edges (sidebands) of the OFDM waveform are energized to represent a binary code word which references a lookup table common to both the receiver PHY and encoder box. OFDM transmitters do not broadcast wireless energy in the channel sidebands to comply with regulatory policies. To avoid violating transmission laws, FII uses a direct connection between the frequency encoder and OFDM receiver. Because FII can deliver a unique code word per packet in real time, FII could potentially allow new applications and optimizations for OFDM systems without requiring a separate API. The FII method is validated through experimentation using SDRs, a GNU Radio IEEE 802.11 receiver, and a V2V radio. A packet reception rate above 90% proves FII operates transparently within existing OFDM architectures. Furthermore, the non-optimized implementation of FII presented in this chapter reveals that FII could reliably deliver up to 360 code words with 94% success and zero false alarms; which is a sufficient performance characteristic for DOAE applications that only require at most 360 code words, capturing 1° of resolution.

In OFDM, spectral efficiency is achieved by dividing the allocated bandwidth into equally spaced overlapping subcarriers. One OFDM symbol contains subcarriers allocated for data and channel estimation. Baseband modulation of the subcarriers is performed in the frequency domain. The OFDM process is implemented by an inverse fast Fourier transform to obtain the time-domain signal that is transmitted over air. However, not every subcarrier is utilized in OFDM systems. The middle subcarrier, direct current (DC), is left unenergized and unmodulated (null). The subcarriers on the edges of the waveform are also nulled to comply with spectral masks defined by radio transmission regulatory authorities [8]. This ensures that interference during wireless transmission into adjacent channels is reduced. Null subcarriers have been explored for several applications, primarily for assist-

ing in the data recovery operation. Typical usage of the null subcarriers includes carrier frequency offset estimation [73], peak average power ratio reduction [74], Doppler scale estimation [75], and channel estimation [76]. In contrast to previous investigations, FII employs the null subcarriers to deliver additional code words conveying information or control signals to OFDM receivers, without violating regulatory spectral masks.

In FII, an external system desires to deliver additional information to an OFDM receiver through a Frequency Encoder (FE) block. The external information is encoded by the FE as spectral energy at the frequencies of the null subcarriers. The frequency content in the null subcarriers are recovered by the physical layer of the receiving radio where a Frequency Decoder (FD) extracts the external information. Simultaneously, the data recovery operation remains unaffected by the introduction of FII.

FII could enable new applications and optimizations in OFDM networks where architectures are limited to single-channel RF front ends that could benefit from additional information as obtained by more dedicated observers or controllers. For example, reliable simultaneous data recovery and DOAE functionality using a single-channel receiver in a doubly selective fading environment is yet to be validated with V2V architectures due to implementation issues [77, Chapter 6]. Using a more reliable DOAE system externally, FII could provide per frame association with the LOS bearing angle between a receiving vehicle and a transmitter, available to all layers (e.g. phy, data, link, network, transport, application) of the radio architecture. Another application of FII could supply external control signals to the PHY such that the communication layers could be reconfigured *per frame* in real time. In summary, FII connects an external system to an OFDM radio without the need for an API by locally exploiting unused subcarriers in the OFDM spectrum. The added advantage is that implementation complexity can be lower than MIMO implementation, sustainable across multiple vendors, and incorporating FII doesn't affect the OFDM communication operation. It is assumed that there is perfect timing and synchronization between the FE and the OFDM receiver.

4.2 Background and Related Works: Direction Finding with Single-Channel Radios

An important measurement needed to provide collision avoidance is the relative location of a transmitting vehicle in azimuth and elevation. Determining the DOA of an incoming SM would provide this safety critical measurement regardless of GPS errors experienced. The limiting factor for performing DOA with existing V2V radios is that accurate DOA methods require a multi-channel RF front end. Currently, a V2V radio is a single-channel system employing affordable IEEE 802.11p chipsets (same architecture of IEEE 802.11a with different software configurations), which enables automakers to deploy V2V radios at production levels. Until multi-channel RF becomes affordable, a single-channel V2V radio is fundamentally restricted from using accurate DOA methods which can be found throughout existing literature [78].

A common component in most DOA methods (either single or multi-channel) is an antenna array. As a signal propagates over an antenna array, the DOA can be determined by exploiting the known phase, amplitude, frequency, and/or noise subspace projection induced by the spatial separation of the array elements. Signal processing is then applied to estimate the incident angle, however, the most accurate methods require each antenna element to have dedicated circuitry. This could possibly include a phase shifter, analog-to-digital converter (ADC), low-pass filter (LPF), and/or low-noise amplifier (LNA). Furthermore, existing methods assume a generalized context (e.g. the signal structure is not known in advance) among multiple impinging signals, which often requires a resource consuming search or optimization of the angle subspace.

It has not been well investigated how to (locally at the receiver) extract the relative azimuth and elevation of a sender in a V2V network. MIMO architectures currently leverage the spatial diversity between multiple receivers and antenna elements. Using MIMO architectures with smart antennas could allow for implementation of direction finding algorithms such as root-MUSIC as simulated by Warty et al. [79]. Yet, as discussed by Attia et al. [80], the implementation cost can be considered too high for any near-term pro-

duction deployment because most direction-finding algorithms require multiple receivers sampling at Nyquist-rates. Compressive sampling could be used to reduce those costs as demonstrated by Gurbuz et al. [81], but this technique has yet to be applied to V2V networks where additional antenna placement adds cost to the car manufacturers bottom line. Narrowband algorithms are most prevalent (e.g. ESPIRT, Root-MUSIC, Compressive Sampling); wideband methods based on the narrowband methods also exist.

Performing single-channel DOA in wireless networks has received attention due to the advantage of lower complexity in exchange for acceptable[2] performance at low SNRs. However, no existing work considers the impact of a single-channel DOA architecture on the data recovery performance of a communication system or performance in doubly selective channels like V2V.

Badawy et al. [82] describe a cross-correlation switched beam system using a 17-element antenna array which samples the incident signal omnidirectionally, then sequentially samples the signal by steering the beam of the antenna array to different azimuth sections. To estimate the DOA, the omnidirectionally sampled signal is cross-correlated with each of the signals captured by the individual beam patterns. The system performs well even in low SNR conditions, but assumes that the signal remains constant over the duration of the switching (the switching delay was not reported). Because of the sequential switching of the antenna beam pattern, data recovery may not be possible if the system scan time is not faster than the required sampling rate of the signal. Furthermore, long dwelling times per sector may capture several uncorrelated frames (e.g. with different modulated data) that are shorter than the dwell time as the beam is switched; potentially reducing this system performance in wideband communication systems operating in burst mode.

Ozaki et al. [83] present a single-channel switched beam system that compares the received power ratio between adjacent beam measurements of a 6-element ESPAR antenna. Due to symmetry, the antenna can only estimate within a 60° range unless physically ro-

[2]The term "acceptable" is used to express that single-channel DOA is inherently less accurate than more complex multi-channel DOA methods.

tated. This system is accurate at an SNR of 20dB, but performance below an SNR of 20dB was not reported. The authors reported this system requires a smaller dwell time than [82], but did not report on the total scan time. It is unclear whether this system would degrade the data recovery performance of a bursty wideband communication signal.

Gorcin and Arslan [84] suggest that DOA could be performed using sequential sampling of two omni-antennas that are physically moved on a platform and processed using the MUSIC algorithm. The LOS system performance for IEEE 802.11g was compared against the popular psuedo-doppler technique [85] in a static indoor environment to reveal that both methods perform reasonably well, above an SNR of 15dB. The authors state that the system requires additional mechanisms for physically adjusting the position of the two-antenna system. The effect on data recovery was not reported, though the experiment durations were 5.04 seconds each. The shortest switching time used was 10ms, which is much longer than the sampling period of IEEE 802.11 signals. Suggesting that this system and the psuedo-doppler technique may not be capable of performing data recovery.

Harter et al. [86][87] introduce a novel single-channel DOA system using a uniform circular array and a bank of digital phased locked loops (PLLs). By comparing phase offsets of the expected PLLs the method is extremely effective at low SNRs. However, additional circuitry not native to current radio architectures is required to estimate the phase shift at the device level. The system is also highly sensitive to the local oscillator (LO) offset between transmitter and receiver, which was reported as being difficult to mitigate without additional processing. Furthermore, switching time and dwell time are not reported; the system was only assessed on a continuous wave narrowband signal, which may not be applicable to wideband communication systems in burst mode.

In the V2V context, it is a safety critical issue for the DSRC radio to estimate θ while not degrading the data recovery operation. The previous works mentioned do not report the single-channel DOAE operation to be simultaneously performed with the data recovery operation.

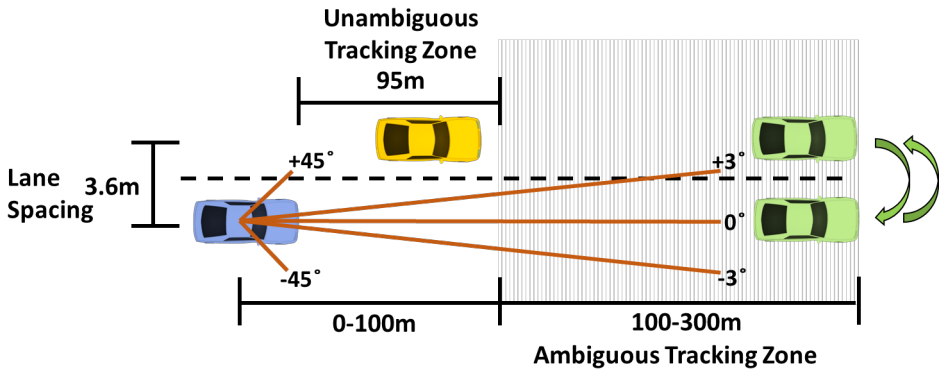

Figure 4.2: The V2V context exhibits an ambiguous DOA region for 100m to 300m appearing in-front of the vehicle.

4.2.1 DOAE in the V2V Context

Highly accurate MIMO DOA methods that employ MUSIC often attempt to estimate the DOA of multiple impinging unknown signals. In the single-channel DOAE system to be presented, the CSMA/CA mechanism of WAVE-802.11p is leveraged to estimate the bearing angle one transmitter at a time. Because CSMA/CA ensures a packet has the best chance of being received without a mid-air frame collision, it is assumed that packet collisions during DOA estimation in the V2V context between only two vehicles will rarely occur. For V2V networks, it is interesting to note that the expected vehicular road configuration of vehicles determines the required resolution for unambiguous DOA estimation, which can also reduce the design complexity of a DOAE system. As in Figure 4.2, a transmitter with a separation distance of 300m to 100m will fall between $\pm 3^{\circ}$ off 0°-heading (boresight), which is approximately 0° given that the lateral separation between centrally located roof mounted antennas is equal to the lane width (typically 3.6m). This angular ambiguity is experienced out to three lanes of separation and arises due to the short lane spacing of vehicles compared to large separation distances between them. This indicates that this ambiguity exists *regardless* of the DOAE method used in V2V networks, and that the SNR will more than likely be very high for distances less than 100m where DOAE would be meaningful. Practically, MIMO DOAE for DSRC radios may be unnecessary

for most road configurations that vehicles will operate in. For a separation distance within 100m, a DOA system that contributes to collision avoidance needs to only provide unambiguous estimation for angles 3° to 45° and -3° to -45°. Furthermore, a $\pm 45^\circ$ FOV equates to an angle tracking range of 95m for a lateral car spacing of one lane which suggests that identifying the lane of the approaching vehicle will be achievable early enough to assist in providing collision avoidance services.

4.3 FII System Description

The main components of the FII system are the FE mentioned previously which contains a lookup table of binary encoded decimal code words to send to the receiver and the FD which decodes the estimated code word using the same lookup table locally in the receiver. The FE is connected to the receiver through a coaxial cable where the antenna of the receiver is combined with the FE signal. Within the receiver, the OFDM physical layer contains an FD to recover the control word sent from the FE. Decoding occurs simultaneously with frame detection, such that additional parameters of the physical layer and up can be adjusted in real time prior to data recovery. The FII operation can be performed continuously per frame as packets[3] are being received from a transmitter. The advantage of FII, is that it allows OFDM radios to have frame-by-frame customization across all functional layers of the communication system by leveraging an external observer or controller without the need for a shared API.

4.3.1 Frequency Encoding

The code words are transmitted in the form of binary code words where each null subcarrier available represents a bit. A bit value of one is represented as non-zero energy at the location of a null subcarrier, and a bit value of zero is represented as no energy. A null subcarrier with non-zero energy is defined as ON, and a null subcarrier with no energy as

[3]Packets are made up of frames.

OFF. With this configuration, a lookup table common to both the FE and FD consists of $2^M - 1$ unique entries, where M is the number of allocated null subcarriers. The number of entries is minus one because the decimal value of 0 is considered the default state of the FII system being off. IEEE 802.11a/g/p provides up to 11 sideband subcarriers, allowing for 2047 code words.

Let a null subcarrier be defined as the signal

$$x_m(t) = A_m \cos(2\pi f_m t + \phi_m) \tag{4.1}$$

where the subscript m is the index of the null subcarrier where $m \in \{M-1, ..., 0\}$, A_m is the amplitude, f_m is the baseband frequency of the null subcarrier, and ϕ_m is the phase. The code word signal, $s(t)$, that is sent to the receiver can be described as a composite signal

$$s(t) = \frac{1}{M_{ON}} \sum_m A_m \cos(2\pi f_m t + \phi_m) \tag{4.2}$$

where M_{ON} is the number of null subcarriers that are ON. Observing eq. (4.1), a larger set of code words or continuous data streaming from an external observer could be obtained with existing digital modulation techniques performed directly on the null subcarriers. For the DOAE application detecting non-zero energy at a null subcarrier location for code word retrieval is sufficient. An example implementation of FII code words for a DOAE application with $M = 3$ can be seen in Table 4.1, where the first two columns would be entries in the tables common between the FE and FD operations.

4.3.2 Frequency Decoding

The FE delivers code words by the composite signal $s(t)$ and is decoded in the receiver after a Fourier transform operation. Let the arriving signal from a transmitter be $w(t)$, described as the OFDM model

$$w(t) = \sum_{k=-K}^{K} A_k e^{j2\pi f_k t} \tag{4.3}$$

Table 4.1: FII Implementation for a DOAE Application

DOAE	Decimal	Binary	ON Null Subcarrier Index (m)	OFDM Index (k)	s(t)
SYSTEM OFF	0	000	-	-	0
$-180°$	1	001	0	31	$A_{31}\cos(2\pi f_{31}t + \phi_{31})$
$-90°$	2	010	1	30	$A_{30}\cos(2\pi f_{30}t + \phi_{30})$
$0°$	3	011	1, 0	30, 31	$A_{30}\cos(2\pi f_{30}t + \phi_{30}) + A_{31}\cos(2\pi f_{31}t + \phi_{31})$
$+90°$	4	100	2	29	$A_{32}\cos(2\pi f_{32}t + \phi_{32})$
$+180°$	5	101	2, 0	29, 31	$A_{29}\cos(2\pi f_{29}t + \phi_{29}) + A_{31}\cos(2\pi f_{31}t + \phi_{31})$

where K is the largest non-zero subcarrier index symmetric about 0 Hz, A_k is the complex amplitude of the modulated baseband data, and f_k is the frequency of the subcarrier at OFDM index k, where $k \in \{-K, ..., -1, 1, ..., K\}$ contains both data and pilot subcarriers.

In this model, $w(t)$ contains frequency content in the range of k, and the code word signal $s(t)$ contains frequency content in the split range of m. Though $w(t)$ has spectrum allocated in the split range of m, the energy in these bands are set to be zero at the transmitter to comply with the spectrum mask as defined by the standards. Thus $s(t)$ and $w(t)$ do not share frequency content, however, subcarriers can undesirably crosstalk each other due to channel and device impairments.

Let the received signal $r(t)$ at the receiver antenna (prior to the RF chain) be

$$r(t) = h_{tx}(t) \star w(t) + s(t) + v(t) \tag{4.4}$$

where $h_{tx}(t)$ is the multipath channel response between transmitter and receiver, $(\star)$ is the convolution operator that applies the multipath channel over each tap (subcarrier), and $v(t)$ is Gaussian noise. Observing $r(t)$ in the frequency domain through the Fourier transform, $R = \mathcal{F}(r)$, the superposition of the code word spectrum with that of the data spectrum is

$$R = G_{loss}(H_{tx}W + H_{tx}^{ICI} + S + V) \tag{4.5}$$

where G_{loss} is the overall attenuation from FE to receiver, and H_{tx}^{ICI} represents the inter-carrier interference (ICI) that the channel introduces into the null subcarrier locations of $w(t)$ coming from the data and pilot subcarriers. It is assumed that S is unaltered by any multipath effects since the FE signal enters the RF front end by a direct coaxial connection.

Device impairments such as carrier frequency offset and sampling offset also introduce additional ICI across all subcarriers [88]. However, the FD only searches for energy content at the null subcarrier locations to signify a bit value of one, rather than measuring amplitude or phase modulation. Thus, the effects of ICI due to the multipath channel and RF front end offsets which affect bit detection can be mitigated through calibration (which increases the

SNR of the code word), without affecting the transmitted frame. Attenuation and system noise are considered to have the most significant impact on the code word recovery, and calibration to be described later can improve the system performance.

For a single OFDM symbol, a 64-point fast Fourier transform (FFT) highlights energy content at the allocated null subcarriers. The FD operation only searches for energy appearing in the null subcarrier indices M. Taking the power spectrum of the FFT output, the m-th null subcarrier that is ON can be detected as

$$\frac{|R_m|^2}{C} > \Lambda \tag{4.6}$$

where Λ is a threshold parameter to signify that a null subcarrier is either ON or OFF, and C is a value on the same order of magnitude as the numerator. The detection is based on a ratio rather than raw values. C could be a static value or the average noise level across data and pilot frequency bins when $w(t)$ is not present, defined as

$$P_{Noise} = \frac{1}{2K} \sum_{k=-K}^{K} |R_k|^2 \tag{4.7}$$

After detecting which null subcarriers are either ON or OFF, the code word is decoded and the reverse lookup table recovers the information sent from the external system.

4.4 FII Implementation

FII can be demonstrated using SDR technology which provides RF chain functionality in software. The implementation of FII is simple, but calibration must be performed to ensure system reliability. The concept of FII is validated by using two SDRs and a commercial off the shelf WAVE-802.11p radio operating at 5.9 GHz. The WAVE-802.11p radio is programmed to broadcast a 100-byte sized SM encoded with Binary Phase Shift Key (BPSK) modulation every 100ms which is typical for V2V operation.

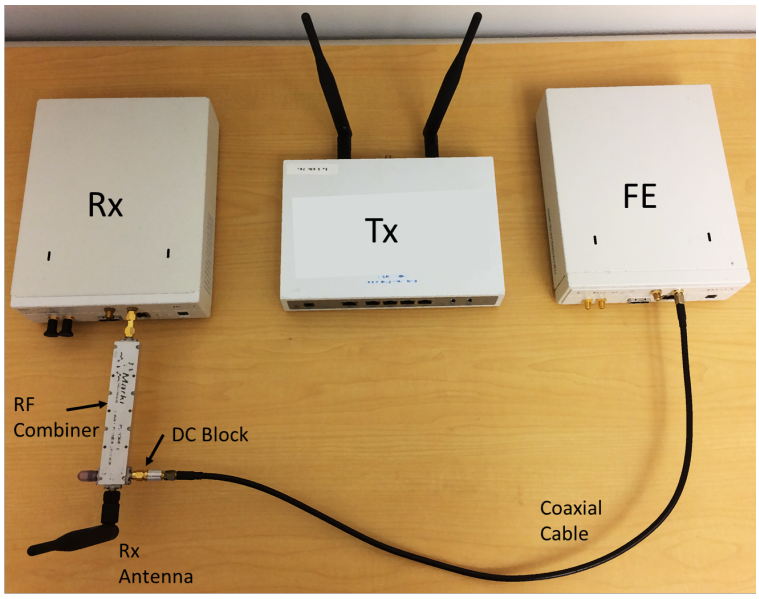

Figure 4.3: Equipment used for FII validation.

4.4.1 Hardware Configuration

As seen in Figure 4.3, one SDR functions as the OFDM Rx, the V2V radio as Tx, and the other SDR functions as the FE. The SDR acting as the FE is connected directly to Rx by a coaxial cable. A DC block is added to the signal path to reduce any DC bias caused by connecting the FE and Rx directly. The Rx antenna and FE coaxial cable are then connected to an RF combiner. This device sums the signal received from Tx with the code word signal from the FE, prior to entering the RF chain of Rx.

Though FII energizes null subcarriers beyond allowed spectral masks, the FE does not transmit wirelessly to Rx. Since the FE doesn't broadcast, the direct line configuration is what allows FII to use the null subcarriers for passing a code word to Rx, while still complying with spectral mask regulation. RF leakage may still occur locally, but the level of radiation should be negligible to other stations since only one DSRC radio will be equipped in vehicles behind the vehicle body. The radiation leakage near the RF ports of the FE and Rx would have to be extremely high to pass through the host vehicle interior and an adjacent vehicle interior to affect the adjacent vehicle DSRC radio. It is this novel configuration, using SDR technology enables the single-channel DSRC radio to leverage the null

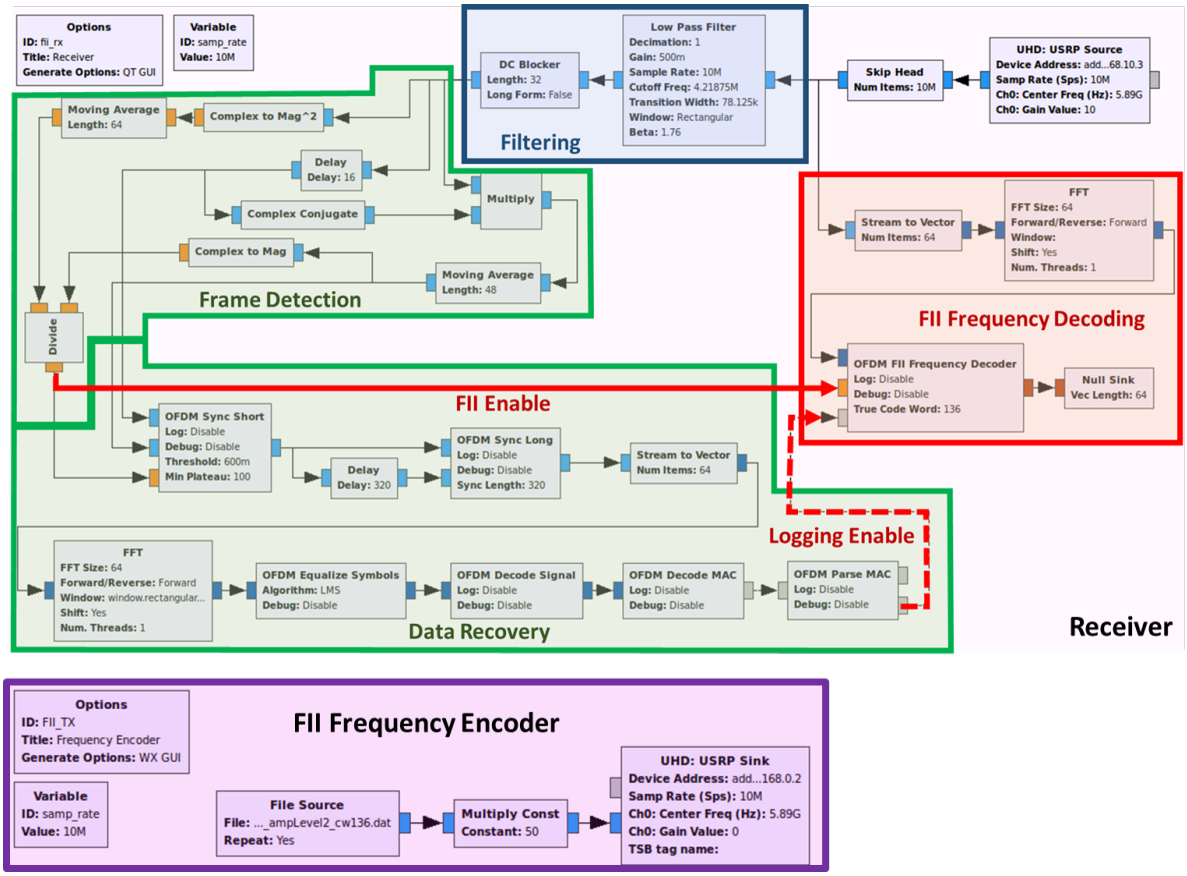

Figure 4.4: Frequency Injection Interfacing flow graphs for receiver and frequency encoder.

subcarriers for a DOAE application. Without the need for a third-party API, the FII method can provide a simple and robust interface between a DSRC receiver and an external DOAE system using a common lookup table between both FE and Rx.

4.4.2 Software Configuration

GNU Radio is used to perform complex baseband sample processing for the FII system and for simultaneously decoding IEEE 802.11p formatted safety messages from Tx. GNU Radio provides a graphical user interface to build flow graphs using drag-and-drop functional blocks of digital signal processing code. The flow graphs for the FE and receiver are shown in Figure 4.4. The FE repeatedly sends a 64-sample duration waveform, per the code word meant for delivery. In this configuration, the FE selects the file with the baseband code word waveform, then repeatedly sends the waveform until a new code word is selected. An

adjustable gain factor is multiplied to the code word to allow for calibration.

The GNU Radio IEEE 802.11a/g/p receiver from Bloessl et al. [89] was modified for the decoding operation at the physical layer of the radio. A custom block created for this prototype performs the detection operation from eq. (4.6). In Figure 4.4 the receiver flow graph is divided into four functional areas: Filtering, Frame Detection, Data Recovery, and FII Frequency Decoding Block.

Filtering

Prior to Frame Detection the added FE signal must be reduced using a low-pass filter along with the removal of any residual DC component. The filtered signal is then sent to the Frame Synchronization and Data Recovery operation from [89]. When a frame is detected, an enable signal is sent to the OFDM FII Frequency Decoding Block. The enable signal acts like a valve so that the FD is only performed during a single frame duration. This keeps the receiver from experiencing overflow due to operations that can be demanding for continuous real time processing. It is assumed that an external observer makes continuous observations, and that the FE begins sending the code word before frame detection. Prior to the enable signal, the FII Frequency Decoding Block continuously computes the noise power per eq. (4.7). For experimentation, a static value for the C parameter is used.

OFDM FII Frequency Decoding Block

Within this functional block a 64-point FFT is performed on the incoming data stream from the SDR. The OFDM FII Frequency Decoding block receives the output of the FFT, but waits until a frame is detected by the Frame Detection operation. Once a frame is detected, the code word decoding is performed by searching for the ON null subcarriers that satisfy eq. (4.6). Once the ON null subcarrier bins are identified, the decoder then calculates the estimated code word decimal value.

4.4.3 Calibration

Not every code word experiences the same spectral intensity, due to the constructive and destructive nature of adding frequency shifted sinusoids. Even if the resultant code word signal is normalized, the spectral content visible from the FFT will remain at the same relative levels to each other, for this reason calibration is required to improve the detection amongst noise. Figure 4.5 identifies discrete levels of spectrum amplitude for all code words created by $M = 11$ null subcarriers. Noticing the various intensities of spectrum content, the overall power level of every code word is adjusted so as not to overload the RF chain of the receiver. The FE sends signals at a 0dB RF power level (lowest setting on SDR), but the overall code word signal power remains adjustable for calibration. Adding this calibration factor, G_{cal}, into the receiver model from eq. (4.5) results in

$$R = G_{loss}(H_{tx}W + H_{tx}^{ICI} + G_{cal}S + V) \tag{4.8}$$

In addition to G_{cal}, a separate calibration must also be performed to set Λ (from eq. (4.6)). Consider the null subcarriers at the FFT edges which are known to experience attenuation due to the circular nature of the underlying discrete Fourier transform which requires an integer number of waveform periods. However, in practice this is not achievable unless synchronization is performed. To keep the processor burden light, code word synchronization is ignored, though if implemented this would benefit the performance of the system overall. Without synchronization, null subcarriers at the edges are more difficult to reliably detect than the null subcarriers closer to the data subcarriers. Windowing could be applied, but windowing is best accompanied with synchronization. Therefore G_{cal} is a practical alternative to increase the intensity of the ON edge null subcarriers above a well-defined Λ.

The threshold Λ can be determined experimentally by observing the average noise generated in the null subcarriers due to the FII system and the received $w(t)$. Doing so can completely reduce false alarms (i.e. a code word is detected when no code word is sent).

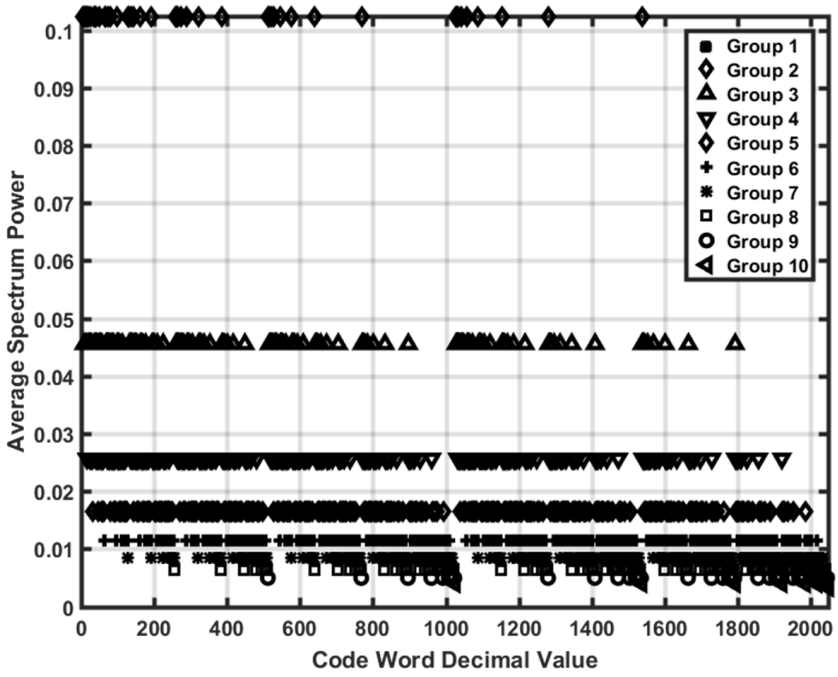

Figure 4.5: Average spectrum power varies depending on the code word, thus calibration is needed. (For M=11, the plot shows 9 discrete levels, however, for clarity the 10th level located at .4096 is omitted.)

Another important reason for calibration is so that the Frame Detection operation doesn't experience false alarms. For OFDM based 802.11 receivers, frame detection is often performed using a time domain autocorrelation operation. The FE could potentially send a code word waveform that exhibits high autocorrelation if the duration is long enough. Because of this, G_{cal} is also set to decrease false frame detections which can overload the incumbent receiver operation.

In summary, the first calibration is to reduce false alarms for both Frame Detection and FD by observing the best Λ when no signal is sent. The next calibration happens per code word to adjust G_{cal} such that the packet reception performance of the data recovery operation remains unaffected and code word estimation performance is maximized. After all calibrations are performed, an output of the complete FII system during real time operation can be viewed in Figure 4.6. The FD operation detects the correct null subcarrier bin that satisfies the threshold, and the data recovery operation remains unaffected since null subcarriers are ignored.

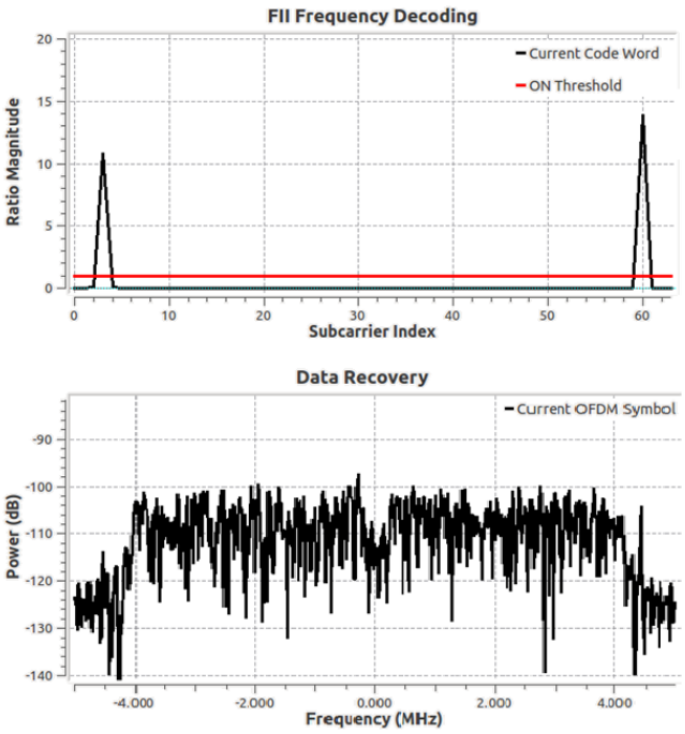

Figure 4.6: Screenshot of FD output (top) and data signal after frame detection and synchronization (bottom) for code word: 136 (i.e. binary 00010001000).

4.5 Experimentation

For experimentation, Tx is placed 3.45m away indoors from the Rx and FE with a direct LOS. The FE continuously sends a code word, while Tx broadcasts SM packets at 10dbm. Tx sends a sequential packet number (modulo 127), with every broadcast. If a packet is correctly recovered by the receiver, this sequential packet number is also retrieved, otherwise Rx will drop the packet because of the CRC32 not being valid.

4.5.1 Methodology

The packet reception rate (PRR) is calculated for the first 100 packets and the code word detection rate (CWDR) is also measured. These two metrics are sufficient to characterize the system since calibration completely removes code word false alarms and frame detection false alarms. The flow graph of the receiver from Figure 4.4, shows the logging enable signal between the Data Recovery and FD operation as a dashed line. When the

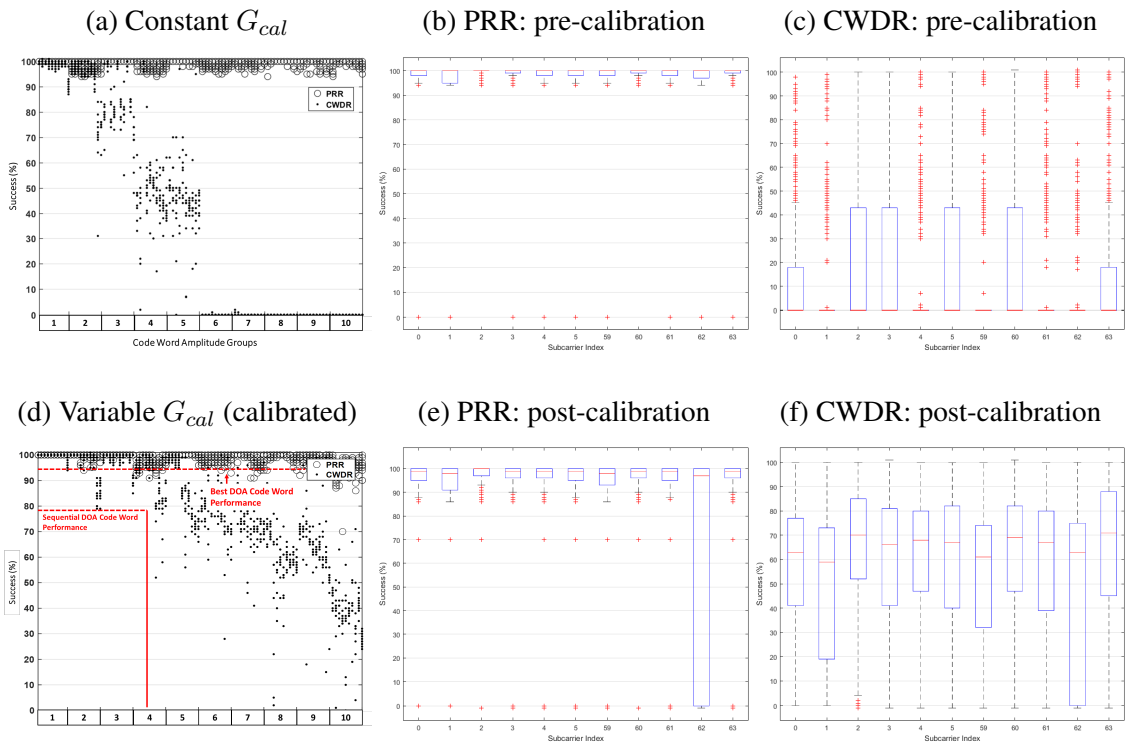

Figure 4.7: Results of PRR and CWDR success rates for uniformly selected code words from 10 different amplitude levels. (a) Constant G_{cal}; (b) PRR per null subcarrier with constant G_{cal}; (c) CWDR per null subcarrier with constant G_{cal}; (d) Calibrated G_{cal} with DOA code word performances highlighted; (e) PRR per null subcarrier with calibrated G_{cal}; (f) CWDR per null subcarrier with calibrated G_{cal}.

Data Recovery operation correctly receives the first packet, a start message is sent to the OFDM FII Frequency Decoding block. The FD block then begins comparing the estimated code word value to the true code word value until a packet number greater than a hundred is received. It is not intended to conduct a test for every code word in the lookup table, instead ten code words are uniformly selected at random from each of the ten amplitude levels from Figure 4.5. Though a test set of only 100 code words is used to validate the FII method, 10 data points for *each* code word under test are obtained. Also, the experiments are first performed with a constant G_{cal} then (if needed) with a calibrated G_{cal} that is tuned manually for code words which performed poorly with the original G_{cal}. Upon finishing each trial, over 1800 data points are manually obtained to validate the FII method for SM packets. A DOAE external observer is not used for this prototype validation, however, it

can be said with confidence that 360 code words with the highest average spectrum power is sufficient for reliable DOAE delivery per frame to the DSRC front end.

4.5.2 Results

Because of the asynchronous message passing between the data recovery operation and the FD block, the CWDR value may represent a nominal value within ± 4 percentage points of error. Comparing Figure 4.7a to Figure 4.7d, the improvement due to calibration is noticeable across all code word amplitude groups identified from Figure 4.5. The PRR remains above 90% across all code words tested, with some data recovery performance degradation in the 10th (smallest) code word amplitude. This is because the G_{cal} is high enough such that the low-pass filter couldn't remove the large spectral influence from the FE signal prior to Data Recovery. One interesting aspect is the variable performance of the code words that contain more ON null subcarriers (i.e. more entropy), see Figure 4.5. If the DOA code words were sequential from groups 1 through parts of 4, the system could deliver at worst 360 code words with 79% reliability. If the DOA code words used only the 360 most reliable code words across all groups, the unoptimized performance would be at an impressive 94% reliability.

To gain insight into this variation, Figure 4.7(b)(c)(e)(d) all reflect the individual performances of each of the null subcarriers tested. Pre-calibration, nearly every subcarrier provides a very high PRR and an unfavorable CWDR. However, post-calibration the performance improves greatly, with a slight performance hit affecting the PRR. The most severe performance degradation occurs in null subcarrier #62, as the spread of the success rate is exceptionally large. This could be due to unforeseen intermodulation due to the mixing of the signals. The other subcarriers remain at a steady performance above 90%, which for the validation set-up is an acceptable PRR, proving that the addition of the FII method into existing OFDM systems is transparent. Without FII the PRR is generally above 90%.

The CWDR performance post-calibration improves across all subcarriers, however, it

is observable that null subcarrier #1 and #62 perform the worst. This is due to the lack of integer value periods reliably entering the FFT. Code words with ON null subcarriers at the edges experience fluctuating amplitudes above and below Λ. As discussed previously, synchronization and windowing could improve this, but for validation purposes the FII system performance for 2047 unique code words is expected to be 67%, which functions well considering the system remained in continuous operation for the duration of each data point. For the DOA performance, at least a 94% code word delivery success rate can be expected even without synchronization and windowing.

4.6 Conclusion

A novel method for delivering external information to OFDM receivers using the null subcarriers was validated. A direct-in configuration with SDR technology demonstrates that the null subcarriers in the OFDM spectrum can be used to deliver binary code words in the form of an analogue signal, which can reliably be detected by the DSRC PHY. The advantage of the system is twofold: 1) an external observer can provide additional information to application layers directly through the radio front end with an expected low complexity, 2) the radio front end can be customized per incoming frame in real time by an external system without requiring an API. With FII in the V2V context, it is possible to enable single-channel DSRC radios to leverage the DOAE functionality of a more robust direction finding observer. The implementation can be cheap and effective, while providing further capability to leverage additional sensors on an autonomous vehicle. There are numerous ways in which this method could optimize V2V and generic OFDM systems to generate new applications never previously considered for SISO or MIMO OFDM radios. For the RSSI PHY-based collision avoidance system, reliably having access to θ measurement would be necessary for enhancing the reliability of the technique.

This concludes the discussion on the RSSI with DOA techniques, which suffers from variability in the measurement. The rest of the document now explores a more reliable

observation through exploiting the Doppler effect.

CHAPTER 5
COLLISION PREDICTION THEORY USING THE DOPPLER DOMAIN IN V2V NETWORKS

Shifting from RSSI and DOA, the attention now focuses on the Doppler phenomenon. The Doppler phenomenon occurs while moving vehicles communicate with each other. The effects of this shift in frequency (that are observable to a DSRC receiver) can be exploited through signal processing to provide 360° awareness. Prior to presenting the PHY-based collision avoidance Doppler techniques, this chapter presents the underlying motivation for predicting collisions using Doppler shift. Collision theory using the Doppler effect is discussed for application in the V2V context through the Doppler domain representation (i.e. time vs. Doppler frequency). Doppler domain analysis is the temporal tracking of the frequency offset from the center carrier due to relative movement. Analysis in the Doppler domain provides insight into the transmitter/receiver dynamics. Doppler spreading is typically viewed as a channel impairment to the IEEE 802.11p waveform. This chapter presents a new paradigm for V2V networks by exploiting the Doppler shift for its capability to predict vehicular collisions[1]. Nomenclature for this chapter and subsequent chapters can be found in Table 5.1.

[1]This chapter does not present a collision avoidance technique, but provides the motivation for the Doppler collision avoidance techniques.

Table 5.1: Doppler Collision Avoidance Model Nomenclature

$\boldsymbol{C_{Rx}}$: Receiving car (host)	$\boldsymbol{S_{Tx}}$: Speed of C_{Tx}
$\boldsymbol{C_{Tx}}$: Broadcasting car	$\boldsymbol{S_{Rx}}$: Speed of C_{Rx}
$\boldsymbol{h_{Tx}}$: Heading of C_{Tx}	$\vec{\boldsymbol{V}}_{\boldsymbol{Rx}}$: Projection of C_{Rx} velocity onto θ
$\boldsymbol{h_{Rx}}$: Heading of C_{Rx}	$\vec{\boldsymbol{V}}_{\boldsymbol{Tx}}$: Projection of C_{Tx} velocity onto θ
$\boldsymbol{\theta}$: Bearing angle from h_{Rx} to C_{Tx}	$\vec{\boldsymbol{V}}$: Relative velocity between C_{Rx} and C_{Tx}
$\boldsymbol{\psi}$: Relative angle from h_{Tx} to θ	$\boldsymbol{p_c}$: Potential collision point
	$\boldsymbol{d_{LOS}}$: Line-of-sight distance from C_{Rx} to C_{Tx}

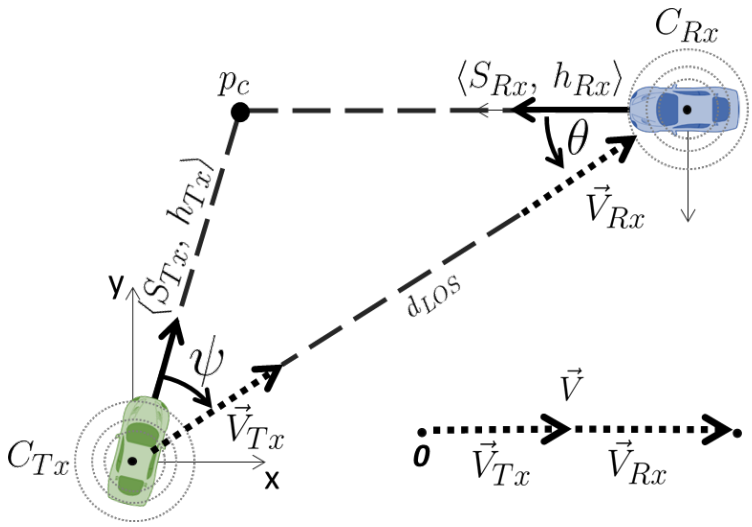

Figure 5.1: Illustration of car dynamics which lead to a collision.

5.1 Introduction

Car velocity is formed of two components operating in independent dimensions: speed and direction (heading). Knowing only the relative velocity between two cars is sufficient for indicating if a collision is likely. This is the basis for all collisions between two objects as defined by classical physics regardless of the choice of the reference frame [90]. For any collision between two cars, Axiom 1 holds:

Axiom 1. ***Unavoidable Car Collision****: If the relative velocity between two cars is positive non-decreasing and the direction (or projection) of their respective velocity vectors remain aligned within some range of the bearing angle formed between the two cars: a collision will occur.*

Observing Figure 5.1 provides an illustration of Axiom 1. If C_{Rx} could track $\vec{V}$ for the duration of the communication link, then a collision could be predicted within adequate time for an on-board autonomous system or driver to react. Axiom 1 is the primary motivation for the Doppler techniques in the PHY-based collision avoidance method presented in this dissertation. As participants in a V2V network maneuver, an accident could be predicted with advanced notice by observing the RF Doppler phenomenon occurring between two vehicles.

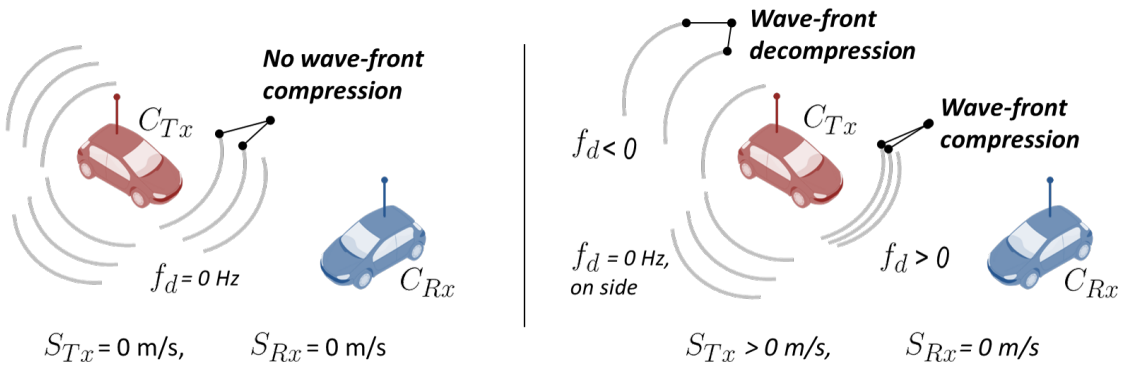

Figure 5.2: The Doppler phenomenon for parked vehicles (left) and moving transmitter (right).

To apply Axiom 1 in the V2V context, the Doppler phenomenon between two V2V equipped cars serves as a proxy to the relative velocity dynamics. Similarly, from chapter 3, RSSI was described as a proxy to RSS which could extract vehicle dynamics. The analogous Doppler shift exploit seeks to do the same. A method accomplishing this was first presented for V2V in [91], which attempted to leverage Axiom 1 to predict a head-on collision by observing the dynamics of the theoretical LOS Doppler shift. Aspects of [91] relevant to this dissertation work are discussed in this chapter.

5.2 The Doppler Effect

The Doppler effect is a phenomenon that signals either transmitted or received from a moving vehicle experience and best illustrated by Figure 5.2. As C_{Tx} moves relative to C_{Rx}, the received carrier signal containing a SM is either compressed or expanded. When the carrier frequency, f_o, of the transmitted signal is received at the RF front end of C_{Rx}, the received carrier frequency is, $f_r = f_o \pm f_d$. The offset is due to the Doppler shift, f_d. The value of f_d in Hertz depends on several factors as described by the Doppler shift equation (5.1), where the carrier wavelength is λ and both transceivers are on the same elevation plane.

$$f_d = \frac{S_{Rx}\cos(\theta) + S_{Tx}\cos(\psi)}{\lambda} \tag{5.1}$$

5.2.1 Small-Scale System Model

To characterize the effect of the Doppler shift on the OFDM waveform it is assumed that C_{Tx} and C_{Rx} are approaching each other on a flat two-lane road traveling in opposite directions. For now, the NLOS Doppler contributions are considered negligible[2] compared to the specular LOS path containing the full $\vec{V}$ between the vehicles. It is also assumed that there are no mid-air frame collisions due to CSMA/CA mechanisms.

Small-Scale Doppler Channel Model

Consider the short training symbol of the preamble from Figure 1.3 to be modelled as

$$x_{STS}(t) = \sum_{k=-24}^{24} A_k cos(2\pi f_k + \varphi_k) \tag{5.2}$$

for associated amplitudes A_k, sub-carrier frequencies f_k, and phases φ_k where k (incremented by four) is the sub-carrier index. The received signal can be modeled as passing through a Rician fading channel $R_f(t)$ in additive white Gaussian noise (AWGN) $n(t)$ with propagation delay t_{LOS} through the shortest LOS path as

$$r_{STS}(t) = x_{STS}(t - t_{LOS}) \star R_f(t) + n(t) \tag{5.3}$$

where $n \sim N(\mu_n, \sigma_n)$ with μ_n as the mean value of the noise, and σ_n is the noise variance. Multipath effects in (5.3) are included for completeness, but are not required for understanding the underlying principles of Doppler for collision avoidance. The realization of $R_f(t)$ is Rician distributed per the *pdf* [92]

$$Rice(q|K, P_r) = \frac{2q(K+1)}{P_r} e^{-K + \frac{(-Kq^2 - Kq^2)}{P_r}} I_0 \left(2q\sqrt{\frac{K^2 + K}{P_r}} \right), q \geq 0 \tag{5.4}$$

[2]Time-domain spreading still occurs due to multipath, however, to explain the concept of Doppler domain collision avoidance it is assumed that the Doppler spread due to NLOS paths are not as prominent as the LOS contribution for affecting f_o. In the next chapter the NLOS paths will play an important role.

where

$$K = \frac{s^2}{2\sigma^2} \tag{5.5}$$

and

$$P_r = s^2 + 2\sigma^2 \tag{5.6}$$

In (5.6), $2\sigma^2$ is the average power level in a scattered component, s^2 is the average power in the LOS component, P_r is the average received power due to fading from eq. (3.1), in (5.5) K is the ratio of the LOS power to all NLOS power, and $I_0(\cdot)$ is the 1st kind 0th order modified Bessel function [92].

5.2.2 Measuring Doppler Shift in OFDM

With device impairments, eq. (5.3) can also be represented as

$$r_{STS}(t) = \sum_{k=-24}^{24} A_k e^{-j2\pi(f_k \pm f_{CFO} \pm f_d^k \pm f_{SO}^k)t + \varphi_k} \tag{5.7}$$

where f_{CFO} is the offset due to local oscillator (LO) mismatch between devices, f_{SO}^k is the sampling offset (SO) due to the ADC inaccuracy which typically uses the same LO, f_d^k is the Doppler shift that affects each kth sub-carrier from its known center frequency f_k, and A_k and φ_k are the final amplitude and phase sub-carrier responses due to all dispersion caused by the multipath channel and device impairments.

Observing the received signal in the frequency domain in Figure 5.3 displays all the frequency shifts experienced per sub-carrier across each short training symbol. Modern recovery techniques are sufficient for locking onto the carrier frequency offset (CFO) induced by LO drift between incoherent DSRC radios [93], but the CFO correction can also remove the effects of the Doppler. The effect of Doppler shift in V2V is small compared to the amount of offset due to the CFO. Thus, the measurement of f_d is difficult to accomplish after the CFO correction. After the CFO correction and synchronization, the signal will still experience an offset due to the residual Doppler effect, $f_d^{Residual}$, residual local offset

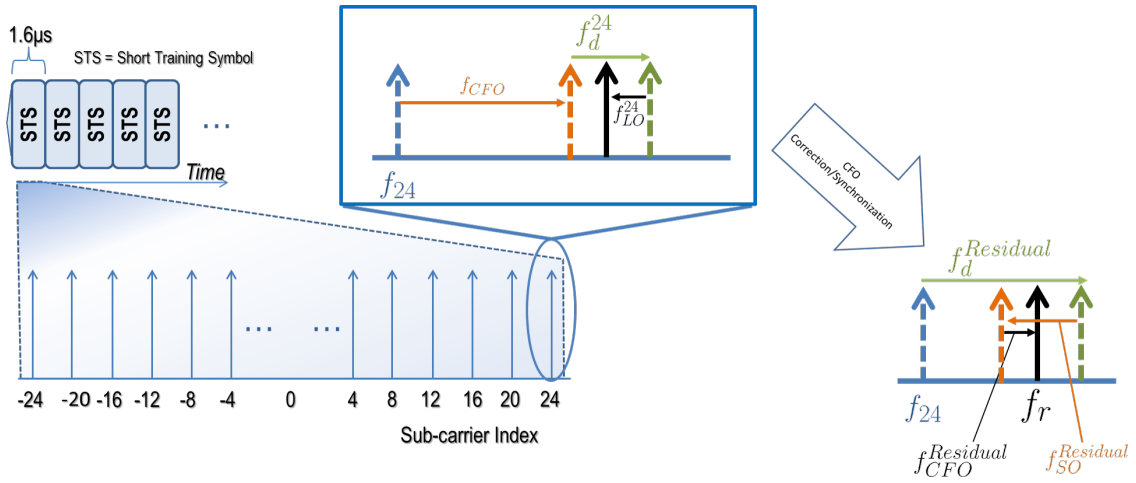

Figure 5.3: Example sub-carrier shifting due to channel and devices impairments.

due to CFO, $f_{CFO}^{Residual}$, and residual offset from the SO, $f_{SO}^{Residual}$. The final shifted received sub-carrier is represented as

$$f_r = f_d^{Residual} \pm f_{CFO}^{Residual} \pm f_{SO}^{Residual} \tag{5.8}$$

where the original Doppler is essentially unrecoverable because it is masked by the data recovery operation removing device impairments. If it is assumed that there is perfect CFO correction and synchronization, then the Doppler shift would be completely recoverable allowing for any measurement of the frequency domain to reveal the Doppler shift across each sub-carrier frequency.

In practice, acquiring f_d directly at the PHY is non-trivial. However, it is possible to achieve a measurement of f_d using the WiSee method first presented by Pu et. al [94]. In this groundbreaking work, a Wi-Fi receiver was demonstrated for the first time to detect perturbations in the NLOS transmit path. The WiSee method leveraged the fact that if the transmitter broadcasted the same OFDM symbol back-to-back, that the receiver could simply take one long FFT to obtain a one Hertz Doppler resolution. This concept was further extended to allow diverse symbols to be transmitted intermittently, while the receiver converts the received frames into the first symbol prior to taking the large FFT. Doing so, all the channel impairments are maintained. Device impairments are also maintained in-

cluding all residual errors mentioned previously, but the Doppler reflections (NLOS paths) contain the full Doppler energy where the LOS path would be located once an alignment is performed. This was the first demonstration that Wi-Fi could be used to detect movement disturbing the segmented electromagnetic field (emf) fields.

5.2.3 Omnidirectional Antenna Model

Since the Doppler reflections will arrive from all angles due to a single omni-antenna on both C_{Tx} and C_{Rx}, it is important to understand the RF restrictions on reception of the LOS contribution. IEEE 802.11p requires -85dBm as the minimum sensitivity of transceivers operating at 3Mbps (the bit rate of the preamble) [8]. It is important that the SM power be above this level to discern the Doppler shift reliably with the incoming waveform. The imposed sensitivity limit will reduce the probability of signal reception for a given communication channel if certain RF characteristics are not met.

The electric field, E_{field}, of the emf delivers max power if delivered to a receiving antenna with the same polarity. The theoretical performance of the omni-antenna to receive a planewave from another omni-antenna is well studied and characterized by the maximum power that an omni-antenna can extract from the incident signal at a given moment in time modeled by

$$P_{Rx}^{max} = \frac{|E_b|^2 \cos(\phi) cos(\theta) G_a \lambda^2}{4\pi Z_o} \tag{5.9}$$

where G_a is the gain, $|E_b|$ is the magnitude of the received E_{field}, ϕ and θ are incident angles of the electric field on the antenna in elevation and azimuth, respectively. λ is the wavelength and Z_0 = 376.73 Ω for free space impedance. The antenna model assumes the emf received by C_{Rx} is a planewave. To ensure the planewave assumption holds for V2V networks, an emf must be received at a minimum distance $R_{FarField}$ from C_{Tx} described by

$$R_{FarField} > \frac{2D^2}{\lambda} \tag{5.10}$$

where D is the largest dimension of the antenna. For a whip omni-antenna, this is along

the vertical axis and the minimum theoretical distance from the transmit antenna for DSRC should be $R_{FarField}$ = 6.4mm. This is more than sufficient for V2V topologies where transmission distance can range from 5.6m (the length of a car) up to 300m for OBUs and 1000m for RSUs.

5.2.4 Estimating S_{Tx}

For the rest of this discussion, $f^k_{CFO} = f^k_{SO} = 0Hz$, so that the focus can be on the large-scale temporal Doppler behavior in the Doppler domain. Recalling eq. (5.1), for an incoming SM if f_d and θ are known to the PHY and host vehicle speed S_{Rx} available to the PHY, then the host vehicle could theoretically determine S_{Tx}. This is valuable for collision avoidance, however, the estimation of S_{Tx} must be made when the two vehicles are far away from each other and approaching each other. For transmitters broadcasting up to 300m ranges, setting $\theta = \psi = 0$ upon initial reception of SMs from the transmitter would enable the host system to estimate S_{Tx} [95]. As the vehicles move closer to each other $\psi = \theta$ but do not equal 0. Thus, the assumption of estimating S_{Tx} reliably must be taken with precaution depending on the initial heading of the vehicles. In the two-lane scenario, if the two cars travel in their respective trajectories, the properties of alternate interior angles for parallel lines is suffice to assume that the θ measurement provided from the FII and external DOAE components of the previous chapter is the same as ψ. For a collision scenario, this assumption may not hold since θ may not be equal to ψ for all time. This suggests that the raw value of f_d alone is not reliable for providing S_{Tx}, neither is knowledge of S_{Tx} without ψ sufficient for collision avoidance. This is because the actual velocity component that corresponds to the Doppler shift is a projection of S_{Tx} onto the line that creates the bearing angle. For this reason, it is more reliable to track temporal changes in the Doppler shift to leverage Axiom 1 and decouple Doppler based collision avoidance from raw f_d values[3]. This tracking occurs in the Doppler domain where the independent

[3]This is analogous to the RSSI technique tracking differences in RSSI values rather than relying on the raw RSSI values.

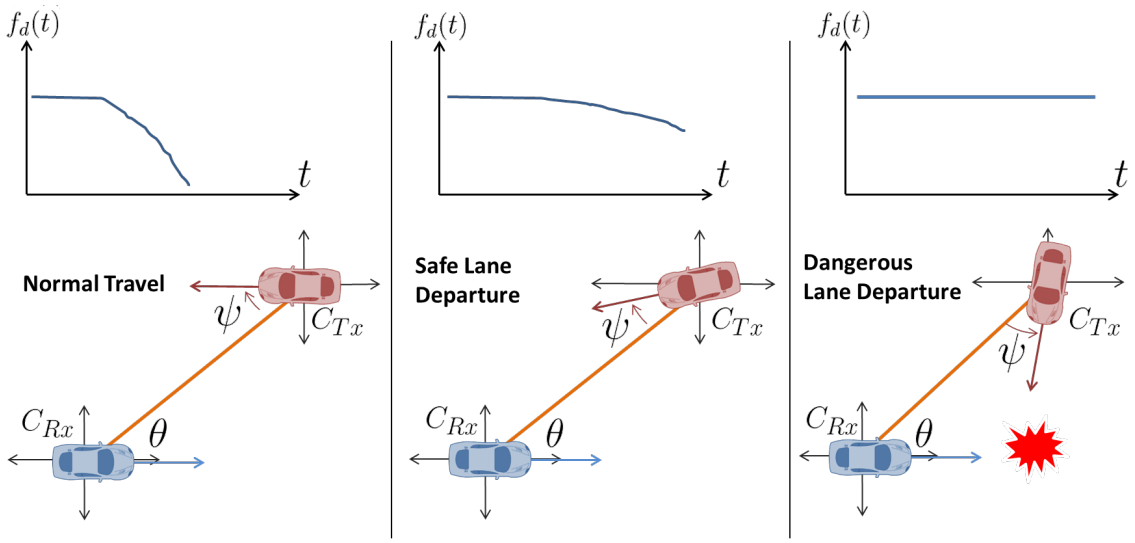

Figure 5.4: Doppler domain dynamics related to collision and no-collision outcomes.

variable is time and the dependent variable is Doppler frequency.

5.2.5 Doppler Domain Analysis

The illustrations of the Doppler domain in Figure 5.4 and their respective scenarios can provide insight into the behavior of the Doppler shift during a collision and no-collision outcome. During normal travel, when C_{Rx} and C_{Tx} are far away the angle between them is very small for a typical two-lane highway, thus $f_d(t)$ is at the highest possible value for their speeds. The maximum velocity vector from each vehicle contributes to the overall relative velocity. As C_{Rx} and C_{Tx} approach, the bearing angle between them increases and $f_d(t)$ decreases as the intensity of the individual contributions start to decrease. If C_{Tx} departs the lane and maintains a constant bearing on C_{Rx}, $f_d(t)$ will not change over time. This agrees with Axiom 1 where the primary focus of Doppler energy from C_{Tx} is captured by sustained proximity of ψ to the bearing angle line relative to the host vehicle and maintain that alignment until a collision occurs.

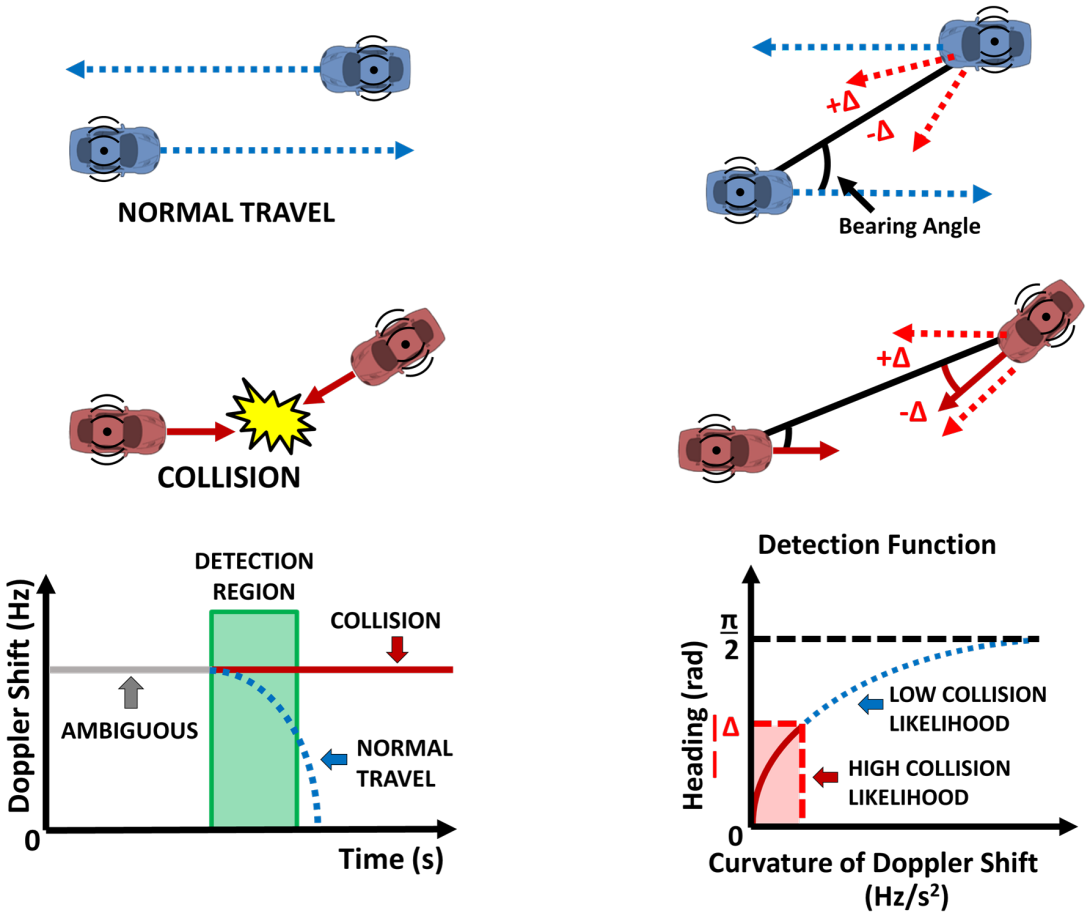

Figure 5.5: Estimating ψ with Doppler domain for predicting a collision.

5.2.6 Estimating ψ from Doppler

To further highlight this concept in the V2V context, Figure 5.5 displays the ambiguous and detection ranges for the same prediction. When the Doppler shift begins to decrease in original value then the likelihood for collision becomes reduced. If the vehicles pass each other safely the Doppler shift will cross 0Hz at the crossing point, as the velocity vectors are orthogonal to each other. As the vehicles begin moving on leaving trajectories the Doppler shift response appears similar as the approaching trend, but inverted. The negative Doppler response is indicative of no collision being possible.

As a thought experiment, it is possible to design an estimate of ψ by relating the curvature of the Doppler domain tracking for predicting a collision. A collision estimator can

be created to map the acceleration of change in the Doppler shift, $f_{\Delta rate}$, to ψ. Estimating ψ may seem like an unreliable approach, but studying a Doppler collision predictor by this method provides valuable insight into the Doppler behavior in terrestrial V2V networks.

For every SM, the Doppler shift is estimated, $\hat{f}_d$, and discretely stored in an observation window be represented by the array

$$\overline{\hat{f}_d} = \begin{bmatrix} \hat{f}_d^1 & \cdots & \hat{f}_d^i \end{bmatrix} \tag{5.11}$$

where $\hat{f}_d^i$ is the most recent $\hat{f}_d$, and $\hat{f}_d^1$ is the oldest measurement from the observation window. Taking the second order derivative of $\widehat{\ddot{f}}_d$ with respect to time and obtaining the average value results in the estimated Doppler acceleration rate defined as

$$f_{\Delta rate} = avg(\frac{\partial \widehat{\ddot{f}}_d}{\partial t}) \tag{5.12}$$

which is then mapped to an estimate of ψ using the half positive parabola defined by

$$\widetilde{\psi} = g(f_{\Delta rate}) = \kappa - \alpha(|f_{\Delta rate}| - h)^2 \tag{5.13}$$

where α and h shape the mapping of $f_{\Delta rate}$ to $\widetilde{\psi}$ and κ will be set to $\frac{\pi}{2}$ because this is the maximum safe angle that C_{Tx} could be from the collision line.

After the Doppler function acquires $\widetilde{\psi}$, the angle estimate is then compared to a threshold denoted Δ. Δ sets the limit as to how far $\widetilde{\psi}$ needs to be off the collision line to ensure a collision will not happen. If $0 \leq |\widetilde{\psi}| \leq \Delta$ then C_{Tx} is assumed to still be on a collision heading with C_{Rx} and the driver is alerted. If $|\widetilde{\psi}| > \Delta$, then it is assumed that h_{Tx} is not on a collision course with C_{Rx}. To reiterate, the key to Doppler shift collision theory is the magnitude of sustained or increasing Doppler shift, indicative of the heading of the threatening vehicle towards the direction of the host vehicle.

5.3 Conclusion

The principles of collision avoidance using terrestrial Doppler shift can be leveraged for adding new "sensor" capabilities to DSRC radios. Methods can be developed to provide 360° awareness. As previously discussed, extracting the Doppler shift measurement is non-trival using existing data recovery methods (IEEE 802.11p chipsets) to detect the LOS Doppler shift using incoherent packetized wireless communication. Instead, the "sensor" view provided by technologies like WiSee can provide the tracking observations necessary for collision avoidance using Doppler shift. It will be shown that the NLOS contributions play the most important role in Doppler-based collision avoidance. The effects of device impairments and the surrounding environment will now be presented in the Doppler-based collision avoidance technique.

CHAPTER 6
AUTOMOTIVE DOPPLER SENSING - THE DOPPLER PROFILE AND MACHINE LEARNING FOR PROVIDING SITUATIONAL AWARENESS IN V2V NETWORKS FOR CONTEXTUAL RECOGNITION AND COLLISION AVOIDANCE

This set of techniques employs a novel sensing operation for V2V networks called: Automotive Doppler Sensing (ADS). ADS provides road safety for connected drivers and connected autonomous vehicles by observing the Doppler profile. The Doppler profile displays the Doppler energy in the form of a high-resolution spectrogram which captures the NLOS reflections between transceivers. The Doppler profile can be analyzed in real time for identifying vehicle dynamics as vehicles maneuver relative to each other. When machine learning is employed, the Doppler profile becomes a powerful new 360° "sensor" to provide contextual awareness of the driving scenario and collision avoidance services. Experimental captures using real devices showcases the ADS capability to provide reliable awareness with high accuracy and low misclassifications in both LOS (highways and surface streets) and NLOS (intersections).

6.1 Introduction

With the range of sensors that auto manufacturers can choose from there has yet to exist any sensor that can provide full 360° coverage in both LOS and NLOS. The Doppler technique is the most reliable method for PHY-based collision avoidance. This is due to the rich content that the Doppler channel response can provide to a DSRC front end. Potentially, ADS is a technology that could enable the V2V radio to exceed all other sensors in terms of stand-alone coverage and safety performance. ADS provides the best of existing sensing technologies:

- Situational awareness can be provided without infrastructure in either LOS or NLOS

conditions (main benefit of V2V)

- Vehicles can reliably determine if other vehicles are threats in real time (primary benefit of active sensors)

- Decoupling safety benefits of V2V from SM content accuracy makes V2V a more reliable system among growing threats to connected cars [26].

This is accomplished by presenting a new sensor view mentioned previously called the Doppler profile and analyzing its output using machine learning. The Doppler profile is a spectral representation of the temporal NLOS Doppler energy as vehicles maneuver. The Doppler profile has a unique potential to enhance the way V2V networks supply collision predictions to operators and autonomous systems. The DSRC spectrum is exploited such that granularities about the driving environment and awareness of potential collisions are made possible. It is assumed that the Doppler profile is generated using the advanced signal processing technique WiSee [94] mentioned in chapter 5. In this work, WiSee is not implemented rather the Doppler profile is created using a continuous wave signal generated from a transmitter at DSRC carrier frequencies to study how the Doppler profile should appear to the radio front end and how it can be used for providing situational awareness to drivers and connected autonomous vehicles (CAV). In that sense, this is the first foundational work to show with omnidirectional incoherent channel illumination the capability to identify driving environments and predict automotive collisions using the Doppler profile.

ADS employs the transmission and reception of incoherent continuous waveforms (iCW) at DSRC. As the vehicles maneuver, the specular and NLOS paths are shifted in frequency creating an energy spread in the frequency domain. By extracting the spectrogram of the received signal with a high-resolution, the Doppler profile can be retrieved and analyzed by machine learning models to determine if there are threats within 300m of the host vehicle. ADS can run continuously to provide reliable situational awareness while the V2V radio channel access provides channel coordination in unused channels. The Doppler pro-

file presents a unique view of the terrestrial V2V channel that can be analyzed for various driving scenarios.

6.2 Spectrogram Analysis: Related Works

The study of Doppler reflections using spectrogram analysis are popular for coherent continuous wave (cCW) radar systems. The general process is to illuminate the channel, capture a raw signal return, generate a spectrogram image by implementing the short-time Fourier transform (STFT) in overlapping FFT intervals, and then analyze the spectrogram contents numerically or using image processing. cCW systems with large FFTs (at least 1 second duration) allow for capturing fine Doppler reflections at a 1Hz Doppler bin resolution called: micro-Doppler. The micro-Doppler creates a high-resolution time-frequency analysis within the spectrogram display. However, the context of these observations in related works are obtained for a stationary observer using directional antennas with high gain.

Bernado et al. [96], presented the time-varying Doppler power spectral density acquired from real-world measurements of vehicles for a carrier frequency range of 5.48GHz to 5.52GHz. The plots featured in the work show NLOS intersection and LOS scenarios suggesting that large-scale Doppler effects can capture moving scatterers and vehicle dynamics, however, the channel sounders used in the measurement campaign did not represent the channel response amid real-device impairments such as local oscillator instability nor did the experiments use single-omni antenna interfaces. Furthermore, the study was limited to small-scale modeling, with no clear analytic description of the macro-Doppler response.

In Anderson [97], a multiple frequency cCW sensor was developed to differentiate between a moving human, vehicle, or animal. The sensor could not only observe micro-Doppler, but also estimate the range of the target by using multiple continuous waves. Based on the Doppler reflections, the complete spectrogram was analyzed offline using

cepstral coefficients and heuristics such as signal energy. The support vector machine (SVM) [98] and Gaussian mixture model classifiers distinguished between targets with 90% overall accuracy. However, the sensor was cCW, remained stationary, used directional antennas, and operated at discrete frequency ranges not within the DSRC band. Furthermore, the analysis was not a real-time classification since the overall spectrogram capture was used for identification.

Andrić et al. [99], analyzed Doppler audio spectrograms using a fuzzy logic approach. The audio spectrums were obtained using a stationary coherent Ku-band short range ground surveillance radar. Fuzzy systems are designed solely by heuristics, but effective in their classification. The authors observed heuristics in the spectrograms such as the central Doppler frequency and the surrounding bandwidth of Doppler spread. Their method accurately characterized between a person walking, running, and wheeled vehicle with 96.7% accuracy. However, fuzzy systems are difficult to design for a wide range of dynamic inputs if expected membership values are not reliable, suggesting that more sophisticated machine learning techniques may be more applicable for a wider range of classification in more dynamic environments; such as the ones that V2V participants communicate in.

In Du et al. [100], Ka-band low resolution radar was used to capture micro-Doppler of vehicle and human movement. The authors identified three energy related features from the spectrogram: entropy (the gathering of large Doppler energy), average entropy for a given spectrogram instance, and maximum energy for a given spectrogram instance. Following these heuristics, the authors developed an SVM classifier with preprocessed training data. Test data was then denoised and preprocessed to classify between targets reliably across a wide range of SNRs, however, the authors also observed these reflections using a stationary system. Furthermore, the system was not designed for real time application since it required a full capture of the target of interest.

Using iCW Doppler reflections, the previously referenced Pu et al. [94] WiSee method demonstrated with a frame-based OFDM waveform that Doppler reflections could be ex-

tracted from a separately located transmitter to classify hand gestures. The authors developed a unique method of reducing the ultrawide-bandwidth signal of IEEE 802.11a[1] to smaller 1Hz Doppler bins. Since both receiver and transmitter were static, only the reflections cause by the user movement were distinguishable. The system was an iCW observer that resulted in a CFO at the receiver because the transmitter and receiver had unsynchronized LO drift. The CFO was corrected by tracking per spectrogram instance the Doppler frequency bin with the largest magnitude, and aligning the carrier wave frequency bin to 0Hz Doppler. Doing so created the first Doppler profile for Wi-Fi devices from which hand gestures moving towards and away from the receiver were detectable. The system could detect nine gestures with 94% overall accuracy among multiple users using a simple pattern matching technique developed specifically for their applications.

Extending this groundbreaking work, this work first presented in [102] considers analyzing the Doppler profile in V2V terrestrial applications where both transmitter, receiver, and other scatterers are moving simultaneously. The outcome of this work is the ADS approach for providing collision avoidance services without relying on the content within SMs. The related works are considered in developing the analysis to classify driving scenarios between vehicles and collision avoidance by only observing received Doppler profiles. This major contribution is achieved by collecting iCW signals using omni-antennas during vehicle maneuvers. The ADS method introduces a new understanding of the Doppler phenomenon in V2V networks and provides the basis for developing future CAV and driver-in the loop applications leveraging the Doppler phenomenon.

[1]V2V may be able to apply this technology to extract Doppler shift since the prominent V2V physical layer protocol is IEEE 802.11p [101], a variant of 802.11a.

6.3 Doppler with Device and Channel Impairments

For simplicity, the spectral Doppler shift of the passband signal can be represented by rewriting eq. (5.1) to the form of

$$f_D(t) = \frac{\vec{V(t)} \cos\left(\theta(t)\right)}{\lambda(t)} \tag{6.1}$$

where $\vec{V}$ is the relative velocity between the two vehicles, θ is the angle they make with each other (assume parallel trajectory lines), and λ is the wavelength. In practice the specular component has a widened bandwidth B due to LO drifts represented by $\lambda(t)$ and channel fading depending on the geometry of the environment [103]. As observed in Figure 6.1a, the spectral component with static transceivers has a 3dB bandwidth of about 20Hz with additional energy out to about $12B$, and temporal jittering due to the LO drift as seen in Figure 6.1b. The drift can cause a translation of up to $\pm$12kHz for an undisciplined LO with a stability of up to $\pm$20ppm. With these impairments, it is unclear what is happening in the real world while these vehicles are maneuvering. Thus, relying only on the specular component is not desirable.

6.3.1 Alignment Operation

The Doppler profile is obtained by performing carrier magnitude tracking first presented by Pu et al. [94]. During translation of either receiver or transmitter, the CFO becomes the dominating factor as the Doppler shift of the specular component takes noticeable dips, but translated in frequency by an offset equal to the CFO at any given time. In the spectrogram of Figure 6.2a, additional energy content around the carrier is also observable, including abrupt phase shifts (discontinuities), partially due to the STFT operation and partially due to uncalibrated baseband processing at the receiver. Due to iCW transmission and reception, an alignment is performed on the signal to remove the CFO by shifting the entire output of each windowed STFT operation of duration T_w, as shown in Figure 6.3.

(a) Actual carrier bandwidth (b) Real LO drift

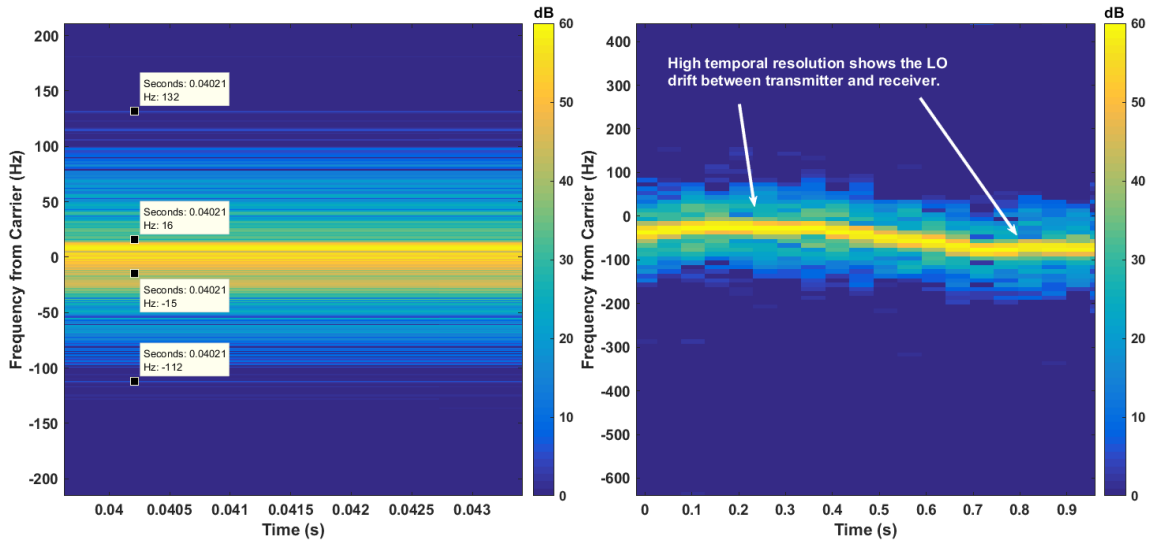

Figure 6.1: Static LOS Doppler shift response with parked vehicles (separation distance $<$ 10m) for a) high frequency resolution and b) high temporal resolution.

(a) Raw spectrogram (b) Aligned spectrogram: Doppler profile

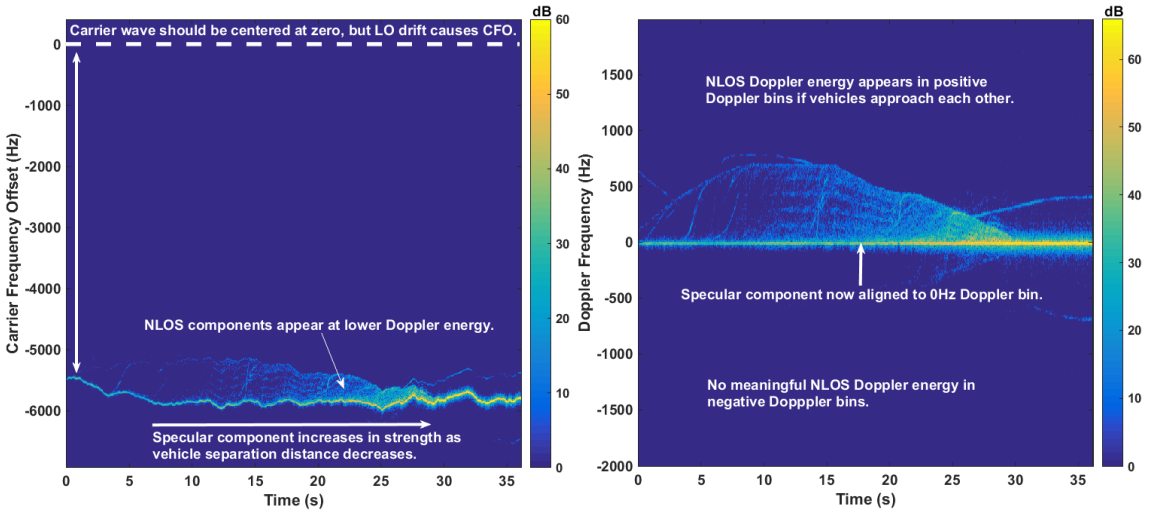

Figure 6.2: Dynamic LOS Doppler shift response shows CFO, LO drift, SO offset, LOS, and NLOS Doppler energy. By removing the CFO, the Doppler profile results which conveys meaningful information about the movement of the vehicles and their environment.

At time $t_0 = T_w$, the received baseband signal, $x[m]$, of length M (which includes all the device and channel impairments during a duration T_w), is converted to the unwindowed

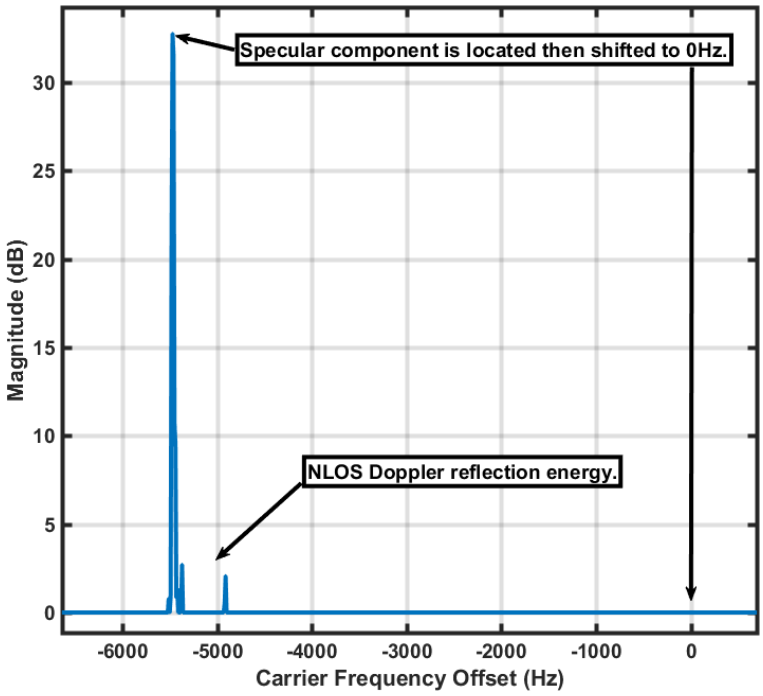

Figure 6.3: One time slice of the spectrogram shows the unaligned Doppler spectrum/spectra for the previous T_w of the received signal.

spectrum representation by the operation

$$\tilde{X}[k] = \mathfrak{F}\{x[m]\} \tag{6.2}$$

where $-\frac{M}{2} \leq k \leq \frac{M}{2}$ and $\mathfrak{F}\{\cdot\}$ is the FFT operation. The associated frequency for the k-th index can be determine by $\tilde{f} = k\frac{F_s}{M}$, where F_s is the sampling rate. After the STFT operation, the spectrum $\tilde{X}[k]$ for the first T_w seconds of the received signal is extracted, as seen in Figure 6.3. Next, the frequency location of the highest magnitude is determined by

$$f_{max} = \max_k \left(\tilde{X}[k]\right) \frac{F_s}{M} \tag{6.3}$$

and the CFO is obtained as

$$f_{CFO} = f_0 - f_{max} \tag{6.4}$$

where f_0 is the known baseband sub-carrier position. Alignment is then performed by

translating the entire spectrum from the carrier bin to the 0Hz bin

$$x_a[m] = \mathfrak{F}^{-1}\left\{x[m]e^{-j2\pi m\frac{f_{CFO}}{F_s}}\right\} \tag{6.5}$$

where $\mathfrak{F}^{-1}$ is the inverse FFT (IFFT). Before applying a final FFT, a window function, $g[m]$, of the same length as the signal segment is applied to the aligned signal, $x_a[m]$, to reveal

$$\hat{X}_a[k] = \mathfrak{F}\left\{g[m]x_a[m]\right\} \tag{6.6}$$

as the final aligned spectrum. The sliding window advances a duration T_a seconds (where $T_a < T_w$), and then the alignment operation is repeated for the duration of the link which comprises the entire STFT operation to generate the overall spectrogram: the Doppler profile as seen in Figure 6.2b.

6.3.2 The Doppler Profile

Performing the alignment operation over consecutive windows advanced by T_a, provides the full Doppler profile. This operation also allows the RF front-end to perform this alignment in real time as additional T_a signal capture is obtained for the duration of the link. The alignment converts an iCW time-frequency response into a cCW time-frequency response. The trade-off is that any variations of the specular component are removed. However, the NLOS Doppler energy is clearly visible at frequencies not within $\pm B$. In the driving scenario of Figure 6.2b the receiver was approaching a parked transmitter. Thus, the Doppler profile does not show any significant energy content in the negative Doppler frequencies compared to the positive range of Doppler frequencies. The NLOS Doppler energy captures the aggregate effects of *all* Doppler shift reflections discernable to the receiver. The Doppler profile is *not* the observation of the specular component except for the energy magnitude over time of the 0Hz Doppler (i.e. signal strength). The Doppler profile captures trends of the dominant NLOS rays which act as a proxy to the shifting of the carrier wave, and features a stable frame of reference (the 0Hz Doppler) for tracking vehicular dynamics

by observing the Doppler energy greater than the bandwidth of the carrier spread. In the Doppler profile, the y-axis is not the true Doppler shift, but rather a profile of the Doppler spectrum across different Doppler frequency bins with resolution $\Delta f = 1/T_w$.

6.4 Doppler Experiments with Incoherent Continuous Wave Signals

Related works performing Doppler analysis seek only to classify what type of object is moving in front of a stationary cCW radar system equipped with high gain directional antennas. For this dissertation work, a new contribution for V2V collision avoidance is made by collecting iCW signals using omni-antennas during real vehicle maneuvers on real roadways.

The observed Doppler phenomenon experienced in the DSRC spectrum was experimentally performed, captured, and analyzed for applications in situational awareness and collision avoidance. Each scenario was performed in environments with various static and moving scatterers. The primary objective was to capture the Doppler effect that occurs for DSRC when a scenario ends in either a safe outcome (normal driving) or a collision outcome. Each experiment was conducted during normal traffic and off-traffic hours depending on the risk involved in simulating the collisions with real vehicles. The results were obtained with one vehicle transmitting a continuous wave, and the other vehicle only receiving while each performed the driving maneuvers. Each experiment was performed three times and the complex baseband signal was stored and processed off-line using custom MATLAB scripts to extract the Doppler profile and classify the driving context and outcome.

6.4.1 Pre-crash Driving Scenarios

In different driving scenarios, the relative position of the vehicles: to each other, to static scatterers, and to moving scatterers can be exploited to identify driving scenarios. These pre-crash scenarios are identified by the US Department of Transportation for having the

(a) ODT (four lane separation; one lane separation; same lane)

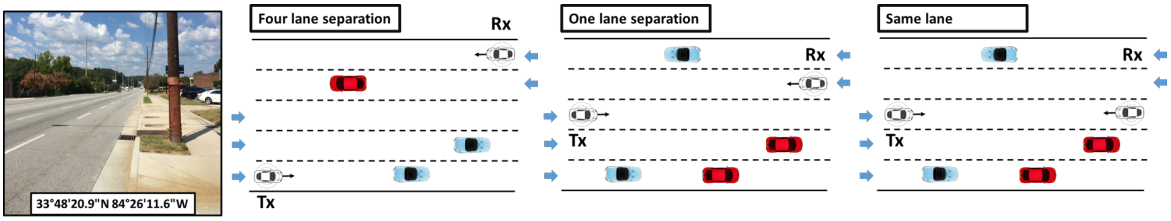

(b) RFC

(c) Convoy

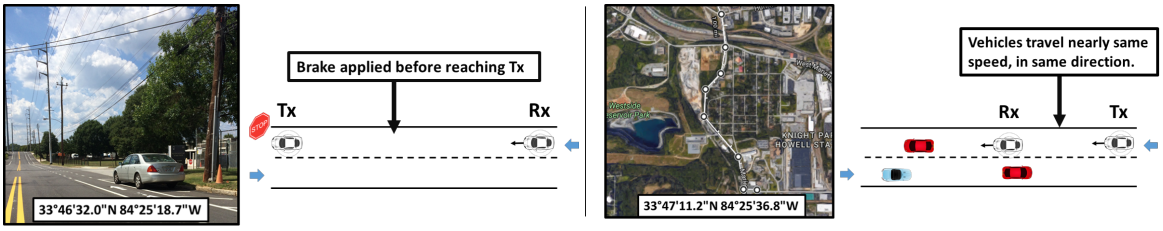

(d) SCP Residential

(e) SCP City

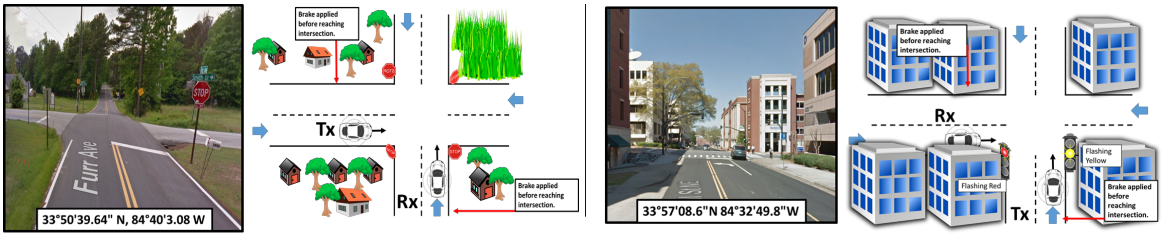

(f) Alt-ODT

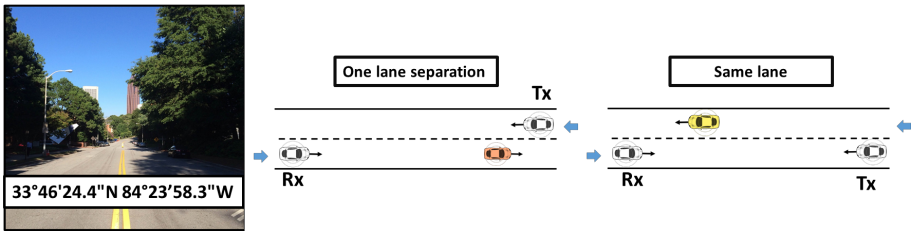

Figure 6.4: Environment locations for experiments. (Photos (c)(d)(e) (Google Maps, 2016))

most societal cost [70]: LOS opposite direction travel (ODT) with no maneuvers, NLOS junction crossing at straight crossing path (SCP), and LOS rear-forward collisions (RFC) due to lead vehicle stopped. In addition to dangerous scenarios where driving context would be beneficial, LOS convoying (CVY) where one vehicle follows another is also considered. The CVY scenario is a purely no-collision outcome to demonstrate that convoying

Table 6.1: Description of Pre-Crash Scenarios for Experiments

Scenario Name	Diagram	Description	Safe	Collision
ODT: Opposite Direction Travel	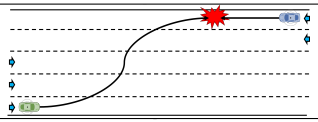	C_{Tx} and C_{Rx} travel opposite directions in their lanes at the same cruising speed of 64 kmh.	Each vehicle maintains their respective lane and passes each other.	Vehicles travel in the same lane while approaching.
RFC: Rear-Forward Collision	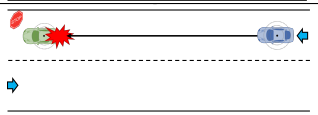	C_{Tx} is stopped while C_{Rx} approaches from behind at a constant speed of 64 kmh.	C_{Rx} brakes at a safe distance from C_{Tx} and stops behind C_{Tx}.	C_{Rx} does not apply the brake.
SU-SCP: NLOS Suburban Straight Crossing Path	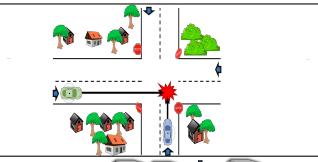	C_{Tx} and C_{Rx} approach a suburban four-way stop at the same cruising speed of 48 kmh.	Both vehicles apply the brakes at a safe distance before the intersection.	Cars maintain their speeds approaching the intersection.
U-SCP: NLOS Urban Straight Crossing Path	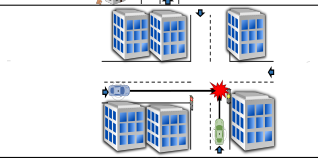	C_{Tx} and C_{Rx} approach an urban intersection with traffic lights at the same cruising speed of 48 kmh.	Both vehicles apply the brakes at a safe distance before the intersection.	Cars maintain their speeds approaching the intersection.
CVY: Convoy	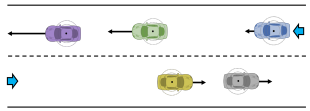	C_{Tx} follows C_{Rx} at different cruising speeds less than 64 kmh.	Each vehicle maintains a safe distance while other vehicles pass.	N/A
Alt-ODT: Alternative ODT	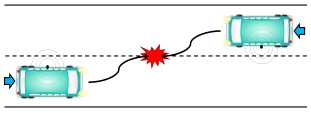	Same as ODT except C_{Tx} and C_{Rx} are larger vehicles.	Same as ODT.	Same as ODT, except antennas are mounted horizontally on the driver doors.

(which is arguably the most frequently occurring driving scenario) can be discernable from others. The ODT scenario can further be broken down into same lane (head-on), adjacent lane (normal), and four lanes over (normal). Similarly, the SCP scenario can be subdivided into suburban intersection and city intersection. To determine the effect of diverse antenna placement, vehicle body, and location, an alternative version of ODT was performed as well. Each of these pre-crash experiments are described below and summarized in Table 6.1. Their locations are also viewable in Figure 6.4.

ODT (suburban environment)

Each vehicle approaches each other from the front, traveling in opposite directions. The vehicles travel at the same speed during each experiment. The vehicles pass each other, continuing in their respective lane. The environment featured many static and moving scatterers, on a five-lane highway, see Figure 6.4a. For one experiment set, the vehicles approached each other from a far distance at the furthest lateral lane separation (four lanes). An additional experiment was performed with the closest lateral lane separation (one lane). This scenario was captured at one location using cars as the test vehicles traveling at 32 kmh (slow) and 64 kmh (fast).

For comparison, an alternate capture of the one lane ODT scenario at 64 kmh was captured. The differences in the alternate capture are: location, larger vehicles, and shorter beginning separation distance. This capture was intended to understand how different starting positions, environments, and vehicle types could change the outcome of the Doppler profile. Also, this alternate capture was used as an alternative test set for the trained classification algorithms that used the training set from the location in Figure 6.4a. Later in the scenario classification section, it is shown that the performance is most sensitive to time dynamics determined by the initial separation distance.

RFC (suburban environment)

In this scenario, the transmitting vehicle is parked a far distance away from the receiver. The receiver then approaches the transmitter at a constant speed. The receiver applies the brakes around 110m to 140m closing distance before gradually coming to a complete stop behind the transmitter. This scenario was performed on a street with very few moving scatterers. Captures were recorded for speeds of 32 kmh (slow) and 64 kmh (fast) at the same location in Figure 6.4b.

CVY (suburban environment)

Both vehicles travel in the same direction following each other. The relative speed and separation distance between them vary during the capture, but the vehicles did not exceed relative cruising speeds greater than 64 kmh. The vehicle separation distance changes most drastically when approaching or leaving a stop. This capture was taken during a long section of road pictured in Figure 6.4c which included at most two stops due to red stoplights.

SCP - Residential

Another common scenario is approaching a NLOS intersection in a residential neighborhood such as pictured in Figure 6.4d. In this scenario, each vehicle starts at the same distance from the four-way stop. Both vehicles then approach the intersection at the same speed (48 kmh), brake at an unknown distance from the intersection, and then slow into a complete stop at the junction boundaries. The residential intersection environment is known to exhibit vegetation (which are not strong RF reflectors at DSRC), and infrequent obstructed LOS. This experiment was performed at night, to limit endangering any additional cross traffic, thus moving scatterers are not captured in this scenario.

SCP - City

Finally, the city intersection is a NLOS scenario that recreates the same vehicle dynamics as the residential intersection, but involves more urban canyon effects and more scatterers such as traffic lights, see Figure 6.4e. The urban canyon effect makes the high walled buildings act like a wave guide for the V2V signal [46], with the strongest single bounce reflection coming from the opposite lane corner [103]. For this experiment, the drivers had to synchronize the approach with additional traffic lights. This experiment was performed at night to limit endangering any additional cross traffic, thus moving scatterers are not captured in this scenario.

6.4.2 Location Features

Driving environments can feature moving scatterers such as other vehicles or the test vehicles themselves[2], along with multiple static scatterers positioned primarily on the sides of the streets [104]. Several of the locations were chosen based on environment and ease of experiment replication. For ODT, a five-lane road with a lane separation distance of 3.6m exhibited intermittent large static reflectors due to industrial warehouses located 15m to 30m away from the roadside. The road does not undulate, and at the time of the experiments featured many moving scatterers. RFC trials were performed on a road with less moving traffic which featured some trees along the roadside, small buildings, and power poles. In SU-SCP an intersection was chosen with some obstructed LOS (OLOS) conditions between the vehicles. Except for rural areas it may be rare that an intersection would have a purely LOS condition, however, in suburban areas OLOS frequently occurs. A few strong reflectors were present due to street signage and small buildings, but dense vegetation along the roadside was the primary obstruction between the test vehicles. The U-SCP scenario is common for city intersections and features a richer scattering environment than SU-SCP. An intersection was searched out which featured high buildings at each

[2]From a channel model perspective, the receiver vehicle body and relative positioning can alter the Doppler shift on double bounced rays received at the antenna.

quadrant of the intersection extending about 70m in each direction from the p_c within the intersection. The Alt-OTLD location was a two-lane surface street located at a university and featured many static scatterers that were closer to the road compared to the OTLD location[3].

6.4.3 Crash Methodology

Prior to performing each pre-crash scenario, the test vehicles start from a far distance away from the expected p_c. For each pre-crash scenario, the experiment either simulates normal driving or driving that results in a collision. Three trials for each experiment are performed, resulting in a data set of 33 individual captures. For each trial the transmitter begins sounding the channel and GPS logging commences prior to the vehicles moving. The vehicles begin accelerating up to their expected cruising speeds. For each experiment that results in a normal outcome, the vehicles follow the expected traffic patterns. For ODT and RFC, a collision is simulated by having the vehicles drive in adjacent lanes, but the antennas relocated[4] from the center of the roof to the side closest to the approaching vehicle, see Figure 6.5. For Alt-ODT collision outcome, the antennas were mounted horizontally on the driver side doors to understand the effects of diverse antenna positioning collision avoidance performance. As the p_c was reached the antennas would pass within 1m of each other at full cruising speed (during the Alt-ODT scenario, the antennas physically contacted each other at full speed). A collision could not be simulated in the same way for the SCP pre-crash scenarios due to safety concerns. However, to simulate a collision at the intersection, the C_{Rx} driver applied a hard brake at a close distance from the intersection, while C_{Tx} continued through at full speed. For SCP, only Doppler information up to the most recent moment prior to braking was used from the data set, and GPS logs helped confirm the point in time of this event taking place. In normal SCP outcomes, both test vehicles applied brakes

[3]From a geometric channel modeling perspective, the Alt-OTLD location is uniquely different from the OTLD location.

[4]Relocating within the roof dimensions does not appear to significantly alter the outcome of the Doppler phenomenon.

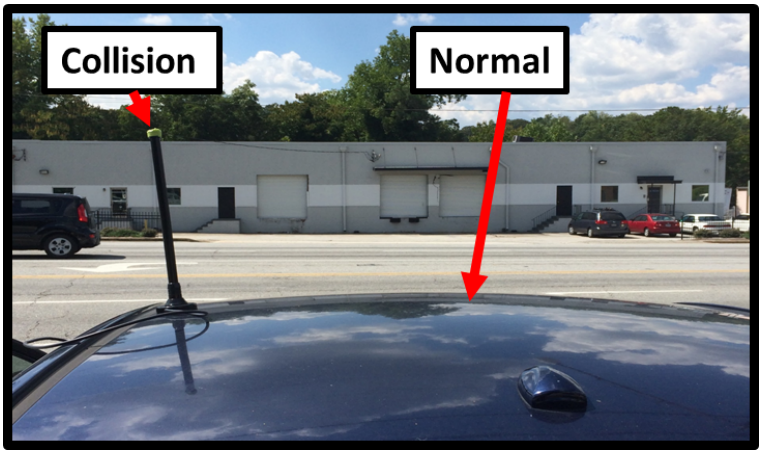

Figure 6.5: Antenna locations for normal and collision outcomes.

much further (and softer) from the intersection than for the collision simulation until both vehicles stopped at the intersection.

6.4.4 Equipment

The equipment for these experiments is based off the novel channel sounding method first introduced in chapter 2, recall Figure 2.1. Instead of only one SDR located at the receiving vehicle and one V2V radio at the transmitter, each vehicle was equipped with an SDR and V2V radio. However, the V2V radio was not programmed to transmit safety messages since the focus of scope of these experiments were to study the effect of iCW Doppler. Instead the V2V radio was programmed to only record its local GPS coordinates to be used later in post-processing. Each vehicle also featured a roof mounted 9 dBi omnidirectional whip antenna.

The equipment was calibrated by performing trial experiments to indicate the best gain settings for the receiver, while the transmitter gain was set per the DSRC regulations. Because of the receiver gain calibration, a trade off was introduced between Doppler reflection sensitivity and signal distortion as the vehicles approached from 300m to near proximity at 3.6m. Automatic gain control could have been programmed into the SDRs, but this was not implemented. Instead it was determined more relevant to study the Doppler reflections from far away (prior to any imminent collision), and reduce the noise effect due to

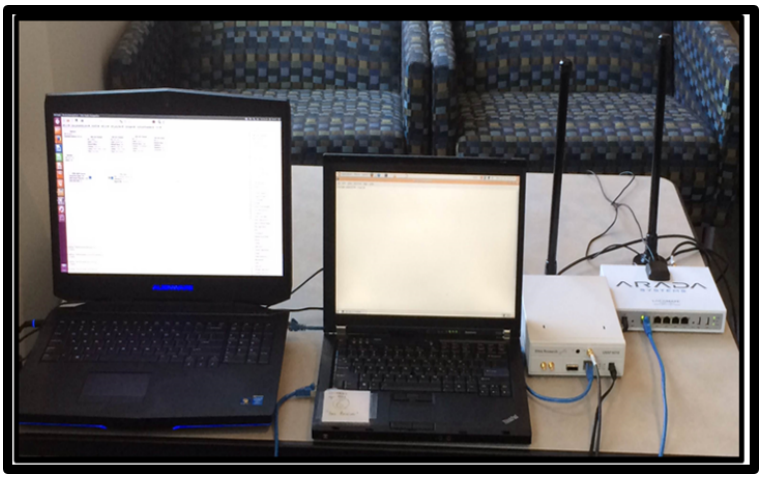

Figure 6.6: Equipment on both vehicles for iCW Doppler capture experiments.

proximity signal distortions in post-processing.

The SDRs were programmed using GNUradio. The flowgraph of the receiver recorded raw complex baseband samples directly to a file at a sampling rate of 1MHz. The transmitter flowgraph was designed to generate a single continuous wave tone at 156.25kHz[5] using a sampling rate of 1MHz. The transmitter then modulated a 5.86GHz DSRC carrier wave by the baseband tone. Bandwidth spreading of the baseband signal due to LO noise was observed to be insignificant compared to the expected Doppler shifts during the experiments. All Doppler processing was performed and analyzed by tracking the baseband signal, since passband Doppler effects are mirrored onto the baseband sub-carrier. The equipment used in each test vehicle is pictured in Figure 6.6.

6.4.5 Post-Processing

From the received complex baseband samples, custom MATLAB scripts were developed to extract Doppler spectra and time sequence in the form of a spectrogram. The alignment operation described previously was implemented with a sliding windowed STFT (to suppress spurious energy in other frequency bins that may have been caused by signal distortion due to proximity) with a window duration $T_w = .1$s which provided a 10 Hz Doppler frequency

[5]The IEEE 802.11p standard identifies this as the baseband frequency for sub-carrier #1.

bin resolution and advancement $T_a = 50$ms. After removing the CFO, the LOS Doppler information becomes lost except for the carrier energy, but the rich scattering environment in V2V allows the receiver to pick up additional reflections that contain Doppler energy.

6.5 Doppler Profile Analysis

The Doppler effect at DSRC exhibits a unique difference between a collision vs. normal driving, including unique identifiers between driving scenarios. To reiterate, in this work the Doppler domain (i.e. tracking the LOS Doppler shift) is not the Doppler profile (i.e. observing Doppler reflections). The effects of $\vec{V}(t)$ and $\theta(t)$ from eq. (6.1) are clearly observable in the Doppler profile. Stronger reflection energy greater than the 0Hz Doppler exhibits similar trends that the LOS shift would exhibit.

The Doppler profile allows NLOS reflections to convey a physical meaning of the driving situation. The Doppler spectrum caused by the NLOS scattering of the signal at terrestrial speeds is preferred for situational awareness rather than observing the LOS Doppler shift. If the LOS Doppler shift were preferred, then the carrier energy itself would be tracked in the unaligned Doppler spectra (like the related works using static coherent systems tracking the LOS Doppler shift). The STFT allows the spectrogram to highlight the temporal dynamics of the vehicles as they maneuver. Figure 6.7, shows an example capture of each driving scenario after alignment for the full duration of the driving scenario and Figure 6.8 shows the Doppler profiles of select half-speed versions of the same scenarios along with an example of the Alt-ODT scenario. The SCP scenarios do not have a capture for different speeds, however, from observing the Doppler profiles in ODT and RFC at different speeds it is likely that the SCP Doppler profile would be scaled depending on the speeds. Each plot is a non-collision outcome. Key observations of driving dynamics are annotated for environmental clues that can assist in determining the driving scenario.

As annotated in Figure 6.7 and Figure 6.8, each pre-crash scenario regardless of the driving speed can feature several distinguishable reflections possibly due to: scattering

(a) 64 kmh ODT: four lanes (ODT4fast)

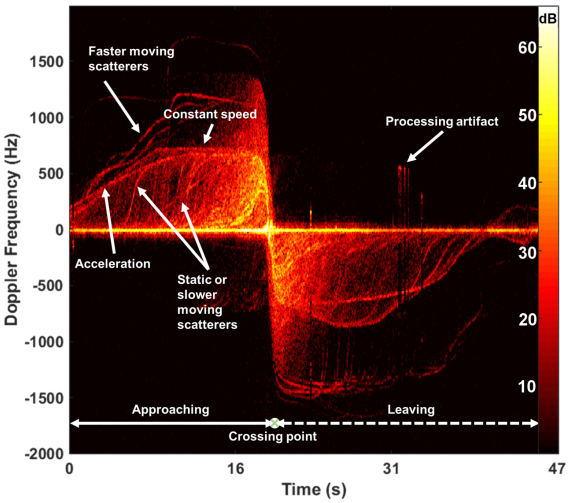

(b) 64 kmh ODT: one lane (ODT1fast)

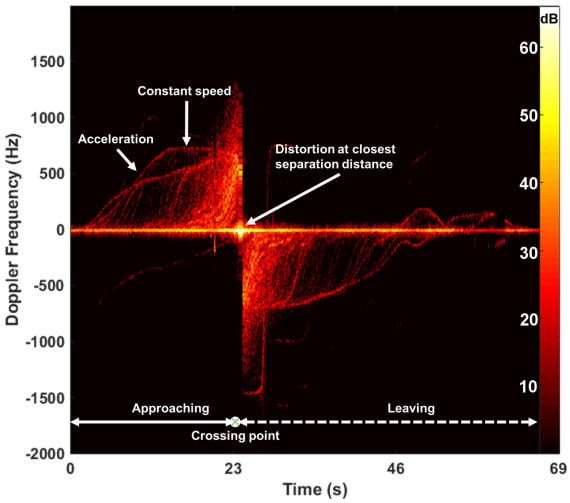

(c) 64 kmh RFC (RFCfast)

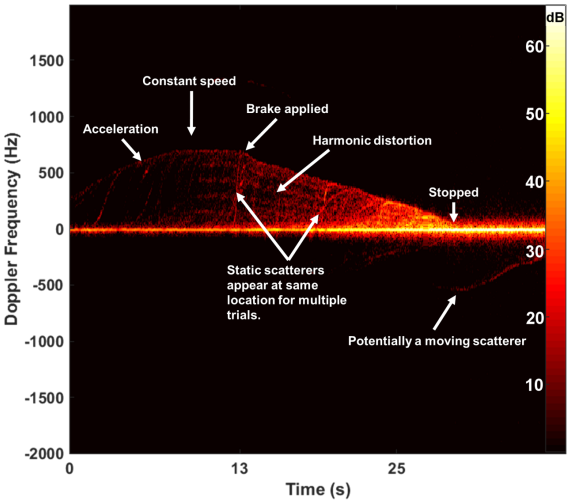

(d) Convoy (CVY)

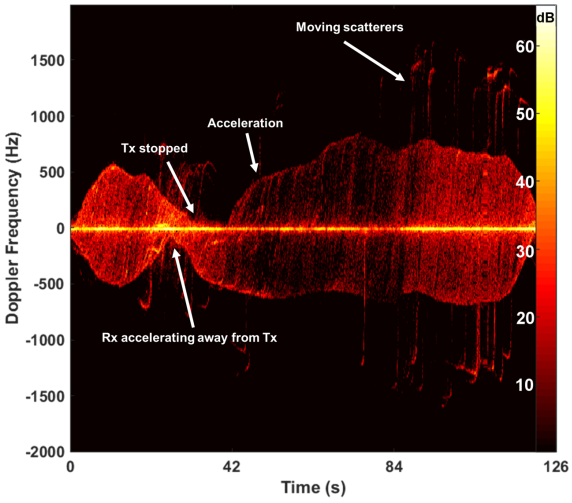

(e) 48 kmh SCP Residential (SCPres)

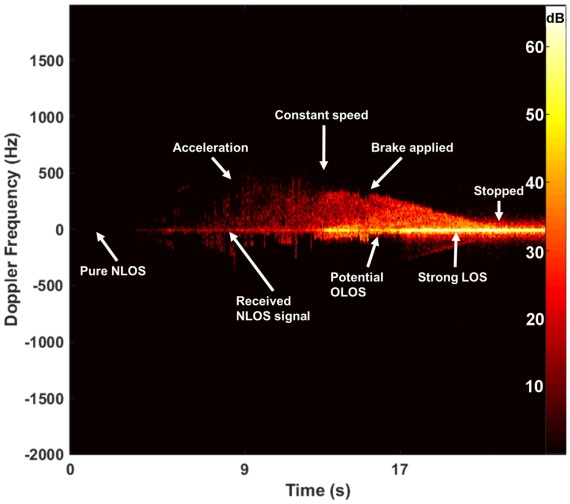

(f) 48 kmh SCP City (SCPcity)

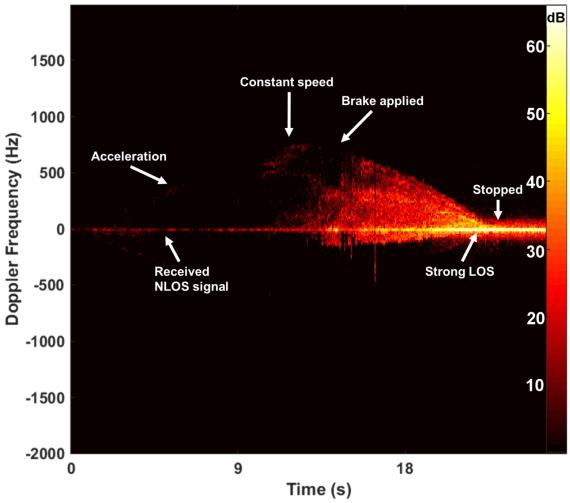

Figure 6.7: Doppler profiles of pre-crash driving scenarios reveal a unique response between pre-crash groups. (Annotations of moving and static scatterers are not confirmed.)

(a) 32 kmh ODT4; (ODT4slow)

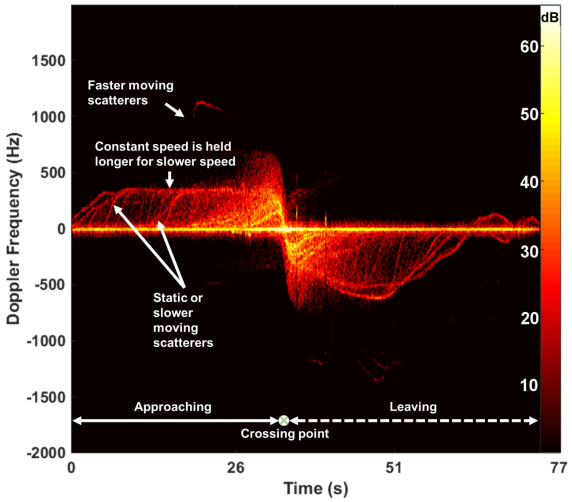

(b) 32 kmh ODT1; (ODT1slow)

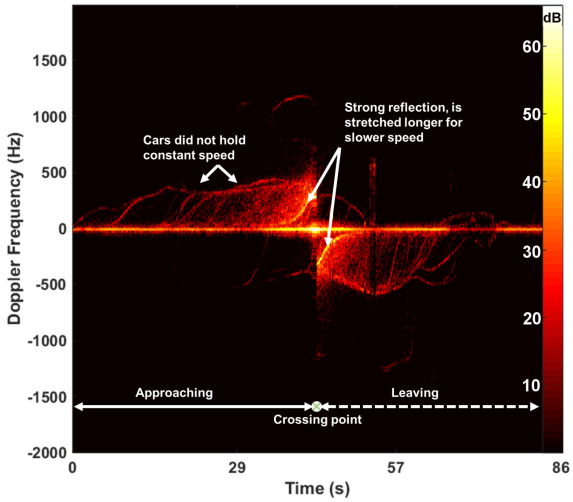

(c) 32 kmh RFC; (RFCslow)

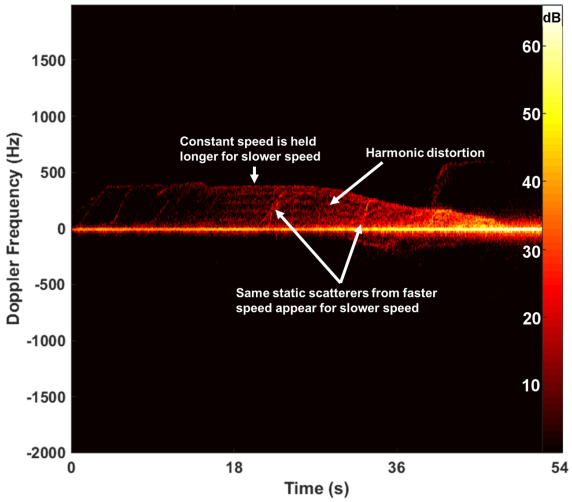

(d) 64 kmh Alt-ODT; (AltODT)

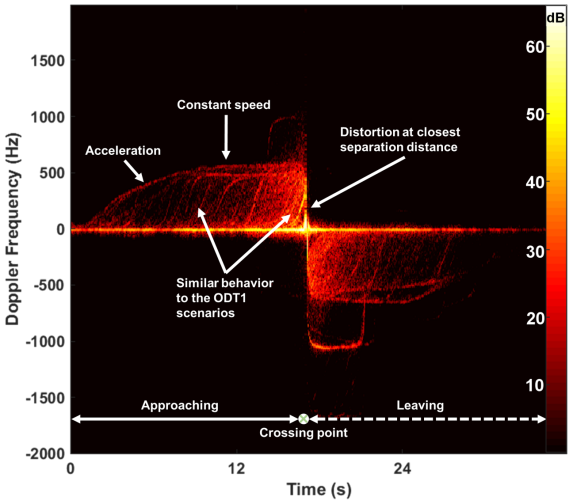

Figure 6.8: (a)(b)(c) Doppler profiles of half-speed driving scenario experiments are scaled down versions of the faster experiments. (d) Doppler profile for Alt-ODT scenario. Notice in (c) the same static scatterers appear as in Figure 6.7c; the same is true for (a) and (b) compared to Figure 6.7a and Figure 6.7b, respectively.

from the test vehicles themselves, the ground ray reflection, static scatterers, and/or faster/slower moving scatterers. Also discernable are unique trends such as constant speed, constant deceleration, and stopping. These results agree with spectrograms of a moving vehicle obtained by a static MFCW radar [97]. The only difference is that the author of [97] noted severe harmonic distortion and inphase/quadrature (I/Q) imbalance at the receiver. Those device impairments appear in the RFC and CVY scenarios, but are not as severe. Individual contributions of the environment to the Doppler profile have not been confirmed, since the scope of these experiments is to observe the *aggregate* Doppler profile from all reflections using real devices. Hereafter, "strong" trends in the Doppler profile will be referred to as a *trace*. Some traces increase in height following an S-shape or an exponential shape.

6.5.1 Doppler Profile Envelope and Reflection Entropy

The NLOS trace which consistently reveals the trend of the vehicle dynamics expected by theory will hereafter be called the Doppler profile envelope (DPE). The DPE is the trace which serves as an upper bound for most of the Doppler energy while most accurately capturing $\vec{V}(t)$ dynamics between the test vehicles. The DPE can also be described as the *strongest* trace that appears to be least like a moving or static scatterer. The DPE can most likely be attributed to the ground reflection ray which is common between the two vehicles along the bearing line between them, or the DPE could be from the double bounced ray scattering off the receiver and transmitter body. These effects were not confirmed because these experiments sought to only study aggregate effects of Doppler shift for extracting driving context, rather than appropriating sources of the Doppler profile which would be more relevant for developing a channel model (this could be left for future work). For the convoy scenario, Figure 6.7d also displays a DPE in the negative Doppler frequencies. This is a characteristic unique to the convoy scenario. The apparent symmetry across the 0Hz line is due to uncorrected distortion[6] in the I/Q complex baseband signal at the receiver or

[6]See [97, Section 8.2] for a discussion on the effects of imaged signals in spectrograms due to non-ideal receivers.

transmitter. However, this device impairment is leveraged to uniquely identify convoy by the appearance of two DPE.

Another differentiator between the Doppler profiles is the amount of Doppler energy due to NLOS scattering. Figure 6.7a to 6.7b display the outcomes of the ODT pre-crash scenarios for four lanes and one lane separation, respectively. The Doppler energy in Doppler frequencies greater than the DPE increases with greater lateral lane separation; indicating that more reflections are receiving a power boost for the same d_{LOS}. Hereafter, the increase in Doppler frequencies with energy content will be referred to as reflection entropy (RE). The increase in RE cannot be due to proximity signal distortion since the RE decreases with the decrease of the DPE (compare Figure 6.7a and Figure 6.7c).

The RE in Figure 6.7a is also overall lower compared to that observed in Figure 6.7b. This can possibly be attributed to the test vehicle bodies creating a waveguide effect as they travel with a shorter lane spacing, such that the DPE has overall more energy than compared to other reflection paths. This difference is not caused by the repositioning of the antennas to simulate collisions (see Figure 6.5), because the path loss measurements reported in chapter 2, which did not alter the antenna positions, also observed a stronger signal power when the vehicles were aligned with one lane spacing compared to two lane spacing (refer to Figure 2.3). Though it is not fully understood why this phenomenon occurs, it is interesting to exploit this outcome in the Doppler profile through the RE observation. Notice that in Figure 6.7c, the RE disappears after C_{Rx} stops behind the parked C_{Tx}. This is expected since parked vehicles do not create any Doppler shift, however, it is interesting that additional moving scatterers around the parked vehicles may be observable.

6.5.2 Faster Moving Scatterers

The Doppler profile can exhibit Doppler frequencies greater than the DPE, and sometimes in negative frequencies. The signal is experiencing Doppler from all angles due to omni-directional antenna transmission and reception. Doppler profile contributions due to faster

moving scatterers seen in Figure 6.7d are treated as noise for identifying the driving scenario. This is because the DPE and RE are proxies to the dynamics between C_{Rx} and C_{Tx}. Traces that extend further than the DPE frequency are treated as noise. Later it will be discussed how to analyze the Doppler profile numerically to reduce the effect of traces that extend beyond the DPE (either positive of negative). For this dissertation work, only the interaction between C_{Rx} and C_{Tx} are studied. Future work could attempt to leverage the Doppler profile for providing collision avoidance among vehicles without V2V radios [105].

6.5.3 Processing Artifacts and Harmonic Distortion

The Doppler profiles also exhibit artifacts due to post-processing or harmonic distortion due to device impairments. The harmonic distortion noticeable in Figure 6.7c and 6.8c does not appear in other driving scenarios. Why this only appears for the RFC scenario is still an unknown, but is exploited for uniquely identifying the RFC scenario. Harmonic distortion is correctable, but was not corrected in this work to include real device impairments. Artifacts due to the STFT process could be a result of I/Q imbalance or signal distortion. The removal of the CFO through alignment did not introduce any artifacts since Figure 6.2a reveals the harmonic distortion exists prior to the alignment process. Having device and channel impairments included in the experimental captures, helps to further validate the true Doppler phenomenon in V2V and observe unique features about the vehicle dynamics.

6.5.4 Capturing Vehicle Dynamics

Vehicle dynamics such as braking status and acceleration can be relayed reliably through the Doppler profile by following the DPE trend, while vehicle alignment can contribute to the RE that is detectable. When the vehicles are aligned in the same lane such as in the RFC scenario, only the C_{Rx} speed contributes to the vehicle dynamics. For ODT and SCP, the vehicles may be offset from each other either by lane spacing or orthogonal trajectories. As

the vehicles traverse in their respective ODT lanes, greater lateral lane spacing can reveal unique trends different from other scenarios. This can be observed in Figure 6.7a where the DPE and RE in four lanes shows a downward sloping trend that begins prior to the crossing point. This agrees with theory since the downward trend is caused by θ and ψ increasing towards $\pm\frac{\pi}{2}$, thus pulling $f_D(t)$ towards the 0Hz Doppler. In ODT one lane, the DPE does not exhibit a significant dip like the four-lane capture because the lateral spacing of 3.6m for an average roadway is not long enough to cause a significant dip in the DPE trend. In these situations, the RE can help differentiate the ODT scenario from the other driving scenarios since the reflection intensity varies at different points in the approach, regardless of scatterers in the environment.

6.5.5 Capturing Environmental Effects

In the SCP scenarios, the suburban and urban environments determine how soon Doppler intensity is detected. Observing Figures 6.7e and Figure 6.7f, the suburban scenarios do not feature a rich scattering environment like the urban scenario. Vegetation in the suburban environment can absorb the signal strength during NLOS/OLOS conditions. Hence, the furthest distance at which the signal is detectable may be closer to the junction in SU-SCP scenarios compared to U-SCP scenario. The amount and quality of reflectors in the environment is known to affect signal reception [106][103], and for the Doppler profile response the number of reflectors available in NLOS conditions can help contribute towards relaying Doppler energy to other vehicles as if there was a LOS path. For example, eq. (5.1) is misleading as one could imagine orthogonal headings resulting in no significant Doppler shift, however, empirical studies show that corridors create a waveguide effect for the signal [46] and that geometric models of junctions indicate some scattering at an urban four-way intersection can serve as relay points for conveying the full Doppler intensity to other vehicles [103]. Consider in any SCP scenario that corner reflections off signage located near the junction openings contribute towards relaying the full Doppler shift contribution

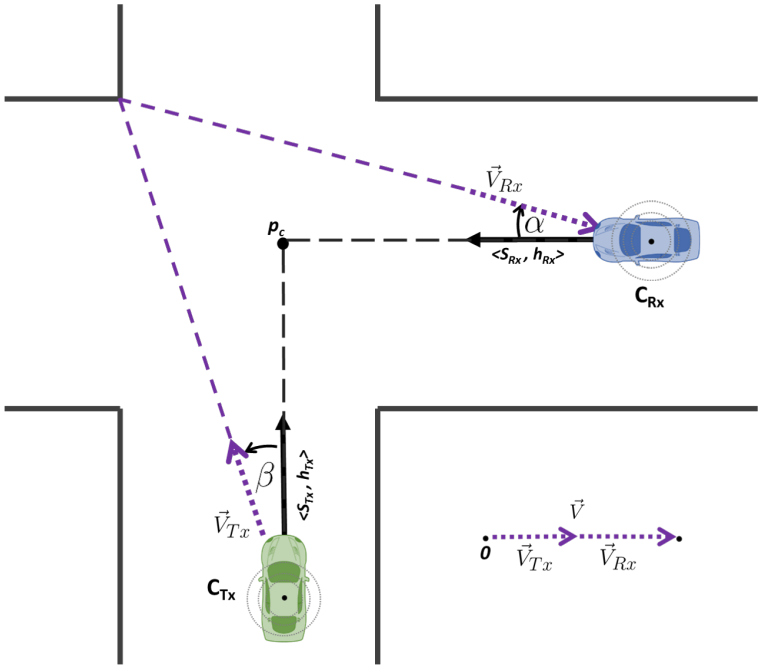

Figure 6.9: Illustration of Doppler contribution in SCP scenarios (not drawn to scale).

by S_{Rx} and S_{Tx} as if $\theta(t) = \psi(t) = 0$. This is illustrated by Figure 6.9, where the single-bounce off a corner scatterer near the junction results in nearly conveying the full Doppler shift between C_{Tx} and C_{Rx}. The angle of departure, β, and angle of arrival, α, are not directed toward the other vehicles like θ and ψ may be, but the geometry makes it seem as if they are.

6.5.6 Doppler Profile Analytic Description

The Doppler profile does not contain any meaningful temporal changes in the carrier wave except for the magnitude of its spectral energy. Each individual Doppler spectra snapshot resulting from an STFT operation of the previous T_w seconds of the received signal reveals the aggregate result of all the NLOS paths that the receiver can resolve at discrete intervals. Hereafter these intervals will be referred to as Doppler bins. The time-frequency varying Doppler profile could be described per discrete Doppler bin within a single Doppler spectra by two components.

Rewriting eq. (5.1) for an omni-antenna, these components are: the Doppler bin with

illumination

$$f(t,k) = \frac{S_{Rx}(t)\cos(\alpha_k) + S_{Tx}(t)\cos(\beta_k)}{\lambda} = \frac{\vec{V}^k_{Rx}(t) + \vec{V}^k_{Tx}(t)}{\lambda} = \frac{\vec{V}_k(t)}{\lambda} \tag{6.7}$$

where $k \in \{0, 1, 2, 3...K\}$ represents the Doppler bin index up to the K-th positive Doppler bin, $\vec{V}^k_{Rx}(t)$ and $\vec{V}^k_{Tx}(t)$ are the individual velocity contributions of the vehicles, $\vec{V}_k(t)$ is the relative velocity for the k-th Doppler bin, α_k represents angle-of-arrival for Doppler bin k, and β_k represents angle-of-departure for Doppler bin k. The λ contribution is now considered a constant equal to the expected wavelength for the carrier frequency since the alignment operation effectively removed its temporal contribution to the CFO. Any residual contribution of LO drift can be ignored since the largest alteration in λ due to LO drift is already on the order of 10^{-6} for DSRC, which produces a negligible influence on the Doppler profile after alignment.

The second descriptive component is the illumination intensity at the k-th Doppler bin

$$I(t,k) = \frac{P_{Tx}G\lambda^{\gamma}}{4\pi d_k^{\gamma}} \tag{6.8}$$

where P_{Tx} is the transmit power, G is the end-to-end system gain, γ is the path loss, and d_k is the path travel distance including bounces for Doppler bin k (assuming a reflection coefficient of 1 for every bounce, which is reasonable for DSRC wavelengths reflecting off scatterers in the driving environment). Notice that α_k, β_k can be assumed uniformly distributed between 0 and $\frac{\pi}{2}$, but the Doppler profile depends on the overall intensity of a reflection path. Therefore α_k, β_k should be restricted in their interpretation as being the *significant* departure and arrival angles of the strongest NLOS paths over the duration of the STFT segment that illuminate a Doppler bin.

Fast-fading effects can also affect the intensity of a Doppler bin; however, these effects are smoothed over by segmentation during the STFT process. T_w should be chosen to be longer than the longest delay spread expected in V2V environments where delay spreads have been recorded no longer than $6\mu s$ in rural areas [107]. The channel effects

due to delay spread is negligible since T_w is expected to be on the order of seconds. By suppressing fast-fading effects with a long T_w, stronger reflections can appear more stable in the Doppler profile as noticeable traces. This is the key advantage of observing the Doppler profile rather than signal strength, CFO, or channel state information (CSI). Furthermore, improved resolution of Doppler bins with longer T_w and shorter T_a can provide a high definition and stable view of the vehicle dynamics to the radio front end at a cost of increased processing delay. Vehicular speed intervals of 16 kmh at DSRC wavelengths results in Doppler steps of 87Hz. Therefore, the length of T_w does not have to be very long to produce meaningful driving context with minimal processing delay. The spreading of the Doppler energy over the frequency range of the Doppler profile gives the resultant spectrograms as the vehicles maneuver. The overall response of this spread will increase the intensity of some Doppler bins over others depending on the vehicle dynamics.

6.6 Feature Selection

Features about the Doppler spectra can be defined for analysis by machine learning techniques. This is the platform from which ADS begins. The features must help isolate the driving scenarios from each other, as well as the safe vs. collision outcomes. This will allow classification techniques using machine learning to numerically discern the context of the interaction that the host vehicle is having with another vehicle. First, a feature set for identifying the type of driving scenario is discussed.

6.6.1 Feature Analysis Part I: Driving Scenario Classification

The unique features needed to properly identify a driving scenario are now defined. The features are numerical definitions of heuristics observed in the Doppler profile that can be applied in a real-time classification architecture, rather than employing spectrogram image processing toolsets over the full capture. Though the full Doppler profiles convey the approach and leaving trajectories, only a duration starting from the beginning of the exper-

iment will be used. This serves for two reasons: 1) so that there is a common alignment point for comparison (acquired by the GPS logs) and 2) for determining how soon a driving scenario can be classified given the selected feature set (this will later be important for collision avoidance). For feature selection, a heuristic approach based on the visual inspection of the Doppler profile data set is used. Features from the Doppler profile that differentiate between the driving scenarios are identified, rather than related works which may focus on identifying the type of vehicle that is approaching. By leveraging unique transmitter-receiver paths, found only in terrestrial driving, the driving scenario between C_{Rx} and C_{Tx} could be identified from observing Doppler alone. This type of sensing provides additional safety benefits for drivers and CAVs that only use a V2V radio for driving assistance.

6.6.2 Driving Scenario Classification: Feature Description

Three key heuristic features that separate the driving scenarios are identified as: Observation Time, DPE, and RE.

Observation Time (N)

The observation time of the Doppler profile is synonymous with the number of STFT windows (segments) that have passed since the beginning of the experiment. Let L be the number of STFT windows that have passed. The instantaneous time, t, can be determined by $t = T_w + L * T_a$. Some unique characteristics are discoverable early on (such as in convoying), other scenarios must wait for a unique event, such as the crossing point in ODT or brake applied in RFC. Let it be defined that after N windows the classification accuracy performs best. Different combinations of expected speeds on the roadways could be used to discover the value of N which provides the most unique information for a given relative speed. This is possible due to the host vehicle being aware of its own speed, heading, and brake status[7]. Calibrating the classification system for different values of N (indexed by the relative speed) could further refine the classification, however, only this non-optimized

[7]It is assumed that these measurements on the host vehicle are reliable; only GPS is assumed unreliable.

system with a fixed N is evaluated for scenario classification.

Doppler Profile Envelope (β)

Let F_{D_i} be the i-th Doppler spectrum after performing a windowed STFT and correcting for CFO using the alignment technique discussed previously. Doppler energy could appear in the positive Doppler bins, $F_{D_i}^{+}$, or negative Doppler bins, $F_{D_i}^{-}$ (0Hz Doppler bin is ignored and assumed to contain the carrier energy). A threshold, Λ_E, is set to determine if the Doppler energy within F_{D_i} is worth processing. If $\max\left(F_{D_i}\right) > \Lambda_E$, then the preprocessing locates the Doppler bin with the strongest reflection energy that exists within $F_{D_i}^{+}$ and $F_{D_i}^{-}$. Within the positive and negative Doppler bins, the Doppler bin that contains energy greater than an energy threshold E_{thresh} is selected as the maximum Doppler bin within the positive bins and within negative bins for the i-th Doppler spectrum. This operation can be described as

$$\begin{aligned} f_{max_i}^{+} &= \max_i \left(F_{D_i}^{+} > E_{thresh}\right) \\ f_{max_i}^{-} &= \max_i \left(F_{D_i}^{-} > E_{thresh}\right) \end{aligned} \tag{6.9}$$

After performing this operation on each STFT window from the beginning of the capture until the N-th Doppler spectrum, the vectors below can be defined as

$$\begin{aligned} \mathbf{f_D^{+}} &= \left(f_{max_1}^{+} f_{max_2}^{+} \cdots f_{max_N}^{+}\right) \\ \mathbf{f_D^{-}} &= \left(f_{max_1}^{-} f_{max_2}^{-} \cdots f_{max_N}^{-}\right) \end{aligned} \tag{6.10}$$

whose elements contain the frequency bin that matched the criteria from eq. (6.9) for every Doppler window from $i = (1...N)$.

After visually inspecting the trends in these vectors for each driving scenario, a numerical description was defined to capture the DPE heuristic that separates the different driving scenarios. Specifically, a curve is fit between $\mathbf{f_D^{+}}$ and $\mathbf{f_D^{-}}$ defined as $\mathbf{C}^{+}$ and $\mathbf{C}^{-}$, respectively. The analytic description of the DPE heuristic is defined numerically as four separate

features based on the trend lines $\mathbf{C}^+$ and $\mathbf{C}^-$ as

$$\begin{aligned} +\mathbf{f}^{\zeta}_{\mathbf{D}\beta} &= \frac{d\mathbf{C}^+}{dt} \\ -\mathbf{f}^{\zeta}_{\mathbf{D}\beta} &= \frac{d\mathbf{C}^-}{dt} \\ +\mathbf{f}^{\varepsilon}_{\mathbf{D}\beta} &= \left|\mathbf{f}^{+}_{\mathbf{D}} - \mathbf{C}^+\right| \\ -\mathbf{f}^{\varepsilon}_{\mathbf{D}\beta} &= \left|\mathbf{f}^{-}_{\mathbf{D}} - \mathbf{C}^-\right| \end{aligned} \tag{6.11}$$

where $+\mathbf{f}^{\zeta}_{\mathbf{D}\beta}$ and $-\mathbf{f}^{\zeta}_{\mathbf{D}\beta}$ describe the slope of the DPE, and $+\mathbf{f}^{\varepsilon}_{\mathbf{D}\beta}$ and $-\mathbf{f}^{\varepsilon}_{\mathbf{D}\beta}$ describe the error from each $f^{+}_{max_i}$ and $f^{-}_{max_i}$ to their associated fit curve instances C^{+}_{i} and C^{-}_{i}. The set of observation vectors

$$DPE : \left\langle +\mathbf{f}^{\zeta}_{\mathbf{D}\beta}, -\mathbf{f}^{\zeta}_{\mathbf{D}\beta}, +\mathbf{f}^{\varepsilon}_{\mathbf{D}\beta}, -\mathbf{f}^{\varepsilon}_{\mathbf{D}\beta} \right\rangle \tag{6.12}$$

becomes the numerical description of the DPE heuristic. The slope ζ is tracked for temporal changes so that the rises, plateaus, and falls in the DPE can be described numerically, and temporal changes in the Euclidean fit error ε are also tracked to differentiate between scenarios that may inherently be more difficult to fit trend lines, such as in SCP compared to RFC. The identified DPE traces in Figure 6.10 capture the overall vehicle dynamics between the two vehicles. The features $+\mathbf{f}^{\zeta}_{\mathbf{D}\beta}$ and $-\mathbf{f}^{\zeta}_{\mathbf{D}\beta}$ track the temporal changes in DPE for their respective ranges since tracking slope removes the dependence on raw Doppler bin values. Recalling that for different relative speeds the Doppler profile can be scaled, further emphasizes the need for tracking DPE and RE without relying on raw values for Doppler bin or illumination intensity. For example, in Figure 6.10 the vectors $+\mathbf{f}^{\varepsilon}_{\mathbf{D}\beta}$ and $-\mathbf{f}^{\varepsilon}_{\mathbf{D}\beta}$ would exhibit low variability from $0 < t < 26$ seconds and then increase as soon as the DPE disappears indicating that the vehicles have stopped. For machine learning models, unique numerical trends like these help to differentiate between the type of driving scenario.

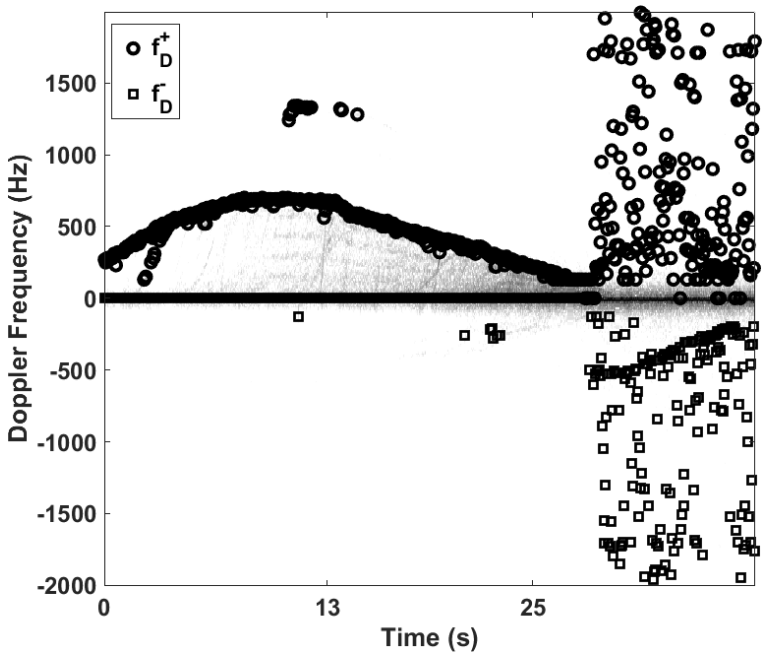

Figure 6.10: RFCfast Doppler profile with overlaid DPE traces for positive and negative Doppler bins.

Reflection Entropy (ρ)

The concept of spectrogram entropy is identified and expressed analytically. Entropy was also identified by [100] for their use case. For this dissertation work, RE is defined by a different definition to better represent the Doppler profile observations in the V2V context. The RE heuristic is numerically defined as the number of Doppler bins appearing further than R bins away from the 0Hz Doppler bin and that feature a normalized magnitude greater than a threshold P_{thresh}. First, the i-th Doppler spectrum is normalized as

$$\tilde{F}_{D_i} = \frac{F_{D_i}}{\max\left(F_{D_i}\right)} \tag{6.13}$$

Next, using the index k from eq. (6.7) to represent the k-th Doppler bin from the 0Hz Doppler bin in the i-th Doppler spectrum, let K be the furthest Doppler bin away from 0Hz Doppler in the i-th Doppler spectrum. Hence, $i = (1...N)$ and $k = (0...K)$ creates a two-dimensional representation of the positive bins and negative bins of the Doppler spectrum

as

$$\tilde{\mathbf{F}}^{+}_{\mathbf{D_{i,k}}} = \begin{bmatrix} \tilde{F}^{+}_{D_{1,0}} & \cdots & \tilde{F}^{+}_{D_{1,K}} \\ \vdots & \ddots & \vdots \\ \tilde{F}^{+}_{D_{N,0}} & \cdots & \tilde{F}^{+}_{D_{N,K}} \end{bmatrix}$$
$$\tilde{\mathbf{F}}^{-}_{\mathbf{D_{i,k}}} = \begin{bmatrix} \tilde{F}^{-}_{D_{1,0}} & \cdots & \tilde{F}^{-}_{D_{1,K}} \\ \vdots & \ddots & \vdots \\ \tilde{F}^{-}_{D_{N,0}} & \cdots & \tilde{F}^{-}_{D_{N,K}} \end{bmatrix} \tag{6.14}$$

where $0 \leq \tilde{F}^{+}_{D_{i,k}} \leq 1$ and $0 \leq \tilde{F}^{-}_{D_{i,k}} \leq 1$, because of the normalization operation. If $2K$ is odd, then the first column in both matrices are equal, since they both are the carrier energy within a Doppler spectrum[8].

The subset of $\tilde{\mathbf{F}}^{+}_{\mathbf{D_{i,k}}}$ and $\tilde{\mathbf{F}}^{-}_{\mathbf{D_{i,k}}}$ for $k = (R+1...K)$ as $\tilde{\mathbf{F}}^{+}_{\mathbf{D_{i,R}}}$ and $\tilde{\mathbf{F}}^{-}_{\mathbf{D_{i,R}}}$, respectively are defined. The value of R can be set greater than the Doppler bin associated with $12B$ to ensure that energy spreading near the carrier wave caused by device or channel impairments are not factored into the RE measurement. The number of subset Doppler bins that surpass the threshold is counted to obtain the values

$$f^{+}_{\rho_i} = \sum_{i}^{N} \left[\tilde{\mathbf{F}}^{+}_{\mathbf{D_{i,R}}} > P_{thresh} \right]$$
$$f^{-}_{\rho_i} = \sum_{i}^{N} \left[\tilde{\mathbf{F}}^{-}_{\mathbf{D_{i,R}}} > P_{thresh} \right] \tag{6.15}$$

where

$$[W] = \begin{cases} 1 & \text{if } W \text{ is true;} \\ 0 & \text{if } W \text{ is false;} \end{cases} \tag{6.16}$$

Eqs. (6.15) represent (for both positive and negative subsets) the number of Doppler bins in the i-th Doppler spectrum that have Doppler reflection energy. Note that the DPE bin is included in RE count, since RE is dependent on the DPE trend (i.e. strongest reflection). This is valid except for faster moving scatterer traces that may contribute unnecessary bins

[8]Strongest energy is more than likely located at the 0Hz Doppler bin for a single Doppler spectrum.

into the RE count. However, faster moving scatterers contribute fewer Doppler bins than the RE count expected between the 0Hz Doppler bin and the DPE bin. Therefore, any RE contribution due to faster moving scatterer traces are considered negligible. Across all scenarios the number of Doppler bins with reflection energy increases as the vehicles approach each other since the Doppler reflection power is more likely to be received. It is cautioned to the reader to not interpret this as increasing distortion energy due to spatial proximity, because most Doppler reflection energy can be found between the DPE bin and 0Hz Doppler bin (see Figure 6.10). In ODT scenarios there is also RE energy that appears above the DPE closer to the crossing point. This RE is specific to ODT and further helps differentiate it from the other driving scenarios. Therefore, the entropy included in the RE count can be attributed solely to the unique scattering environment around and between the vehicles.

Observing the measurements of eqs. (6.15) from the first STFT to the N-th STFT, defines the arrays

$$\begin{aligned} \mathbf{f}_{\rho}^{+} &= \left(f_{\rho_1}^{+}, f_{\rho_2}^{+}, \cdots f_{\rho_N}^{+}\right) \\ \mathbf{f}_{\rho}^{-} &= \left(f_{\rho_1}^{-}, f_{\rho_2}^{-}, \cdots f_{\rho_N}^{-}\right) \end{aligned} \tag{6.17}$$

Similar to the DPE analytic description, a curve is fit between $\mathbf{f}_{\rho}^{+}$ and $\mathbf{f}_{\rho}^{-}$ that is defined as $\mathbf{C}_{\rho}^{+}$ and $\mathbf{C}_{\rho}^{-}$, respectively. The RE heuristic is also defined numerically as four separate features based on these trend lines as

$$\begin{aligned} +\mathbf{f}_{\mathbf{D}\rho}^{\zeta} &= \frac{d\mathbf{C}_{\rho}^{+}}{dt} \\ -\mathbf{f}_{\mathbf{D}\rho}^{\zeta} &= \frac{d\mathbf{C}_{\rho}^{-}}{dt} \\ +\mathbf{f}_{\mathbf{D}\rho}^{\varepsilon} &= \left|\mathbf{f}_{\rho}^{+} - \mathbf{C}_{\rho}^{+}\right| \\ -\mathbf{f}_{\mathbf{D}\rho}^{\varepsilon} &= \left|\mathbf{f}_{\rho}^{-} - \mathbf{C}_{\rho}^{-}\right| \end{aligned} \tag{6.18}$$

where $+\mathbf{f}_{\mathbf{D}\rho}^{\zeta}$ and $-\mathbf{f}_{\mathbf{D}\rho}^{\zeta}$ describe the slope of the RE, and $+\mathbf{f}_{\mathbf{D}\rho}^{\varepsilon}$ and $-\mathbf{f}_{\mathbf{D}\rho}^{\varepsilon}$ describe the error from each $f_{\rho_i}^{+}$ and $f_{\rho_i}^{-}$ to their associated fit curve instances $C_{\rho_i}^{+}$ and $C_{\rho_i}^{-}$. The set of observation vectors

$$RE : \left\langle +\mathbf{f}_{\mathbf{D}\rho}^{\zeta}, -\mathbf{f}_{\mathbf{D}\rho}^{\zeta}, +\mathbf{f}_{\mathbf{D}\rho}^{\varepsilon}, -\mathbf{f}_{\mathbf{D}\rho}^{\varepsilon} \right\rangle \tag{6.19}$$

becomes the final numerical description of the RE heuristic. Temporal changes in the slope ζ and error ε are tracked, based on visual inspection of how the RE heuristic can be unique across different scenarios. For example, the RE can appear much higher near the crossing

point for ODT compared to the RE appearing to decrease in RFC.

Considering the related work in [100] that developed a different interpretation of entropy, the definition for this dissertation work is based on the Doppler profile. A direct comparison to their entropy definition is moot, since the authors obtained spectrograms using a static coherent radar that tracked the LOS carrier wave illuminating various moving targets. The spectrograms of this dissertation work are obtained from an incoherent observation of the NLOS reflections due to roadway environments and vehicle dynamics.

In summary, nine features are tracked for numerically representing the Doppler profiles for classifying the pre-crash scenario. Four represent the DPE, four represent the RE, and the observation time represented by the number of STFT windows that have passed. A feature ranking analysis revealed that each feature is equally important to the overall performance of the classification system. This was also confirmed by visually inspecting the feature set across the different driving scenarios. The analytic descriptions presented are the first for incoherent spectrogram analysis between two vehicles maneuvering. This work is significantly differentiated from WiSee, where classification was based on gesture movements assigned to a subspace of $\langle -1, +1, 2 \rangle$ (See [94, Section 3.2]) representing movement toward, away, or neutral.

The nine-column feature set just described is one realization of what a feature set could be for the Doppler profile. This feature set could also be useful for other applications yet to be investigated. In machine learning, it is important to consider many different features that could be attributed to the classification objective. The collision avoidance feature set to be described next employs a more rigorous selection process based on the DPE and RE heuristics.

6.6.3 Feature Analysis Part II: Collision Classification

Extending the feature descriptions from driving scenario classification, collision classification requires a more rigorous approach due to the importance of real time collision avoidance. It can be argued that the collision classification feature set is the most important set within the sub-system, due to the safety of life objective. Therefore, the feature set considers a range of descriptions beyond the visual inspection conducted for the driving scenario classification. While still using the heuristics of DPE and RE, their definitions are further refined. The real world DSRC Doppler phenomenon during a collision is presented in Figure 6.11 and Figure 6.12.

The Doppler profile for collisions is represented as a spectrogram with the y-axis as the

Doppler bin from the carrier wave, and the x-axis as either the time to collision (TTC) or time until a safe event. The plots for the safe outcomes are focused versions of the plots from Figure 6.7, to follow Axiom 1 such that only positive Doppler bins are of interest since the primary objective is to predict car collisions before they occur[9]. This includes not raising false alarms when an outcome is safe.

The objective of this feature analysis is to leverage Axiom 1 through the Doppler effect with the assistance of machine learning classification algorithms. Specifically, numerical characteristics in individual Doppler spectra (through the DPE and RE heuristics) are exploited to extract meaningful information indicative of a collision. Extracting features per Doppler spectra allows implementing the collision avoidance method in real time. This approach also has the advantage of not assuming *a prior* knowledge of the channel, nor positional and velocity information of C_{Tx} through SMs; the sub-system only observes the Doppler profile in real time to predict if a collision will occur. For SCP scenarios, the number of reflectors in the environment determines how soon Doppler intensity is detectable. Hence, the earliest time prior to an SCP collision where the Doppler profile is meaningful may occur more often in city rather than residential environments.

Safe travel can also be revealed early on depending on lane spacing. Observing the ODT Figure 6.11c, the DPE and RE in four lanes shows a downward sloping trend that begins around 1.3s prior to the crossing point. Whereas the DPE and RE in ODT one lane can appear like an ODT head-on collision because the lateral spacing of 3.6m for an average roadway is not far enough to cause a significant dip in the RE trend. In these situations, the RE can help distinguish between one lane and a head-on collision in ODT since the reflection intensity is clearly different at different points in the approach regardless of other scatterers in the environment.

As described earlier, the Doppler shift can serve as a proxy to the relative velocity between two DSRC equipped vehicles. A Doppler shift less than or equal to zero is (per Axiom 1) not possible to result in a collision. Recalling eq. (6.7) it is expected that the relative velocity prior to a collision is always positive due to the addition of the individual velocity components. The relative velocity (i.e. closing velocity or range-rate) is the addition of individual velocity vectors from C_{Tx} and C_{Rx} in the direction of θ. Except for the SCP scenarios where θ has no meaning to the velocity during NLOS. Thus, angles of departure and arrival are preferred to generalize the Doppler profile. The Doppler profiles validate the collision theory of chapter 5 since the negative Doppler bins do not exhibit

[9]The negative Doppler bins either did not have significant energy content, or the negative energy content was gathered near the 0Hz Doppler bin.

(a) ODT Collision (Head-On)

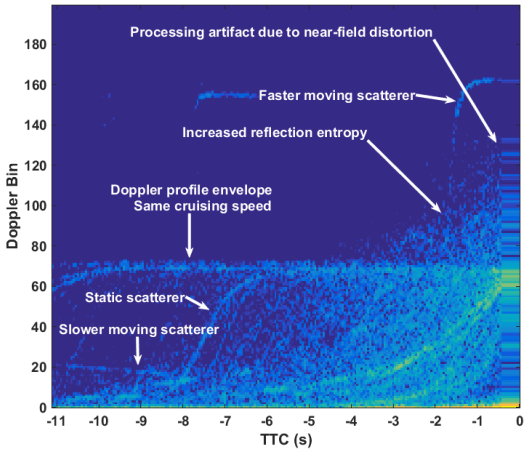

(b) ODT Safe: One Lane Separation

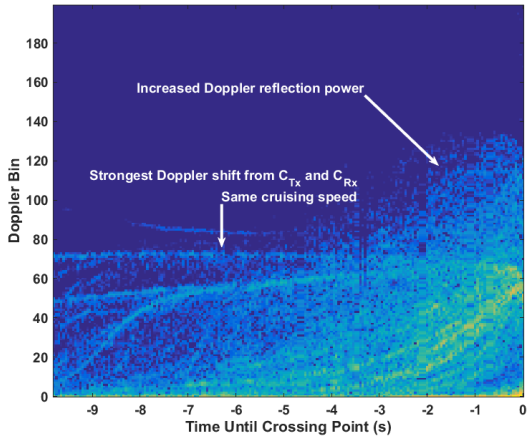

(c) ODT Safe: Four Lane Separation

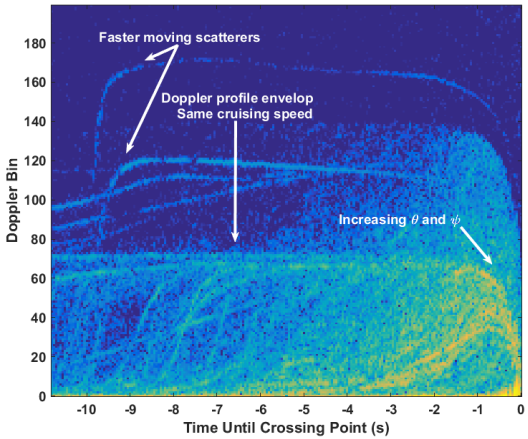

(d) Alt-ODT Collision

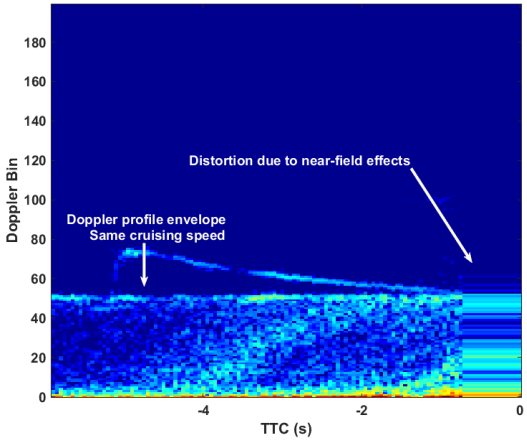

(e) Alt-ODT Safe: One Lane Separation

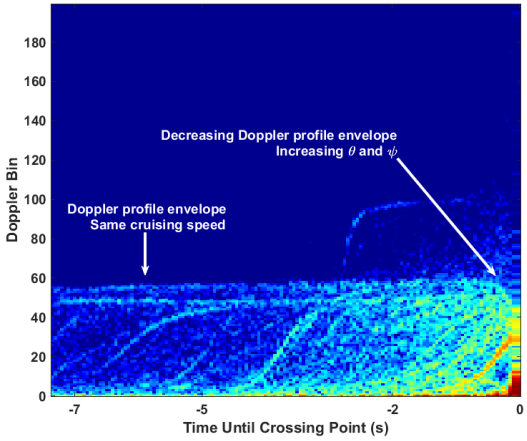

(f) Color Bar

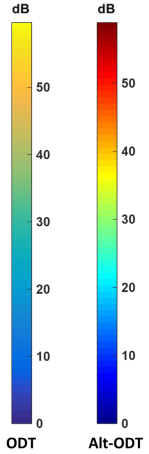

Figure 6.11: Doppler profile for ODT and Alt-ODT pre-crash scenarios in collision (a)(d) and safe (b)(c)(e) outcomes.

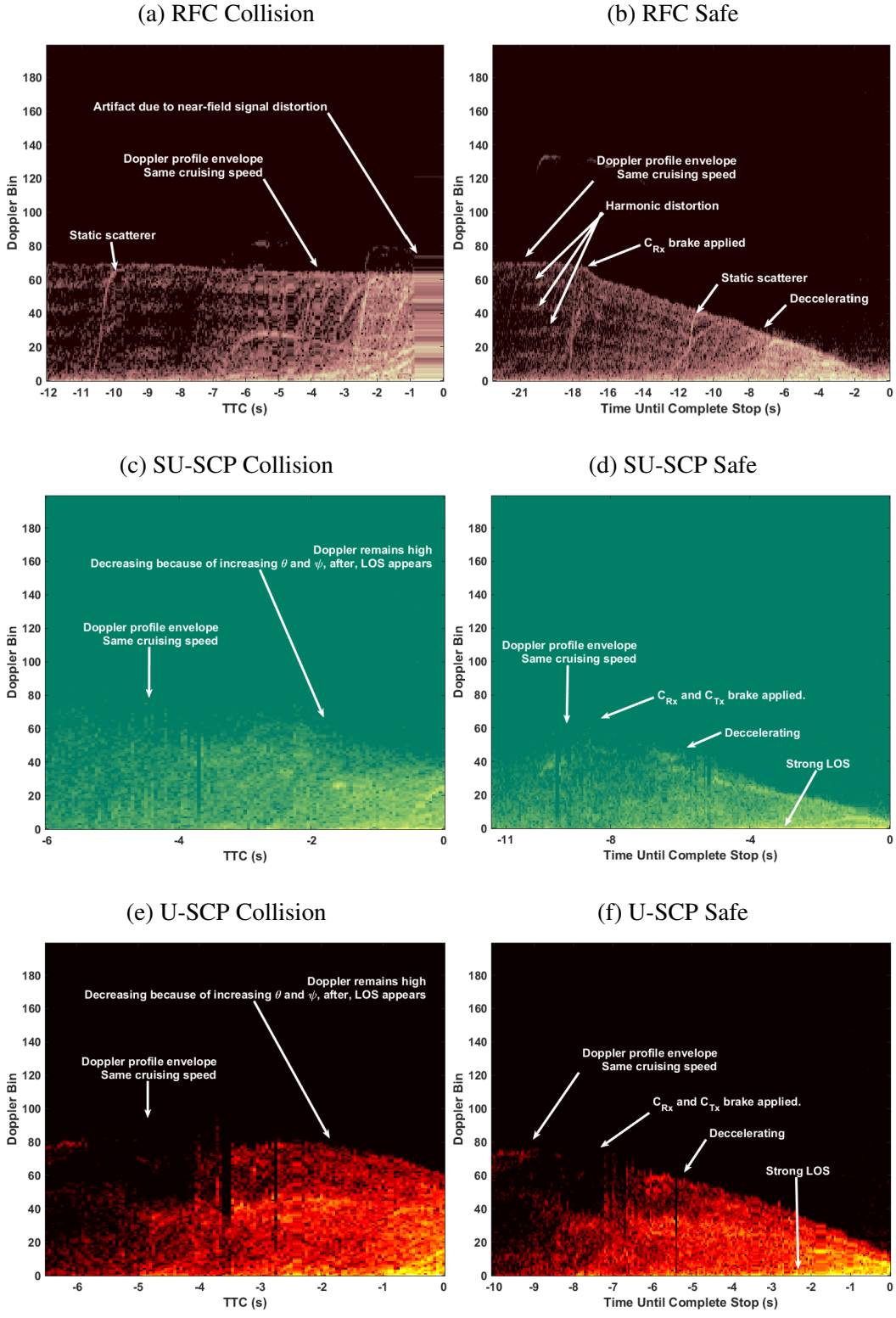

Figure 6.12: Doppler profile for RFC, SU-SCP, and U-SCP pre-crash scenarios in collision (a)(c)(e) and safe (b)(d)(f) outcomes.

significant Doppler energy. Furthermore, the LOS Doppler trends are validated by the DPE and RE trends. This is supported by the observation in Figure 6.11c where both DPE and RE descend toward the 0Hz Doppler bin for a safe/normal outcome. This is the same behavior that the LOS Doppler shift would exhibit. In a collision outcome, the DPE remains flat which is predicted by the collision theory. Incredibly, this trend is also observable in both SCP collision outcomes during NLOS conditions, compared to their respective safe outcomes. This is due to the reflection geometry described from Figure 6.9 inducing a Doppler effect as if the vehicles were approaching each other in LOS. This is another key exploit of terrestrial V2V that enables the ADS method for providing collision avoidance in NLOS.

6.6.4 Collision Classification: Feature Description

Considering the aggregate response of the Doppler profile due to all dynamic and environmental effects, the heuristics identified previously as DPE and RE need to have a more reliable numerical representation to employ machine learning into the collision prediction. Relationships between the DPE and RE features are also considered which could provide more insight into discernable nuances between collision and safe outcomes. Additionally, cepstral coefficients calculated per Doppler spectra, not the entire Doppler profile, are also considered for feature extraction. The collision classification feature set is now described analytically.

Carrier Bin Magnitude ($E_{i,0}$)

Let $I_{i,k}$, be the illumination intensity of the k-th Doppler shift in the i-th Doppler spectrum following the windowed STFT and CFO correction operations. With $0 \leq k \leq K$, the 0Hz Doppler bin (carrier bin) magnitude is calculated as

$$E_{i,0} = 20 \log_{10}(I_{i,0}) \tag{6.20}$$

DPE Bin (k_{DPE})

The carrier wave is spread in frequency due to the translation of the vehicles [108, Example 10-24], and thus influences neighboring reflection bins which can mask reflection content caused by smaller Doppler shifts. Therefore R still represents the Doppler bin number that separates the carrier and reflection content of the Doppler spectra. To limit the effects of noisy Doppler measurements at far distances, the log magnitude of $I_{i,k}$ for $R < k \leq K$ as

$E_i = 20\log_{10}(I_{i,k})$ is applied then normalize with $\hat{E}_i = \frac{E_i}{\max(E_i)}$. The DPE bin location can be estimated by performing

$$k_{DPE} = \max_k \left(\hat{E}_{i,k} > E_{thresh}\right) \tag{6.21}$$

where $0 \leq E_{thresh} \leq 1$ is a threshold parameter for locating the DPE.

Ranges of the Doppler spectra bins can be defined that are segmented by k_{DPE} and R, such as the range of upper Doppler bins above the DPE as

$$U \in k_{DPE} + 1, ..., K \tag{6.22}$$

and lower Doppler bins below the DPE as

$$L \in R + 1, ..., k_{DPE} - 1 \tag{6.23}$$

Furthermore, the number of bins within these ranges can be defined as

$$N_U = K - k_{DPE} + 1 \tag{6.24}$$

$$N_L = k_{DPE} - R + 1 \tag{6.25}$$

For clarity, Figure 6.13 illustrates the segmentation of each Doppler spectra that makes up the Doppler profile.

RE Count (N_ρ)

Like the driving scenario feature analysis, the representation of the RE heuristic is to count the number of reflection bins that are above E_{thresh}

$$N_\rho = \sum_{k=R+1}^{K} \left[\hat{E}_{i,k} > E_{thresh}\right] \tag{6.26}$$

where

$$[W] = \begin{cases} 1 & \text{if } W \text{ is true;} \\ 0 & \text{if } W \text{ is false;} \end{cases} \tag{6.27}$$

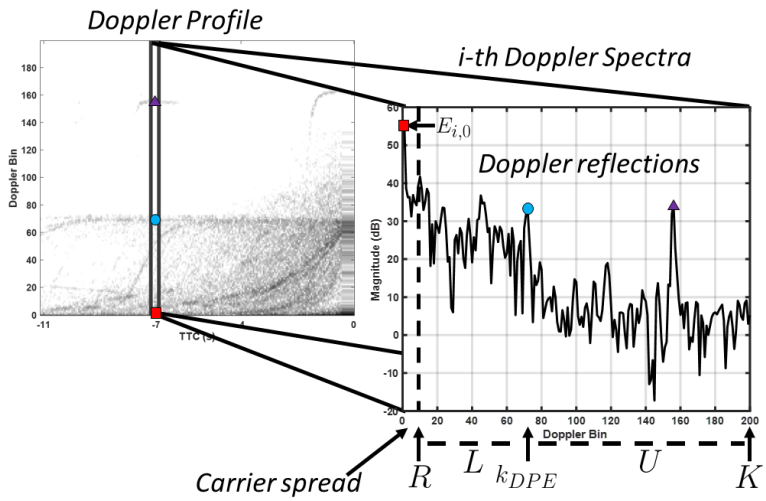

Figure 6.13: Segmentation of Doppler spectra by R, k_{DPE}, and K.

this feature also includes the DPE bin into the count. The reasoning by this method is that more entropy will have more reflection bins with greater intensity.

Relational Features

From the previous definitions, additional features of interests can help capture nuance relationships between features. These are briefly identified below as

Estimate of C_{Tx} speed:

$$\widehat{S}_{T_x} = |\frac{k_{DPE}\lambda}{T_w} - S_{R_x}| \tag{6.28}$$

RE count in L:

$$N_{L_\rho} = \sum_{k=R+1}^{k_{DPE}-1} \left[\hat{E}_{i,k} > E_{thresh}\right] \tag{6.29}$$

RE count in U:

$$N_{U_\rho} = \sum_{k=k_{DPE}+1}^{K} \left[\hat{E}_{i,k} > E_{thresh}\right] \tag{6.30}$$

Average magnitude in L

$$\tilde{E}_L = \frac{\sum 20\log_{10}(I_{i,L})}{N_L} \tag{6.31}$$

Average magnitude in U

$$\tilde{E}_U = \frac{\sum 20\log_{10}(I_{i,U})}{N_U} \tag{6.32}$$

Difference between lower and upper magnitude:

$$\Delta\tilde{E}_{LU} = \tilde{E}_L - \tilde{E}_U \tag{6.33}$$

Magnitude of DPE bin:

$$E_{DPE} = 20\log_{10}(I_{i,k_{DPE}}) \tag{6.34}$$

Difference between DPE and carrier magnitude:

$$\Delta E_0 = E_{DPE} - E_{i,0} \tag{6.35}$$

Difference between DPE and lower magnitude:

$$\Delta E_L = E_{DPE} - \tilde{E}_L \tag{6.36}$$

Difference between DPE and upper magnitude:

$$\Delta E_U = E_{DPE} - \tilde{E}_U \tag{6.37}$$

Difference between DPE magnitude and lower with upper:

$$\Delta E_{total} = E_{DPE} - (\tilde{E}_L + \tilde{E}_U) \tag{6.38}$$

Average magnitude of reflections:

$$\tilde{E}_{refl} = \frac{\sum_{k=R+1}^{K} 20\log_{10}(I_{i,k})}{K-R} \tag{6.39}$$

Difference between lower magnitude and all reflections:

$$\Delta\tilde{E}_{Lrefl} = \tilde{E}_L - \tilde{E}_{refl} \tag{6.40}$$

Difference between upper magnitude and all reflections:

$$\Delta\tilde{E}_{Urefl} = \tilde{E}_U - \tilde{E}_{refl} \tag{6.41}$$

Cepstral Features

In addition to the features described previously Cepstral coefficients are considered as features for their application to spectrogram analysis of cCW Doppler classification [97][109]. Though the Doppler profile is a representation of dynamic iCW Doppler, Cepstral coefficients are widely used in speech recognition because they are a numerical representation of the entire spectrogram or individual Doppler spectra, which can be useful for classification. Let the n-th Cepstral coefficient of the i-th Doppler spectra be defined by

$$c_i[n] = |IDFT\left\{\log(|I_i|^2)\right\}|^2 \tag{6.42}$$

where $IDFT\{\cdot\}$ is the inverse discrete Fourier transform, and $n \in \{0, 1, 2...\}$. Typically, only the real part of the Cepstral domain is used (i.e. $\mathbb{R}\mathrm{e}(\cdot)$ instead of the outer $|\cdot|^2$), however, because of the time-series nature of the Doppler profile the outer $|\cdot|^2$ operation is to ensure stark separation between coefficient realizations over successive Doppler spectra while disregarding the sign of their value. The size of c_i is equal to $K + 1$, but not every coefficient is necessary [109]. Typically, only the first few coefficients are useful; therefore, only the first 12 coefficients are considered.

Feature Tracking

The features identified may experience outliers that can throw off the detection performance. For example, locating the correct DPE bin is important for collision avoidance since the LOS component is not trackable. Locating the correct DPE bin reliably requires a tracking method. Let a feature be represented as an array by the place holder, y, with the first index being the oldest observation, and the last value being the most current (as extracted from the i-th Doppler spectra). An outlier criteria $\Delta\tilde{e}$ can be computed as

$$\Delta\tilde{e} = \alpha_t \frac{\sum_{n=i-N_{track}}^{i-1} y_n}{N_{track}} \tag{6.43}$$

where N_{track} is the number of previous values in y, and $0 \leq \alpha_t \leq 1$. If the current $y_i > \Delta\tilde{e}$, then an outlier has been discovered, and the average of the previous N_{track} values is used as the current value of y_i. This operation is performed for every feature identified previously, to ensure that the data is conditioned to the trends they should be following. Recalling in the driving scenario features outliers were considered negligible. For collision classification, outliers can throw off prediction performance. An illustration of this tracking operation for

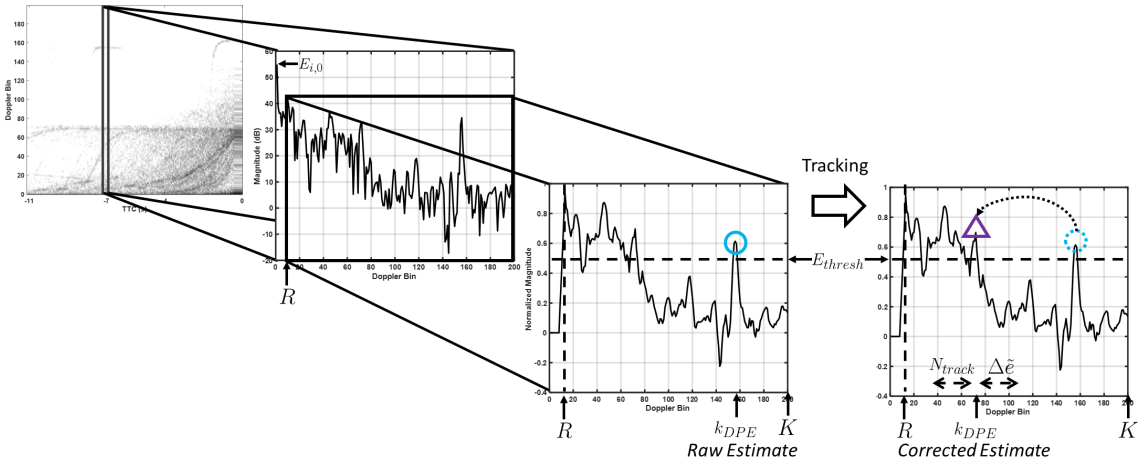

Figure 6.14: Break out operation of k_{DPE} tracking.

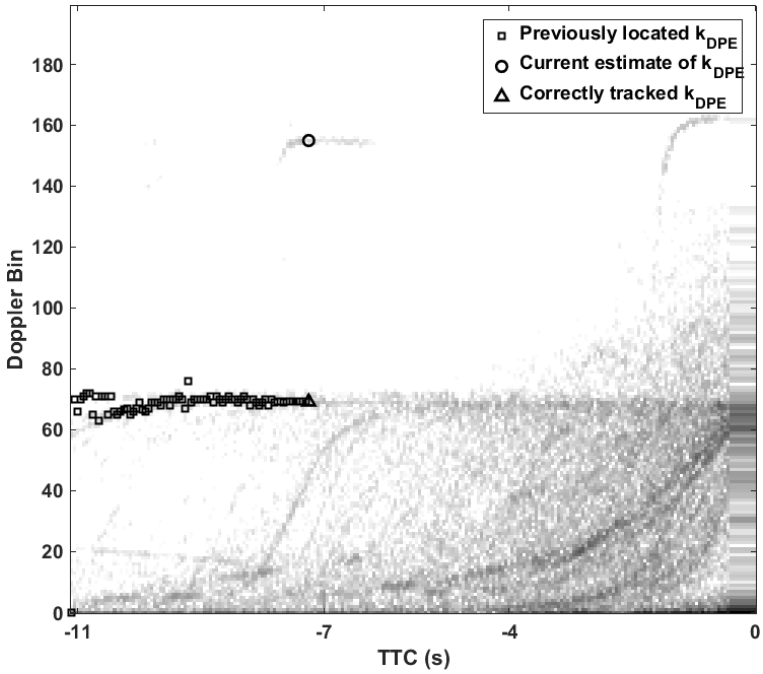

Figure 6.15: k_{DPE} tracking correctly ($N_{track} = 5$, $\alpha_t = .5$).

the k_{DPE} feature can be observed in Figures 6.14 and 6.15.

Dynamic Features

After tracking the feature, temporal derivatives and linear curve fitting errors are identified for each of the previously mentioned features including Cepstral coefficients. The purpose of the temporal derivatives is to extract the dynamic nature of the Doppler profile features. For every T_a advance of the STFT window, the Doppler spectra will change. The temporal

derivative at the i-th Doppler spectra for any feature y is taken as

$$\dot{y}(i) = \begin{cases} \frac{y(i)-y(i-1)}{T_a} & i > 1 \\ \\ 0 & i = 1 \end{cases} \tag{6.44}$$

Like the method from chapter 4, the curvature trend of the feature is considered. Specifically, the past N_{fit} STFT windows are employed for fitting a line between the previous N_{fit} samples of y including the i-th observation. The slope of the best linear fit line is then recorded for the i-th Doppler spectra. The fit error, like driving scenario features, is also considered as a feature to capture the variance of the previous N_{fit} observations which may be lower in collision outcomes compared to normal outcomes.

6.7 Machine Learning

ADS is the next advancement of PHY-based collision avoidance by providing the context of the driving scenario and collision avoidance services through machine learning. This is due to the Doppler profile capturing rich information about the environment and vehicular dynamics. ADS provides continuous 360° coverage of the host vehicle through a single roof mounted omni-antenna. Currently, no other "sensor" can achieve this level of situational awareness in LOS and NLOS. As ADS processes the baseband signal in T_a increments, the heuristics are analyzed numerically as feature sets. Diverse machine learning models form the core of the prediction engine, enabling classification of driving scenarios and collision prediction. The performance of the driving scenario classification is assessed first.

6.7.1 Driving Scenario Classification

Three popular machine learning methods for classification are studied and assessed for their performance in driving scenario classification. These methods are: k-nearest neighbors (kNN), complex decision trees (CDT), and support vector machine (SVM) [98]. Following convention, 2/3 of the data set is for training and 1/3 for validation. Each training set uses 10-fold cross-validation to protect against overfitting. After generating the training sets, assigning the appropriate classification labels, and generating test sets, the performances of the three machine learning methods are assessed. The classification models are trained using MATLAB toolboxes; some trial and error was performed to configure each model.

When testing the models, it is assumed that the receiver and transmitter begin capture from the same starting point in time. This does not provide a comprehensive assessment for every driving scenario, but it is effective for assessing the performance of the classification method as a proof of concept. Recalling that the fit curves for the DPE and RE depend on the N-th STFT window, searching for the N-th window simulates real time operation. The objectives are to understand how long ADS listens until the driving scenario is correctly identified and what factors affect its performance. Ideally the classification model would be unaffected by changes in vehicles or surroundings, and correct classification would occur as early as possible after the first signal reception.

Performance

The configuration for each of the models are presented in Table 6.2. Table 6.3 describes the sets used for each test defined in Table 6.4. The tests described in Table 6.4 are examined for the ADS ability to identify driving context using the driving scenario feature set. The first test examines general classification performance based on selecting the minimum duration of observation time needed. The best N is then used for the rest of the tests. After reporting the generic classification performance, sub-classification performance is then reported for the SCP and ODT scenarios. The effect of speed on the classification performance is also tested for ODT and RFC scenarios. Finally, overall classification using every set is reported for completeness.

Selection of N

Based on the data set, a value for a single N to classify the driving scenarios is discovered using the generic sets. Assuming all scenarios are measured from the same initial capture time, insight can be provided into how long the signal must be observed before an accurate prediction would be reliable. Recalling that the selection of N is a proxy to the total observation time, Figure 6.16 highlights that an N representing between 350 to 400 STFT windows is needed. This equates to a minimum of 17.6s to 20.1s of total observation time when using any of the models. This occurs before the crossing point in ODT and before the stopping points in RFC and SCP[10], indicating that reliable classification could occur before a unique event (e.g. crossing point, stopping point). Following the performance trend from small N to large N, improvements in the detection accuracy could be achieved if the Doppler profiles are trained based on segmentation. For example, at N=150, CDT

[10]Convoy is a continuous ebb and flow; thus, it is moot to consider the observation window.

Table 6.2: Model Configurations

Classifier	Configuration
kNN	Number of neighbors: 1; Distance metric: city block; Distance weight: equal; No standardized data.
CDT	Max splits: 200; Split criterion: Gini's diversity index; No Surrogate decision splits.
SVM	Kernel: Cubic; Box constraint level: 1; Auto Kernel scaling; Multiclass method: One-vs-One; Standardized data;

Table 6.3: Experiment Sets for Driving Scenario Classification

Set Name	Trained with:	To Classify:
Generic	ODT4fast, ODT1fast, RFCfast, SCPres, SCPcity, Convoy	ODT, RFC, SCP, CVY
LaneAll	ODT4fast, ODT1fast	ODT4, ODT1
SCPall	SCPres, SCPcity	Residential, City
Alt-ODT	N/A	ODT, CVY
Fast	ODT4fast, ODT1fast, RFCfast, Convoy	ODT, RFC, CVY
Slow	ODT4slow, ODT1slow, RFCslow, Convoy	ODT, RFC, CVY
Fast-Slow	ODT4fast, ODT1fast, RFCfast, ODT4slow, ODT1slow, RFCslow, Convoy	ODT, RFC, CVY
Total	All training sets (generic, speed, alternate)	ODT, RFC, SCP, CVY

Table 6.4: Tests for Driving Scenario Classification

Test Name	Training set	Tested with	Purpose
Selection of N	Generic	Generic	Discover N that best classifies the generic scenarios.
Lane Type	LaneAll	LaneAll	If ODT is classified, determine sub-classification of lane separation.
SCP Type	SCPall	SCPall	If SCP is classified, determine sub-classification of SCP type.
ODT Full	Generic	Alt-ODT	If ODT can be detected regardless of vehicle type or location.
Speed64	Fast	Slow	If Fast can classify Slow
Speed32	Slow	Fast	If Slow can classify Fast
CombinedSpeed	Fast-Slow	Fast-Slow	If one training set of all speeds can classify ODT and RFC.
Overall	Total	Total	If entire training set can classify all generic classes.

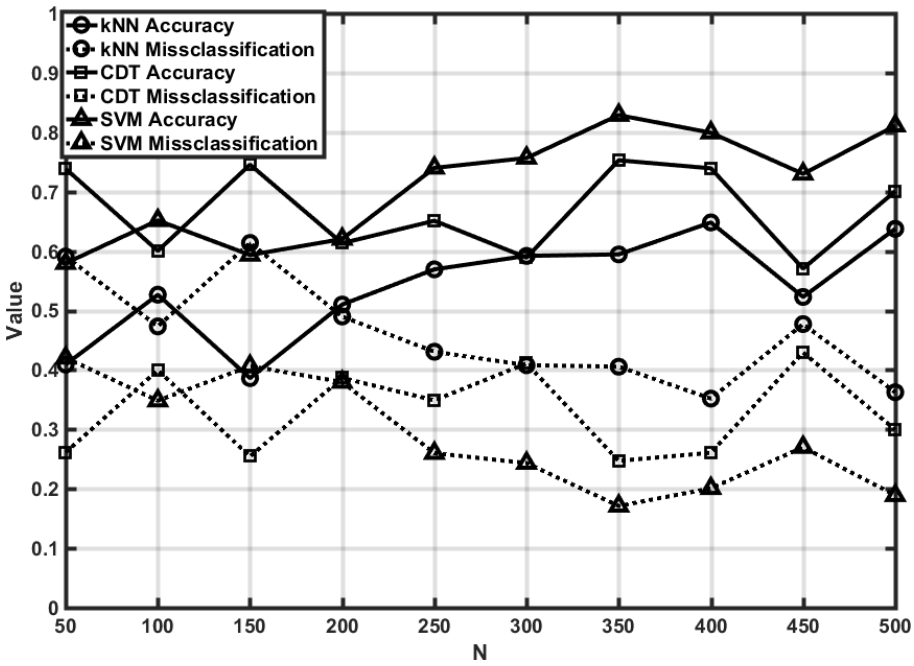

Figure 6.16: Performance of classifiers based on a fixed N.

outperforms SVM, however, longer observations could switch to using SVM to improve the performance of the system.

Figure 6.17 shows the confusion matrix of SVM for a fixed N of 350. The ODT and RFC scenarios are the most similar resulting a high rate of misclassifications. RFC doesn't appear drastically different from ODT until braking occurs, which might not occur immediately upon signal reception. Convoy performs the best because Doppler energy exists profoundly in both positive and negative bins compared to other driving scenarios.

Sub-classification

From Table 6.5, the SCP sub-classification performs very well compared to the ODT sub-classification in Table 6.6. If the generic estimation correctly identified either ODT or SCP, the SCP generic scenario is more likely to be sub-classified correctly than ODT when using the same N. The kNN model performs best for both SCP subclasses and better than SVM for ODT.

The ODT subset performance in Table 6.6 shows difficulty in identifying between lane separation. Further analysis reveals that using a lower N of 150 is better for classifying ODT subclasses, see Table 6.7. This is due to RE differences early on at the beginning of the approach. The early Doppler reflections in Figure 6.7a are at the same strength as the DPE, whereas for a similar distance in Figure 6.7b the DPE has a stronger presence over

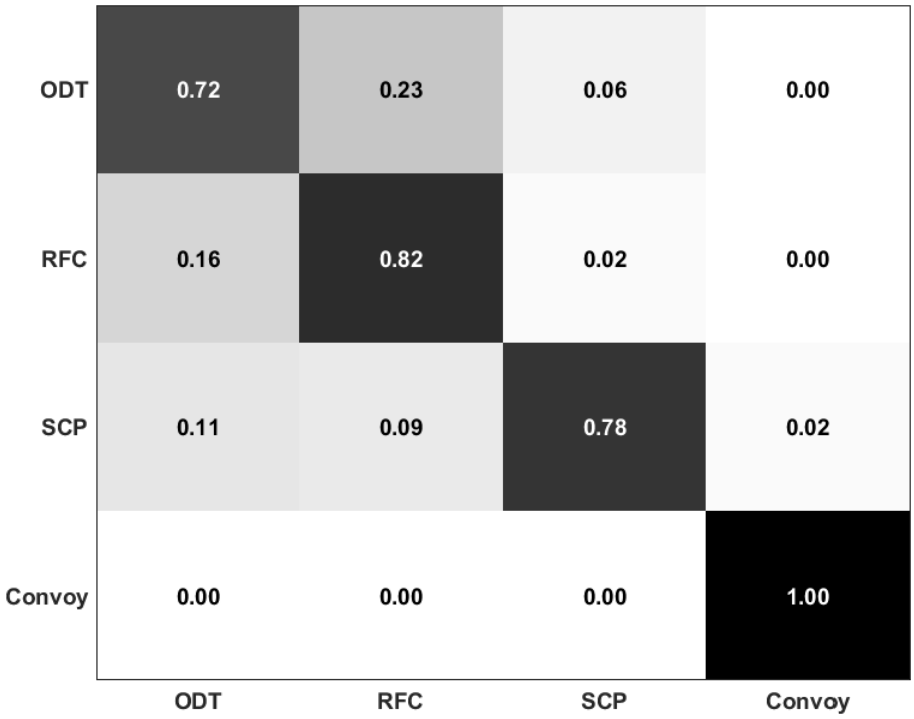

Figure 6.17: Confusion matrix for SVM with N=350. (row=true class, column=predicted class)

other reflections. Extracting more reliable lane separation from Doppler profiles is an area for optimization. Nevertheless, the results show that Doppler shift observation can provide granular details of the driving context when classifying with the appropriate model.

Effect of different location and vehicles

Table 6.8 highlights that an N of 350 may not be enough observation time to correctly identify the ODT scenario across different locations and vehicles. However, Figure 6.18 reveals that the Doppler profiles are very similar in DPE and RE heuristics. For ODT, the major factor is not the location nor vehicle bodies, but the time dynamics from the beginning of the capture. For the Alt-ODT scenario, the crossing point appears sooner

Table 6.5: Confusion Matrix of Test: SCP Type (N=350)

	kNN		CDT		SVM	
	Resi.	City	Resi.	City	Resi.	City
Residential	.90	.10	.79	.21	.75	.25
City	.11	.89	.04	.96	.13	.87

Table 6.6: Confusion Matrix of Test: ODT Type (N=350)

	kNN		CDT		SVM	
	ODT1	ODT4	ODT1	ODT4	ODT1	ODT4
$ODT1$	.21	.79	.26	.74	.16	.84
$ODT4$	.81	.19	.99	.01	.73	.27

Table 6.7: Improved Confusion Matrix of Test: ODT Type (N=150)

	kNN		CDT		SVM	
	ODT1	ODT4	ODT1	ODT4	ODT1	ODT4
$ODT1$	.64	.36	.26	.74	.16	.84
$ODT4$	.65	.35	.78	.22	.44	.56

than in the training set from the beginning of the experiment (though the cruising speeds were the same). Using a longer observation time for both training and test sets that include the unique crossing point event can substantially improve the classification performance as reported in Table 6.9, with a trade-off of not being usable for collision avoidance.

Effect of speed

The effect of speed on the classifiers across changing vehicle dynamics is now considered. The confusion matrices reported in Table 6.10, Table 6.11 and Table 6.12 indicate that a combined set performs best when compared to the individual tests. The separation between higher speeds and lower speeds for the same scenarios is apparent to the classifiers early on since an N of only 350 does not include a unique event in the slower tests. Future work recommends designing an adaptable classifier that switches between training models based on the estimated speed of C_{Tx} and the host vehicle speed.

Overall performance

Finally, the total performance of the classification using the largest training set is reported. The accuracy and false alarm percentage reported in Table 6.13 indicates that providing sub-classification can help reduce false alarms, since the largest test set doesn't perform as high as the separate performance of generic and sub-classification sets. This can be attributed to more relevant data within the sub-class training sets. Also, because of a fixed N the false alarm rates tend to be higher because of similar constant speeds trends. This can be observed between ODT and RFC which do not show differences until after the vehi-

Table 6.8: Confusion Matrix of Test: ODT Full (N=350)

	kNN				CDT				SVM			
	ODT	RFC	SCP	CVY	ODT	RFC	SCP	CVY	ODT	RFC	SCP	CVY
ODT	.46	.09	.29	.16	.38	.00	.43	.18	.28	.05	.53	.14
RFC	N/A	N/A	N/A	N/A	N/A	N/A	N/A	N/A	N/A	N/A	N/A	N/A
SCP	N/A	N/A	N/A	N/A	N/A	N/A	N/A	N/A	N/A	N/A	N/A	N/A
CVY	.18	.02	.41	.39	.00	.00	.31	.68	.00	.00	.02	.98

Table 6.9: Improved Confusion Matrix of Test: ODT Full (Trained: N=500; Tested: N=450)

	kNN				CDT				SVM			
	ODT	RFC	SCP	CVY	ODT	RFC	SCP	CVY	ODT	RFC	SCP	CVY
ODT	.63	.01	.25	.11	.81	.13	.07	N/A	.70	.01	.23	.06
RFC	N/A	N/A	N/A	N/A	N/A	N/A	N/A	N/A	N/A	N/A	N/A	N/A
SCP	N/A	N/A	N/A	N/A	N/A	N/A	N/A	N/A	N/A	N/A	N/A	N/A
CVY	.39	.00	.50	.11	.01	.15	.84	N/A	.01	.00	.04	.95

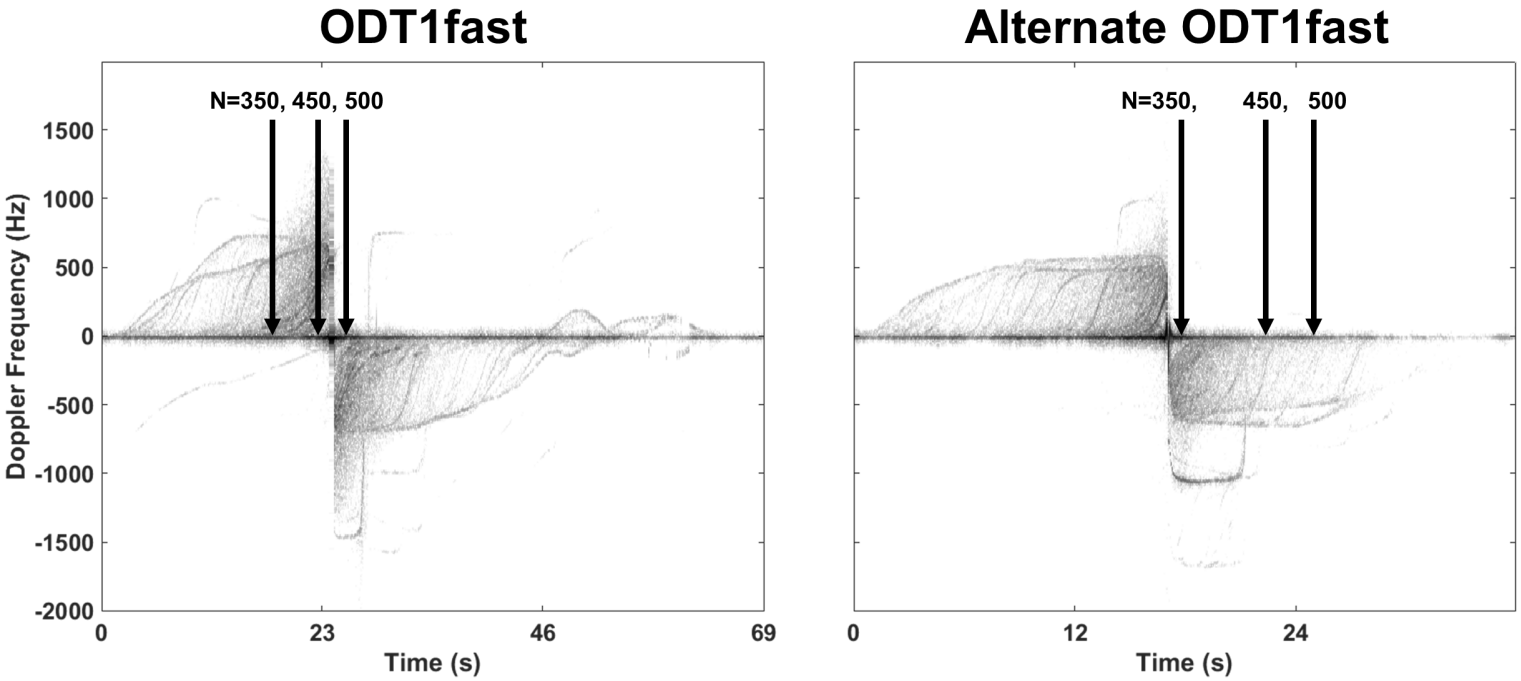

Figure 6.18: Comparison of ODT1fast to alternate ODT1fast location with different vehicles.

Table 6.10: Confusion Matrix of Test: Speed64 (N=350)

	kNN				CDT				SVM			
	ODT	RFC	SCP	CVY	ODT	RFC	SCP	CVY	ODT	RFC	SCP	CVY
ODT	.52	.29	N/A	.82	.58	.29	N/A	.13	.69	.26	N/A	.05
RFC	.47	.53	N/A	.00	.67	.33	N/A	.00	.35	.65	N/A	.00
SCP	N/A	N/A	N/A	N/A	N/A	N/A	N/A	N/A	N/A	N/A	N/A	N/A
CVY	.18	.00	N/A	.82	.00	.00	N/A	1.0	.00	.00	N/A	1.0

Table 6.11: Confusion Matrix of Test: Speed32 (N=350)

	kNN				CDT				SVM			
	ODT	RFC	SCP	CVY	ODT	RFC	SCP	CVY	ODT	RFC	SCP	CVY
ODT	.79	.15	N/A	.06	.51	.48	N/A	.01	.25	.73	N/A	.02
RFC	.75	.24	N/A	.01	.89	.11	N/A	.00	.38	.59	N/A	.03
SCP	N/A	N/A	N/A	N/A	N/A	N/A	N/A	N/A	N/A	N/A	N/A	N/A
CVY	.20	.07	N/A	.73	.03	.00	N/A	.97	.00	.00	N/A	1.0

Table 6.12: Confusion Matrix of Test: CombinedSpeed (N=350)

	kNN				CDT				SVM			
	ODT	RFC	SCP	CVY	ODT	RFC	SCP	CVY	ODT	RFC	SCP	CVY
ODT	.74	.21	N/A	.05	.83	.17	N/A	.00	.76	.24	N/A	.00
RFC	.44	.56	N/A	.00	.53	.47	N/A	.00	.38	.62	N/A	.00
SCP	N/A	N/A	N/A	N/A	N/A	N/A	N/A	N/A	N/A	N/A	N/A	N/A
CVY	.22	.05	N/A	.73	.03	.00	N/A	.97	.00	.00	N/A	1.0

Table 6.13: Confusion Matrix of Test: Overall (N=350)

	kNN				CDT				SVM			
	ODT	RFC	SCP	CVY	ODT	RFC	SCP	CVY	ODT	RFC	SCP	CVY
ODT	.77	.09	.12	.01	.82	.08	.09	.00	.82	.11	.06	.01
RFC	.41	.48	.1	.00	.49	.47	.04	.00	.28	.70	.02	.00
SCP	.45	.09	.45	.00	.35	.03	.59	.03	.16	.04	.79	.00
CVY	.10	.00	.04	.85	.01	.00	.00	.98	.00	.00	.00	1.0

cles begin applying brakes in RFC. Convoy always performs the best because it is the only scenario that contains both positive and negative shifts, sometimes simultaneously. For the classifiers, this can be attributed to higher entropy measurements in both positive and negative Doppler bins compared to the other scenarios. This is an added advantage considering that convoying is likely the most typical driving scenario that may occur between two DSRC equipped vehicles. Perhaps the other scenarios can be identified more reliably with more data captures for training. Overall, the classification capability of ADS to identify the correct driving scenario exhibits an average detection rate of 82.75% and average false alarm rate of 9.71%, using a supervised SVM model. There does not exist a related work to compare to, given the specific characteristics of ADS. Further optimization could improve the performance and the feature set may perform better in a different application.

6.7.2 Collision Classification

The driving scenario feature set did not provide robust classification performance. The underperformance occurred because: 1) the feature selection was based on visual inspection, and 2) the training data size was spread thinly across four subclasses. The collision classification requires a more robust approach towards feature selection and classification to ensure driver safety, but also depends on the driving conditions (LOS vs. NLOS) being identified correctly. The 116 features for collision classification are now thoroughly assessed to identify the most influential features. The superiority of numerical ranking vs. visual inspection will show to be invaluable to the system performance.

Collision classification improves on the scenario classification by abstracting the driving scenario to only two classes: NLOS or LOS. SCP are grouped as NLOS, and ODT and RFC are grouped into LOS. Convoy is not considered for collision classification, however, the original nine features for identifying convoy driving performed perfectly. Dividing the driving scenario classification into only two classes creates larger training sets which can improve performance. Once the driving scenario is determined, the collision classification can then be discerned using a more focused data set. This staging approach is inspired by the SCP sub-classification tests that performed better than generic classification.

The collision classification uses three separate models defined into stages for providing a collision avoidance service. The first stage (Stage 1) classifies the driving scenario as

either NLOS or LOS. The second stage then chooses a collision classification model specific to either the NLOS (Stage 2a) or LOS (Stage 2b) driving scenarios. Stage 2 classifies observations as either COLLISION or SAFE. Therefore, three models (either kNN, CDT, or SVM) using large training sets can enable robust collision avoidance services through ADS. The collision classification is now explored for ADS.

Feature Ranking

Prior to training the models, a rigorous feature ranking process is executed to select the ten highest scoring features (for each stage) out of the 116 identified earlier. Features are ranked using the RELIEFF [110] algorithm with different configurations for the nearest neighbors parameter, and the *rankedfeatures* function in MATLAB [111] using various criteria. In total, 13 independent opinions for each classification stage are analyzed. After normalizing all feature scores across each of the 13 opinions, the ten features with the highest median score for all opinions are selected as the final recommendations for a feature set. Figure 6.19 shows the results of feature ranking for Stage 1, Stage 2a, and Stage 2b classifications. A scatter plot of the highest scoring three features for each stage is included to visually show the class separation. Stage 1 depends on DPE and carrier magnitude (which could be a proxy to RSS), Stage 2a depends on a mixture of relational features and the RE heuristic, Stage 2b depends on RE heuristics. All stages are strongly dependent on Cepstral coefficients and none of the dynamic features are useful (as they are currently defined). From the original nine features, dynamic features such as the slope of the fit curves made up most the set. It is now apparent why the driving scenario performance was not optimal though all features were verified as equally important (they were just not all optimal features). Selecting the appropriate feature set in machine learning is a challenging task, but the observable separation in class labels in each stage verifies that the features extracted can provide reliable classification for each stage. Furthermore, the Doppler profile has now been verified to display unique trends indicative of a collision and driving scenario.

Training and Test Sets

The best features from each classification stage are now used to train machine learning models. The models are configured to maximize performance. By convention 2/3 of the Doppler profile data sets are used for training and 1/3 reserved for testing. A reference data set is comprised of ODT, RFC, SU-SCP, and U-SCP captures. The Alt-ODT data set consists of a totally new environment with different vehicles and different antenna mounting

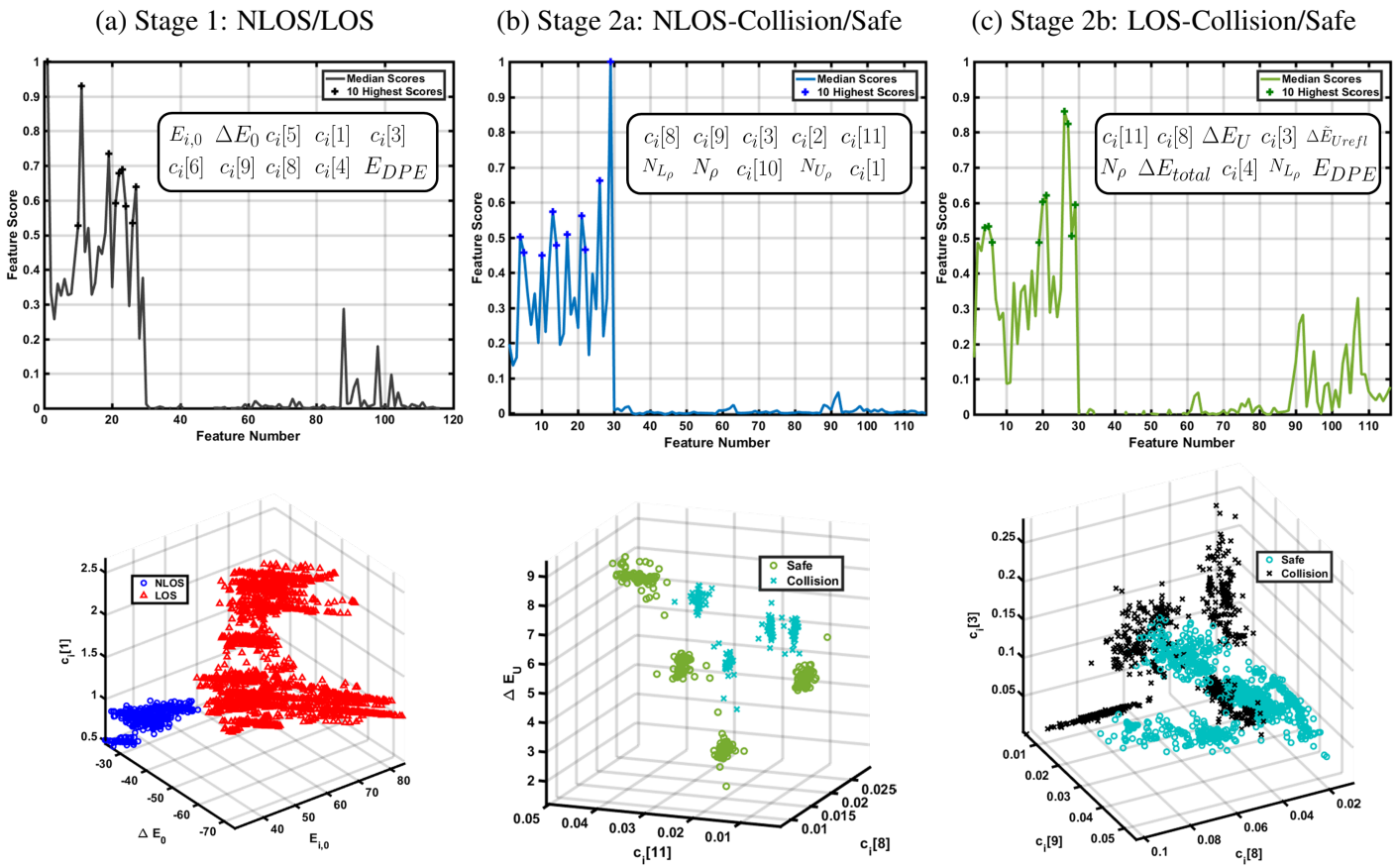

Figure 6.19: Feature selection for each classification stage showing normalized feature scores with ten highest annotated (above) and highest three plotted to show separation (below). Feature numbers: 1: $E_{i,0}$; 2: k_{DPE}; 3: $\widehat{S}_{T_x}$; 4: N_ρ; 5-17: N_{L_ρ}, N_{U_ρ}, $\tilde{E}_L$, $\tilde{E}_U$, $\Delta\tilde{E}_{LU}$, E_{DPE}, ΔE_0, ΔE_L, ΔE_U, ΔE_{total}, $\tilde{E}_{refl}$, $\Delta\tilde{E}_{Lrefl}$, $\Delta\tilde{E}_{Urefl}$; 18-29: $c_i[n]$; 30-58: temporal derivatives of features 1-29; 59-87: slope of fit line for features 1-29; 88-116: linear fit error for features 1-29.

locations for the collision outcome. The trained models from the reference set are tested for their performance when given this unknown Alt-ODT data. If the reference set performs poorly when tested with the Alt-ODT data set, then retraining the reference set by including 2/3 of the previously unknown data can help improve the classification performance. When training each model, cross-validation protects against overfitting. After generating training sets, assigning classification labels, and generating test sets, the performance of the three models are analyzed considering various configurations. The models are trained using MATLAB toolboxes and tested using custom MATLAB scripts.

Determining Feature Extraction System Parameters

The system parameters of the feature extraction are varied to determine the best performing configuration and classification model to use for Stages: 1, 2a, and 2b. All configurable parameters described earlier in the feature extraction section are recalled again in Table 6.14. A Monte Carlo simulation with fixed seed is used to assess the best performance of a classification operation. Only the experimental data which makes up the reference set is used. The best parameters and classification models are reported in Table 6.15. The performance of the best system parameters is reported in Figure 6.20 as confusion matrices. Each row is the true classification and each column is the estimated classification by the respective model identified in the last column of Table 6.15. The overall accuracy rates are very high and misclassification rates are very low for the reference set, indicating exceptional performance. The kNN model performs the best because the isolation between classes for Stage 1 and Stage 2a is very high. The CDT model is required for Stage 2b because the features are not as isolated, but segmented enough to not require an SVM.

The performance of the same system parameters and classification models trained with only the reference data set are now tested to classify observations from the entire Alt-ODT data set (i.e. data that was not used in training the models). The results shown on the left-hand side of Figure 6.21 seem to indicate that LOS collision classification may be sensitive to unknown data. The Alt-ODT set is in LOS conditions, but Stage 1 erroneously classifies 0.3% of observations as NLOS. Those three observations that were misclassified as NLOS, when passed through Stage 2a are misclassified as safe, when they resulted in a collision. However, the LOS classification performance for Stage 1 is still very high, indicating that LOS and NLOS conditions exhibit uniquely identifiable features. When the Alt-ODT test set is classified using Stage 2b, the performance takes a significant hit. However, when the classifiers are retrained with 2/3 of the Alt-ODT data set, the performance improves

Table 6.14: Feature Parameters

Feature Extraction	R, K, E_{thresh}, α_t, N_{track}, N_{fit}

Table 6.15: Best Performing Feature Extraction System Parameters ($R = 10$, $K = 200$)

	E_{thresh}	α_t	N_{track}	N_{fit}	Classification Model
Stage 1	.2	.1	10	15	kNN (k=1; Non-standard; Euclidean)
Stage 2a	10	.1	5	6	kNN (k=200; Standardized; Euclidean)
Stage 2b	.5	.3	5	10	CDT (Splits: 10)

Table 6.16: Best Performing Retrained Feature Extraction System Parameters ($R = 10$, $K = 200$)

	E_{thresh}	α_t	N_{track}	N_{fit}	Model	Feature Set
Stage 1	Unchanged					
Stage 2a	Unchanged				SVM Gaussian; Box: 1; Scale: .79; Standardized;	Unchanged
Stage 2b	.5	.1	10	20	SVM Cubic; Scale: auto; Standardized	N_{U_ρ}, $c_i[11]$, $c_i[1]$, ΔE_L, $\Delta \tilde{E}_{Lrefl}$, N_{L_ρ}, $c_i[2]$, ΔE_{total}, N_ρ, $c_i[9]$

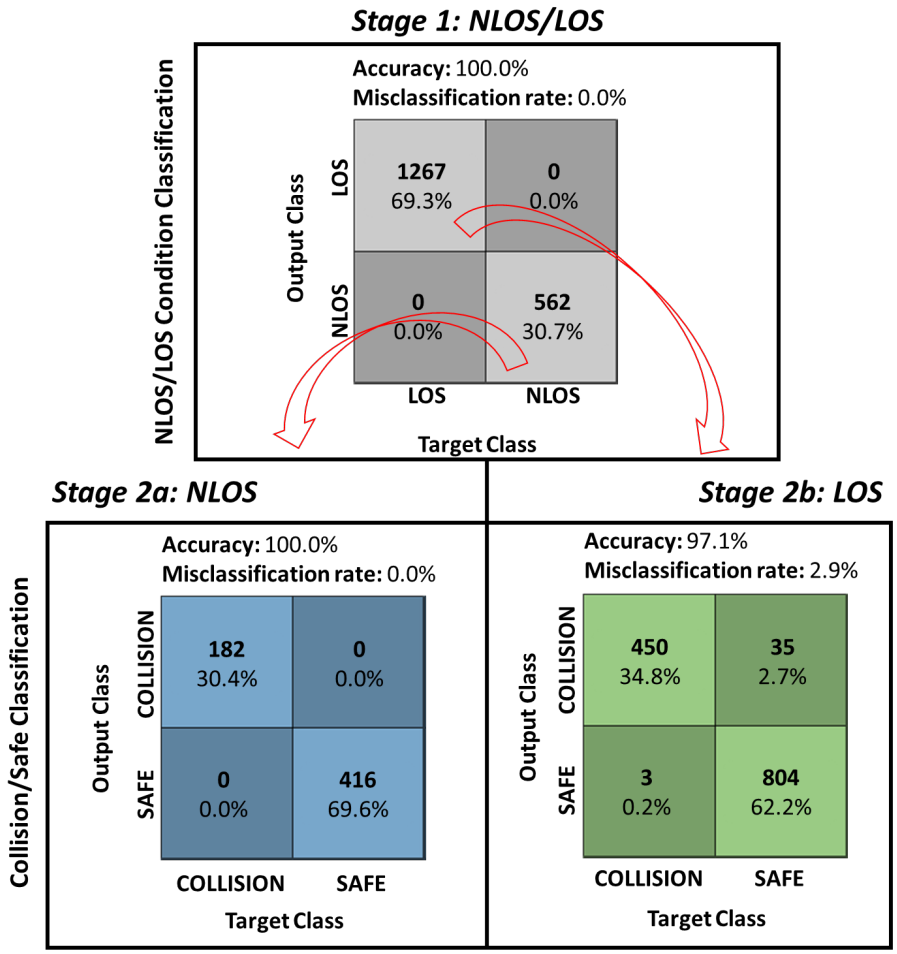

Figure 6.20: Confusion matrices for classification operations with same reference data - each cell is interpreted as: **X** number of STFT windows corresponds to Y% of all STFT windows tested. (The total number of observations for each classification are slightly different because of different N_{fit} for Stage 1, 2a, and 2b. This does not affect the outcome since classification does not start until after N_{fit} observations have passed.)

significantly and can maintain or improve accuracy from Figure 6.20. This is a common behavior of most machine learning based systems that experience performance gains when supplied more reference data to lower the misclassification rate when given unexpected observations.

When retrained, new system parameters must be chosen and a new feature set must be used. Table 6.16 reports on the differences in system parameters for the retrained reference set with Alt-OTLD data. The length of historical observations must be doubled for Stage 2b, while depending more evenly on DPE, RE, and Cepstral features compared to the previous Stage 2b reference feature set. The classification models chosen and configuration settings are different depending on the classifier and feature set. With more training data, the SVM model begins to perform better than kNN or CDT. It could be typical for larger training sets to use an SVM model in which higher dimensions of features can improve performance. A diversity of machine learning algorithms being used throughout the system could also provide more robust classification procedures by considering the output from multiple classifiers. However, to reduce system complexity and processing delay kNN, CDT, and SVM have demonstrated to be sufficient classification algorithms for Doppler profiles. How these stages become integrated into the ADS collision avoidance operation is presented next.

6.8 ADS Collision Avoidance

Classification stages 1, 2a, and 2b are now maximized for highest performance in predicting collisions reliably. Next, they are integrated into the ADS real time collision predictor. The collision predictor for ADS leverages the major concepts of the Doppler collision theory from chapter 5. Specifically, throughout the link duration as the vehicles approach p_c the predictor initially assumes a collision is likely while actively seeking to discover normal behavior. This is counterintuitive considering that this means *normalities* are discovered rather than *abnormalities*. Therefore, ADS assumes a collision for some duration of time until a safe outcome is predicted. While the classification stages are predicting, decision timers are defined for Stages 1 and 2. Timers introduce a time dimension into the classification operations to provide meaningful context in regards to collision avoidance. This is like the observation time heuristic identified for driving scenarios, except now this heuristic is not a feature for classification, but a parameter for safety.

The collision prediction method described in Algorithm 2 centers around the two timers. When the system turns ON, real time observations of the feature sets are passed through

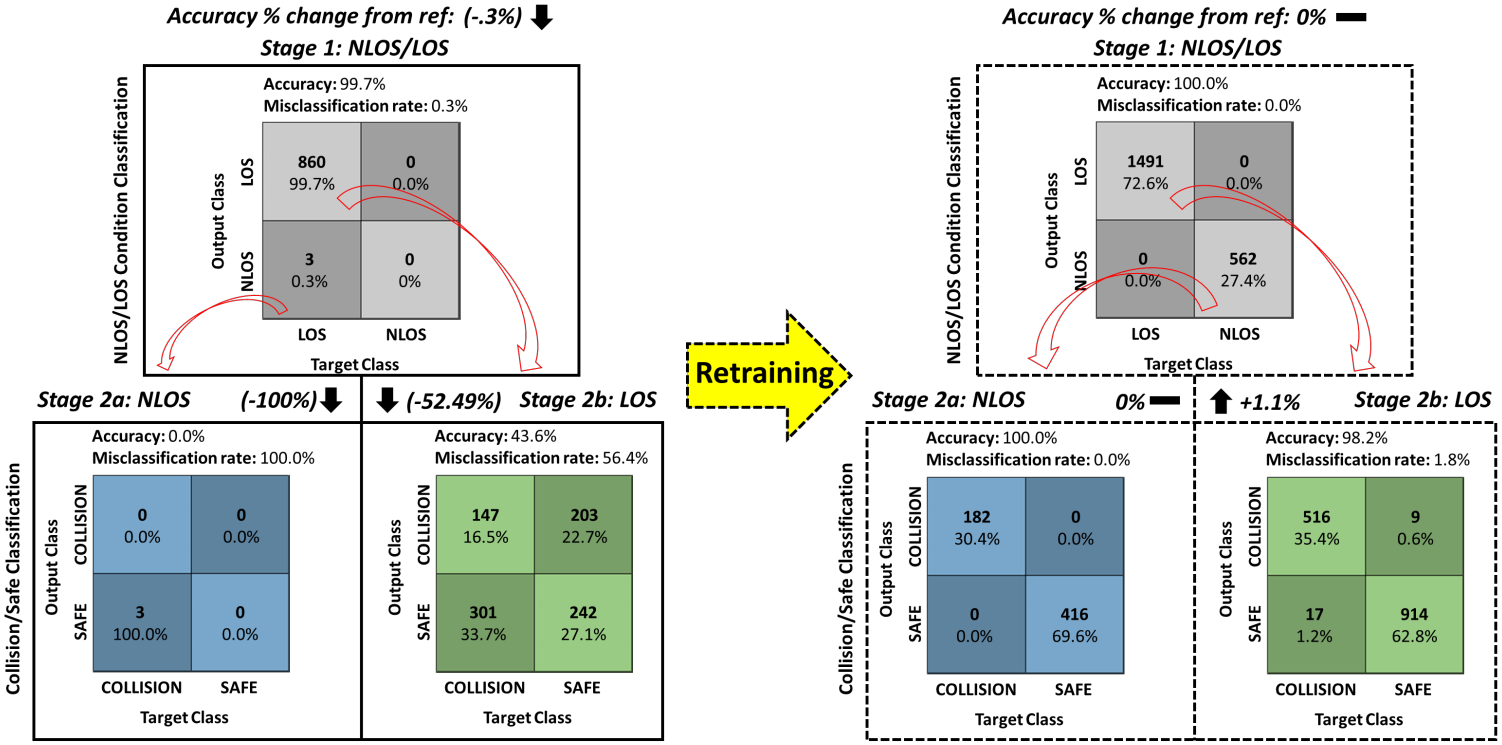

Figure 6.21: Confusion matrices for classification operations with Alt-ODT data set, using trained models from reference set. Retraining with more data can help improve overall performance. (The total number of observations for each classification are slightly different because of different N_{fit} for Stage 1, 2a, and 2b. This does not affect the outcome since classification does not start until after N_{fit} observations have passed.)

the machine learning models for classification. Preliminary simulations revealed that improved classification performance can be achieved when the first stage of the algorithm identifies if the vehicles are operating in NLOS/LOS after ADS turns ON. This is how classifying the driving scenario context can help direct the collision classification more precisely, since collision and safe outcomes within NLOS/LOS exhibit subtle differences, while differences in NLOS vs LOS are more apparent. A fixed timer T_1 is defined such that upon expiration, the vehicles need to be deemed in NLOS conditions or not. The importance of this stage is that in NLOS conditions (see Figure 6.12) there may be less time to safely decide due to signal absorption at far away NLOS distances. Once the NLOS/LOS scenario is determined by majority vote, the second stage decision timer T_2 is set as

$$T_2 = \begin{cases} \frac{\eta(T_{react}\widehat{S}+.1\widehat{S}+.006\widehat{S}^2)}{\widehat{S}} & NLOS; \\ \\ \frac{\eta(T_{react}\widehat{S}+.1\widehat{S}+.006\widehat{S}^2)}{S_{Rx}} & LOS; \end{cases} \tag{6.45}$$

where $\widehat{S} = S_{Rx} + \widehat{S}_{T_x}$, η is a weighting parameter, and T_{react} is the C_{Rx} driver reaction time. Eq. (6.45) is adapted from [112] where the numerator (except for η) is the total safe braking distance. During Stage 2, a sub-classification is performed to determine if the observation is for a collision or safe outcome. For example, if Stage 1 determined LOS then Stage 2 only uses classification configurations for LOS collisions. When T_2 expires, a final stage (Stage 3) then decides if a collision is likely using majority voting. Stage 3 is immediately executed with a majority vote taken for all classifications on Doppler spectra since the ending of T_1, and a final decision is made to either throw an alert or disregard.

The timers are areas of optimization for ADS to provide reliable collision avoidance early enough prior to an accident, and not introduce instability through false alarms while approaching a safe event (e.g. crossing point, stopping point). Though the classification analysis revealed high performance and reliability, omitted was *where* the misclassifications were happening since the system turned ON. Though the classification operations may be generating multiple estimations of which class Doppler spectra falls into (in real time), per Algorithm 2 only one final prediction is determined once the final timer expires and the final majority voting enacted. For ADS, adding timers and majority voting implements a management layer onto the raw classification operations that were analyzed previously. This ensures a reliable method of collision avoidance in case the underlying classification operations unknowingly perform with low accuracy due to an unforeseen input vector. These management operations can help reduce noise produced from the un-

Algorithm 2 Collision Predictor

With system status: ON
Pending collision
Set T_1;
{Stage 1}
while $T_1 \geq 0$ **do**
    Advance STFT window by T_a;
    Extract features;
    Classify: $NLOS$ or LOS
    $T_1 = T_1 - T_a$
end while
Determine majority NLOS or LOS
Set T_2;
{Stage 2a/b}
while $T_2 \geq 0$ **do**
    Advance STFT window by T_a;
    Extract features;
    Classify: $COLLISION$ or $SAFE$
    $T_2 = T_2 - T_a$
end while
{Stage 3}
if Majority SAFE **then**
    Collision not likely
else
    Collision likely $\Rightarrow$ alert
end if

derlying classification operations. It is not sufficient to determine where the classification is most likely to be reliable[11], because a decision must be made given a wide range of unknown driver reaction times, which can affect the meaningful performance of ADS to provide a collision avoidance service.

6.8.1 Collision Prediction Performance

The collision prediction algorithm is now analyzed for providing reliable and stable collision avoidance services by only observing the Doppler profile. Custom MATLAB scripts implement Algorithm 2 and multiple analyses are performed using the real-world data sets. In the analyses, only historical observations are used for the system parameters defined previously. ADS does not know anything *a prior* about the newest observations being sourced

[11]For example, given a classification operation: plot a cumulative distribution function of accuracy for different TTCs.

from the test sets, except for the supervised models. The performance is optimized by tuning T_1 and η for various T_{react}. It is assumed that a CAV would react much faster than a human driver; therefore, the worst-case performance of the collision predictor is assumed for the driver reaction times reported in [113] where $T_{react} \sim \mathcal{N}(r * \mu, \sigma = .2569s)$ with $\mu = .9723s$, and with $r \in \{1, ..., 5\}$ to simulate distracted driver reaction times [114]. Before obtaining prediction metrics, the best performing T_1 and η parameters are discovered through Monte Carlo simulations. Then, for each pre-crash scenario tested, additional Monte Carlo simulations generate 10,000 realizations of T_{react} for a given r and report the performance metrics. Specifically, the objective of these analyses is to report on metrics which characterize the ADS capability for providing reliable collision avoidance services to drivers. These metrics are divided into three groups:

Time metrics

The time metrics quantify the moment when Algorithm 2 makes a correct prediction. This is interpreted as the average duration of time, $T_{predict}$, that it takes from ADS turning ON until a correct prediction is made. This is determined by

$$T_{predict} = N_{fit} T_a + T_1 + T_2 \tag{6.46}$$

if $N_{fit} \geq N_{track}$ is always true[12]. The moment at which ADS turns ON may occur at different times relative to a critical point in space; therefore, the average duration of time, T_{prior}, from a p_c for a correct prediction is also considered. This characterizes each pre-crash scenario by how soon a correct prediction is made prior to a collision/crossing point/stopping point being reached. Inspecting eq. (6.45) and eq. (6.46), reveals that the time metrics will depend on ADS parameters: T_1 and η, while susceptible to the unknown reaction time of the host driver.

Prediction metrics

The prediction metrics quantify the overall performance of Algorithm 2, while ignoring the time at which the prediction occurs. Both NLOS and LOS are characterized separately for how often a *collision is correctly predicted* as the detection prediction rate, P_D. Also, separately for both NLOS and LOS conditions, how often *a safe outcome is incorrectly*

[12]The initial delay of the first T_w does not matter, since the Doppler processing operation could run in the background from vehicle ignition start. If the T_w buffer is filled, then signal segmentation through STFT can be performed continuously.

Algorithm 3 Criteria for P_C and P_S

if ODT or Alt-ODT or SCP **then**
  $\tau = \frac{T_{react}(2S_{Rx})+.1(2S_{Rx})+.006(2S_{Rx})^2)}{2S_{Rx}}$
else if RFC **then**
  $\tau = \frac{T_{react}(S_{Rx})+.1(S_{Rx})+.006(S_{Rx})^2)}{S_{Rx}}$
end if
if Correctly Predicted: COLLISION and $|T_{prior}| > \tau$ **then**
  P_C : True Collision Avoidance
else if Correctly Predicted: SAFE and $|T_{prior}| > \tau$ **then**
  P_S : True Safe Prediction
end if

predicted a collision as the false alarm prediction rate, P_{FA}, is also considered. Similarly, to the classification analysis the overall rate of combined safe and collision outcomes correctly predicted, known as the *Accuracy* of the prediction is reported. The combined number of misses for collision and safe outcomes, known as the *Failure Rate*, is also recorded.

Collision avoidance metrics

The collision avoidance metrics represent the intersection of the time and prediction metrics that are meaningful for understanding how effective ADS is at providing a collision avoidance service within the data sets. Algorithm 2 does not define *how* the system turns ON, instead it is left to the implementer of ADS. Based on Axiom 1, ADS turns ON the moment that the DPE becomes level. This may not always result in the best performance considering that there may exist behaviors that are detectable sooner than the DPE levelling. Furthermore, the data set is specific to the experimentation. Different equipment and configurations could lead to better or worse performance than what is reported.

The collision avoidance metrics for this data set are captured in two behaviors. The first is how often the system correctly predicts a collision with enough time for the driver to react, this is the true collision prediction rate: P_C. The second is how often ADS correctly predicts safe with enough time prior to the crossing/stopping point; the true safe prediction rate: P_S. The criteria for both metrics are described in Algorithm 3.

6.8.2 Analysis of Collision Prediction

The Monte Carlo simulation finds the best ADS parameters, T_1 and η, that produce the highest performance for $T_{react} \sim \mathcal{N}(\mu = .9723s, \sigma = .2569s)$. First, the T_1 that maximizes the *Accuracy* and P_C is discovered. Next, the best performing η for only for LOS is

Table 6.17: Best Collision Prediction System Parameters

	T_1	η
LOS Reference	.2s	.1
NLOS Reference		.2
LOS Retrained		.3

determined. Then, the best performing η for only NLOS. Also considered are the retrained versions which include the Alt-ODT data set to determine the best retrained configuration for only LOS, since the retrained Stage 1 classification performance (see right side of Figure 6.21) correctly classifies Alt-ODT as LOS every time. The best performing parameters are reported in Table 6.17. The metrics $T_{predict}$ and T_{prior} for correctly predicted collision and safe outcomes are reported in Figure 6.22. Since $T_{react} \sim \mathcal{N}(r * \mu, \sigma)$, the time metrics are also normally distributed with different μ while maintaining the same σ as T_{react}. With the reference test set and Alt-ODT test set, the performances for $T_{predict}$ are typically under 2 seconds. With the retrained test set, the average $T_{predict}$ can reach up to 4.5s. This is expected since, as η increases, the time to make a prediction can take longer. This is consistent for correctly predicted collision and safe outcomes. Furthermore, when a collision is correctly predicted, the minimum expected T_{prior} in LOS occurs sooner than -5s of advanced warning for these speeds. The SCP scenarios provide a shorter T_{prior}, however, this could be improved by changing how ADS turns ON. An earlier ON status results in earlier notification to the driver. For the retrained sets, as expected, the larger η increases then the closer the alert is thrown to the collision point. Overall, safe predictions occur much earlier from the event point primarily because the normal driving behavior can be observed more clearly than a collision outcome. Again, this supports the theory that *collisions* should be expected first, while searching for normal behavior as the anomaly. Given T_a, the metric $T_{predict}$ can also be represented as the number of STFT windows that are used to make the prediction, which can be between 14 and 90 windows.

For the prediction metrics, Figure 6.23 and Figure 6.24 indicate the performance of the collision predictor. For $T_{react} < 2$, the collision predictor using the reference test set performs perfectly, even though the underlying classification operation in LOS (see Figure 6.20), has 97.1% accuracy with some misclassifications. This is because the management layers of timers and majority voting help to reduce noise produced by the classification stages. Drivers would not be distracted by false alarm rates, neither would drivers be tempted to turn ADS off, since it can perform reliably with more than double the aver-

age driver reaction time. As expected for Alt-ODT test sets, the *Accuracy* and *Failure Rate* performs slightly better than the underlying classification operation (see left side of Figure 6.21), but the retrained parameters help to improve the overall *Accuracy* and *Failure Rate* to near perfect performance; no matter how delayed the reaction time of the driver is.

The collision prediction metrics show the usefulness of ADS when applied to real world scenarios. Figure 6.25 shows ADS is highly reliable up to a driver reaction time of about 2 seconds. This indicates that when the collision predictor issues a warning to the driver, that the warning is truly given with enough time to allow the driver to make a defensive maneuver. This is a critical advantage of ADS, considering that the predictor has not received any high-level information about the sender, except for only tracking the Doppler profile and running classification algorithms. The real-time collision prediction verifies superb performance, given real world data leveraging supervised machine learning. ADS can make accurate and timely predictions to provide realistic collision avoidance services to drivers in both NLOS and LOS conditions.

6.9 Conclusion

The Doppler profiles presented were not based on wireless channel models, but real world iCW reflections through omnidirectional antennas. Consider the spectrograms featured in this dissertation work as the true Doppler profile that the OFDM-based V2V signal would also encounter. The Doppler shift is typically seen as a channel impairment to the data recovery operation, however, as shown by this dissertation work the Doppler reflections contain valuable information related to the driving context when viewed in the Doppler profile perspective. The application of the Doppler profile for V2V was inspired by the groundbreaking work of [115][116][94], specifically in [94] that first demonstrated frame-based incoherent communication architectures could extract the Doppler profiles to detect hand movement. This was the motivation for this dissertation work: if human Doppler shifts could be extracted from ultrawide-band OFDM signals, then surely the Doppler shifts expected from vehicle maneuvers in V2V networks could also be viewed in the Doppler profile. The difference between the DSRC Doppler profiles and those of [94], are that the DSRC Doppler profiles were generated from a CW signal to understand the clearest picture of how a Doppler profile appears to an IEEE 802.11p receiver front end. It is hoped that this work inspires future investigations to continue to leverage the physical layer directly for improving V2V reliability.

V2V is a cyber-physical system susceptible to hacking attacks and garbage in, garbage

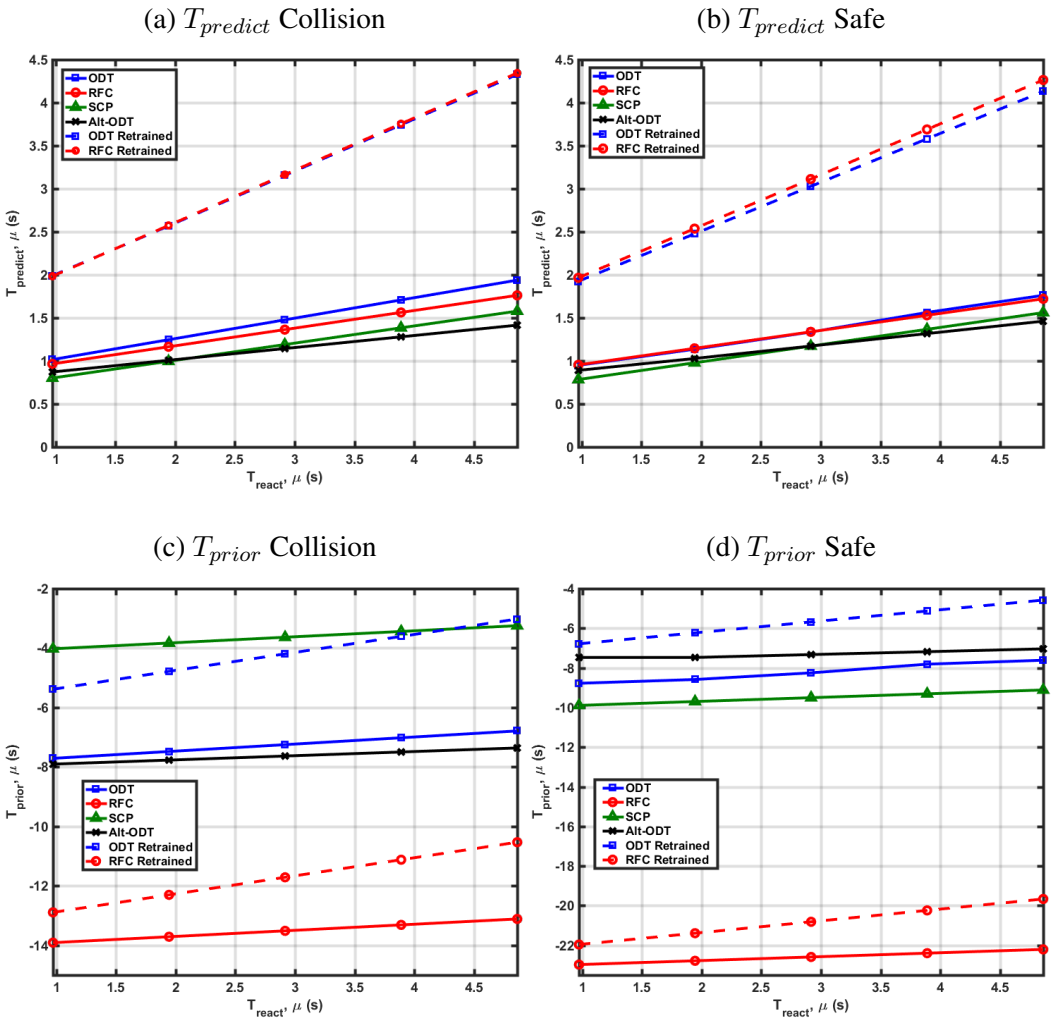

Figure 6.22: $T_{predict}$ and T_{prior} for correctly predicted collision and safe outcomes.

(a) Reference Test Set (b) Alt-ODT Test Set (Unknown) (c) Retrained Test Set

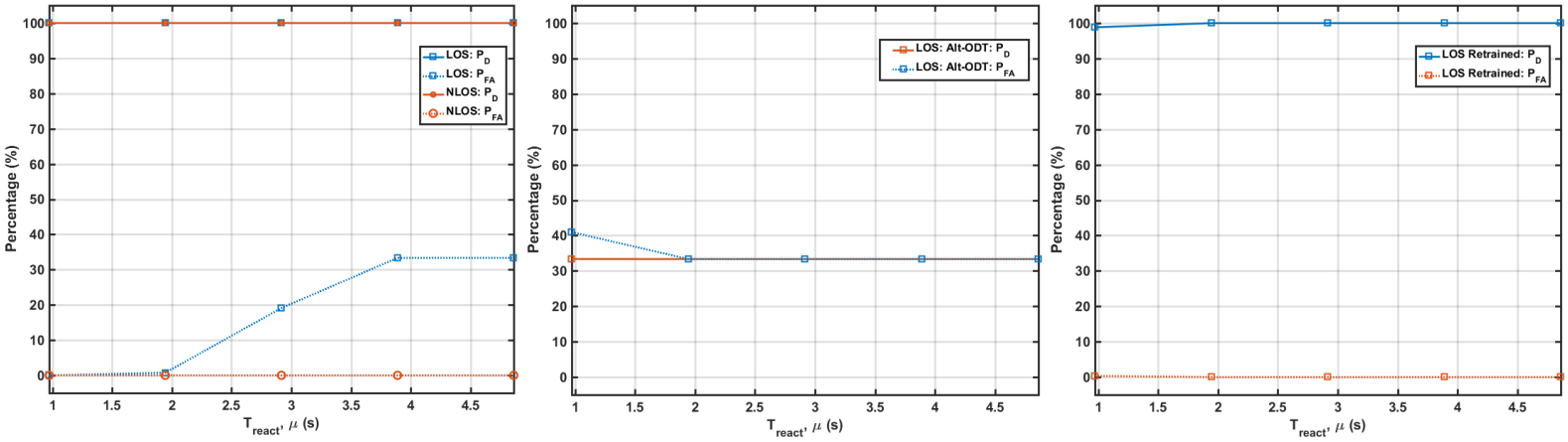

Figure 6.23: P_D and P_{FA} metrics.

(a) Reference Test Set (b) Alt-ODT Test Set (Unknown) (c) Retrained Test Set

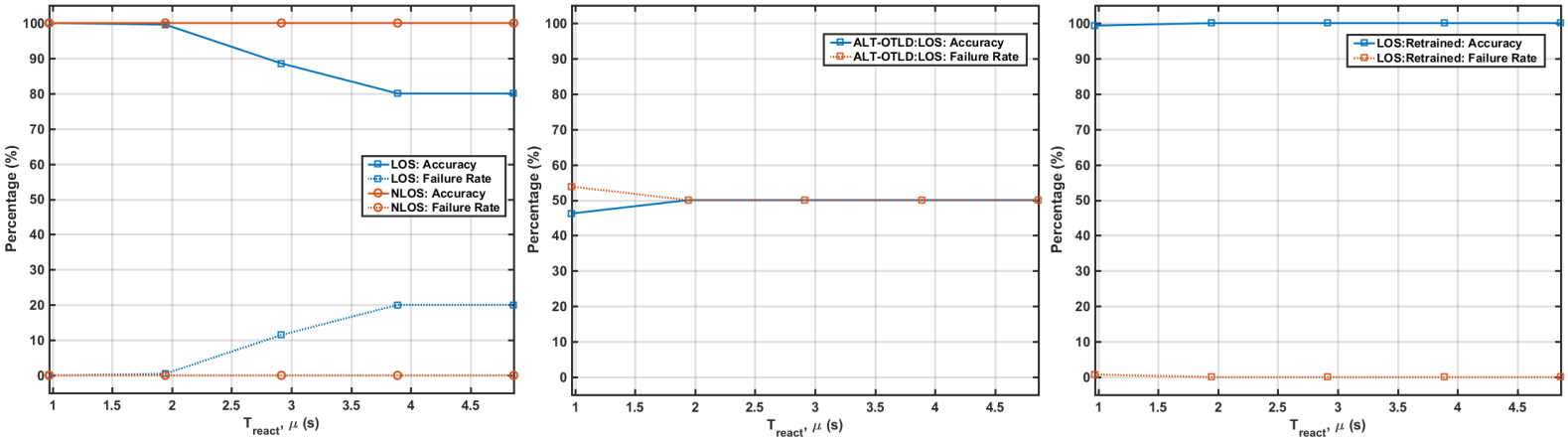

Figure 6.24: *Accuracy* and *Failure Rate* metrics.

(a) Reference Test Set

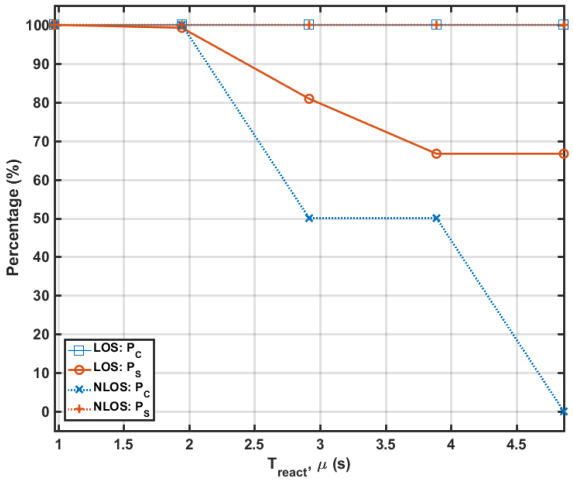

(b) Alt-ODT Test Set (Unknown)

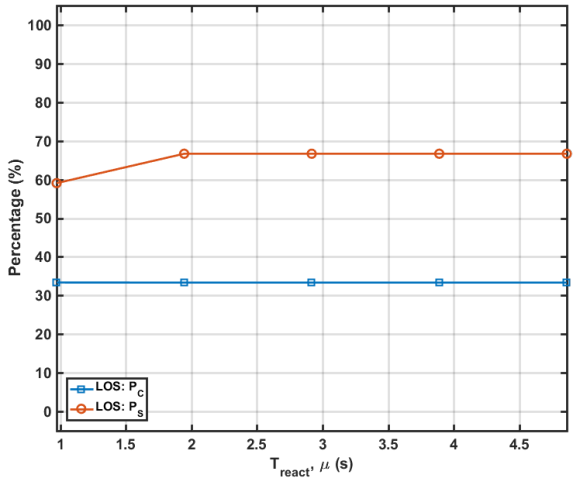

(c) Retrained Test Set

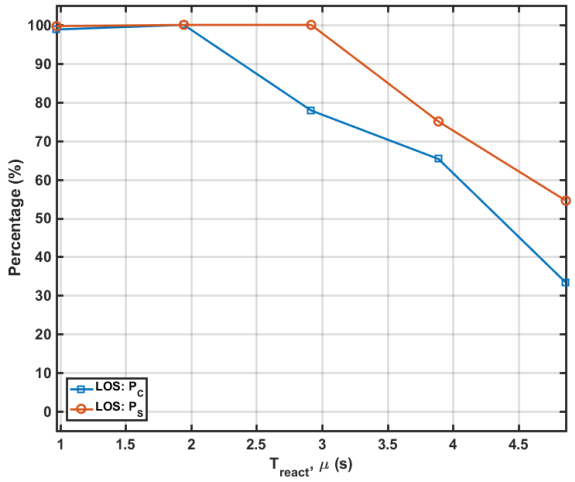

Figure 6.25: P_C and P_S metrics.

out data. Even if every vehicle is transmitting and receiving correctly and securely, the correct safety information is not guaranteed to be correct every time due to connected car vulnerabilities [117]. Ideally, the contents exchanged between two vehicles during any given driving scenario would deliver accurate and trusted information, but this has yet to be verified for all driving conditions at full deployment. To mitigate these threats, this dissertation work showed that observing the Doppler effect between two V2V participants provides invaluable insight to improving collision avoidance services and the V2V radio operation, reliably.

In the 5.9GHz DSRC frequency band, the communication signal can experience reflections from a wide range of scatterers in both NLOS and LOS driving environments. It was never intended for the data sets used in this work to represent the vast number of environments and maneuvers on the roadways, which feature more complicated driving dynamics. To detect a collision across a wider range of vehicle dynamics would require an in-depth extension of pre-crash scenarios; therefore, given the current data set at constant speeds the system was only assessed for detecting collisions commonly seen with distracted driving vehicle dynamics. Distracted driving due to smartphone use and other activities now accounts for over 10% of all fatal vehicular collisions [113]. As vehicles become more cyber connected, new user interfaces and nuisance collision avoidance warnings may ironically also lead to more crashes due to distracted driving. In the analyses presented it was assumed the worst-case scenario in V2V where both radios are misbehaving and both drivers are distracted by relying on the incumbent V2V radio collision avoidance through SM passing.

It is more probable that the host vehicle speed and heading information is locally available and correct, but the transmitting vehicle SM data may not have high fidelity. If the SM is well-formed, the expected transmit power and expected channel are used, then signal processing could be accomplished at the PHY to obtain information needed to satisfy Axiom 1. Though prediction of a collision with only one transmitter was presented, the IEEE 802.11p protocol features typical channel access coordination of broadcast stations. Thus, employing RF fingerprinting techniques [118] may be a way to separate identities of transmitters without relying on the SM contents at all, however, this was out of scope.

The Doppler profile system correctly identifies collisions up to a distracted driver time of twice the average reaction time of drivers. When the classification algorithms are trained with enough data, then the performance can reflect significant gains. It was demonstrated that the collision avoidance service is reliable and the system parameters highlighted are

tunable for specific driving conditions. Most significantly it was demonstrated that it is possible to provide reliable 360° collision avoidance coverage in NLOS. One-hundred and sixteen features were identified that could be observed in real time to describe the Doppler profile and only the most relevant of these features for collision avoidance was selected. Other features may perform better depending on the use case of the Doppler profile, which is not only limited to collision avoidance. Ensuring that the detection rate is high, while the false alarm rate is low is the most challenging part of collision prediction using a single observer like the radio front end. However, as previously shown the Doppler profile is a unique "sensor" view that leverages additional Doppler reflections for detecting a collision. The novelty of the proposed method is highlighted as a pioneering approach to explore an overlooked area in V2V research for developing PHY-based collision avoidance services specifically in V2V networks.

The data was gathered and analyses performed to report the fundamental observations of Doppler related to collision avoidance through ADS. Through this work it was shown that by observing the Doppler reflections, the type of driving scenario between two vehicles can be determined and assessed for behavior indicative of a collision. For most of the Doppler profiles shown in this study the Doppler energy between two transceivers is in the direction of $\vec{V}$. It could be of interest to model the Doppler channel characteristics using an appropriate channel model to simulate the Doppler profile for rapid prototyping of new ADS-based collision avoidance algorithms. This would help further understand the Doppler channel dynamics and contributions to the Doppler profile due to static and moving scatterers, perhaps even to detect non-V2V road users.

CHAPTER 7
RESEARCH CONTRIBUTIONS AND FUTURE RESEARCH DIRECTIONS

7.1 Research Contributions

The contributions on this research are summarized as follows:

1. An improved Vehicle-to-Vehicle (V2V) path loss model was derived from a novel static measurement campaign which captured the effect of vehicle orientation, approach direction, and lane separation. Differences in reported path loss values in the background literature suggest that the vehicle road configuration plays an important role in the signal power response. The model extends the classic power law path model, to include a y-intercept and a path loss exponent as a Gaussian distribution obtained from the static channel measurements. The model is apparently effective at distances less than 100m to fit a variety of dynamic vehicle scenarios. The proposed model leverages the line-of-sight (LOS) dominance as an opportunity to uncover a detailed realization of the channel, which on average could perform better than the classic power law and two-ray ground reflection models. [39]

2. The received signal strength indication (RSSI) within Wireless Access in Vehicular Environments 1609 and the IEEE 802.11p (WAVE-802.11p) based V2V networks is shown to provide collision avoidance to drivers among misbehaving nodes. Experimental observations reported by this work demonstrated during a collision that RSSI can be differentiated from the RSSI during a no-collision outcome. If the direction-of-arrival (DOA) is available, then false alarms due to multiple vehicles can be reduced. The RSSI collision avoidance technique leverages the relationship between vehicle dynamics and sharpness in the RSSI curvature. By checking the third derivative of a discrete array against zero, the technique does not have to set a specific threshold to define what collision "curvature" is, which could vary for many different channel conditions. Generally, vehicular collisions occur because the relative velocity between two vehicles remains positive. The prediction methodology attempts to detect this behavior in RSSI among varying channel conditions, whereas the traditional RSS-distance method attempts to guess the varying channel conditions; a much more difficult task to accomplish in practice for vehicular environments. [52]

3. A novel method for delivering external information to Orthogonal Frequency Division Multiplexing (OFDM) receivers using the null subcarriers is presented. A direct-in configuration with software defined radio technology demonstrates that the null subcarriers in the OFDM spectrum can be used to deliver binary code words in the form of an analogue signal, which can reliably be detected by the OFDM receiver physical layer. The advantage of the technique is twofold: 1) an external observer can provide additional information to communication layers directly through the radio front end with low complexity, 2) the radio front end can be customized per incoming frame in real time by an external system without requiring an application program interface. With frequency injection interfacing, there are numerous ways in which this method could optimize OFDM systems and generate new applications never considered for even single receiver OFDM radios. The most critical for this dissertation is that the DOA could be passed to a V2V radio for tracking transmitters per frame in supporting collision avoidance services. [72]

4. The theory of Doppler-based collision avoidance was presented to explain how the Doppler phenomenon can be leveraged in terrestrial V2V networks. Using a theoretical collision avoidance system, the Doppler trend was tracked to estimate the likelihood of a head-on collision by estimating the transmitter heading proximity to the bearing angle to the host receiver. The collision avoidance theory is the first to suggest the Doppler effect could be exploited to provide a collision avoidance service, regardless of the accuracy of the contents in a safety message (SM). [91]

5. A collision and driving scenario classification technique based on the Doppler profile was presented called: automotive Doppler sensing, which can decouple the safety benefits of V2V communications from relying on SM content. The Doppler profile in V2V networks shows rich data about the vehicles and their environments and can be exploited to potentially provide a reliable collision avoidance service directly from the radio front end. Using the Doppler profile, a feature set was described and extracted to numerically represent the time-series data acquired through a large measurement campaign in real-world scenarios. The classification algorithms used in the study, demonstrated a reliable average overall performance of 82.75% detection rate and 9.71% false alarm rate. Compared to other studies, this work was the first to prove incoherent continuous wave signals on non-stationary platforms using omnidirectional antennas could be used in terrestrial V2V for determining the surrounding environment. The Doppler profiles acquired, revealed unique information about the

driving scenario between the two platforms, including sub-classification capabilities such as identifying what type of intersection is being approached and what the lateral lane spacing between the radios might be. [102]

6. A novel collision avoidance technique based on the Doppler profile was presented to decouple the safety benefits of V2V communications from relying on SM content. To date, there have been no validated physical layer techniques for V2V that can provide 360° collision avoidance services to drivers in both LOS and non-LOS (NLOS) amid misbehaving nodes. The ADS technique is the first to do so through the processing of the Doppler profile. The system performs exceptionally well when given sufficient training data, and can be optimized by the adjustable system parameters. The system can provide reliable collision avoidance services to autonomous systems and distracted drivers reliably without false alarms. Through real-world data, extensive design optimization, and system analysis it was demonstrated that the Doppler technique could operate with high reliability and stability in real-time. [102]

7.2 Future Research Directions

In this dissertation, physical layer techniques were explored to enable collision avoidance services to drivers in LOS and NLOS. Specifically, the RSSI, DOA, and Doppler shift were exploited for discovering trends that were indicative of a collision between two V2V equipped vehicles. The future of driving will undoubtedly exhibit more sensors and driver assistance technologies to help improve roadway safety and efficiency. Future work would seek to develop these different techniques into a unified system for collision avoidance. Several advancements would need to be made in the areas of software defined radio technology which may achievable soon.

The Doppler-based technique proved the most reliable, suggesting that ADS could be the premier sensing method in V2V networks for protecting driver-in-the-loop and autonomous systems. Exploring the implementation of the ADS function either integrated in the V2V radio (using technologies like WiSee), or developing a separate ADS sensor could open new opportunities for connected vehicles.

Also in this dissertation work, a novel method for delivering external information to the V2V radio was explored. Future work would develop the hardware to implement this technique and paired with a DOA estimation system for application to vehicles. The platform could also be extended to enable other devices in the Internet-of-Things (IoT) to sense the

surrounding world while providing numerous new applications for enhancing radio communication.

A subtle notion of this dissertation work was the heavy reliance on software defined radio technology. This dissertation suggests that the software defined physical layer is the new frontier technology for bridging the connected and mobile world of devices and machines by a safer, more reliable means. Where cyber-attacks and real world issues can exploit the cyber-physical nature of V2V, the flexible physical layer can provide the means to ensure V2V communication reliability.

REFERENCES

[1] USDOT, "49 cfr part 571," Department of Transportation National Highway Traffic Safety Administration, Tech. Rep. Docket No. NHTSA-2016-0126, 2016.

[2] "Connected vehicle pilot deployment program," Department of Transportation National Highway Traffic Safety Administration, Tech. Rep., 2016.

[3] D. N. Patel, S. B. Patel, H. R. Kothadiya, P. D. Jethwa, and R. H. Jhaveri, "A survey of reactive routing protocols in manet," in *International Conference on Information Communication and Embedded Systems (ICICES2014)*, 2014, pp. 1–6.

[4] N. S. Patel and S. Singh, "A survey on techniques for collision prevention in vanet," in *2016 International Conference on Wireless Communications, Signal Processing and Networking (WiSPNET)*, 2016, pp. 1663–1666.

[5] "Fcc allocates spectrum in 5.9 ghz range for intelligent transportation systems uses," Federal Communications Commission, Tech. Rep. No. ET 99-5, 1999.

[6] M. Ashour, A. Attia, A. ElMoslimany, Y. Mohasseb, and A. El-Keyi, "Mimo vehicle to vehicle channels: An experimental study," in *2014 IEEE 80th Vehicular Technology Conference (VTC2014-Fall)*, 2014, pp. 1–5.

[7] "Ieee guide for wireless access in vehicular environments (wave) - architecture," *IEEE Std 1609.0-2013*, pp. 1–78, 2014.

[8] "802.11-2012 - IEEE Standard for Information technology–Telecommunications and information exchange between systems Local and metropolitan area networks–Specific requirements Part 11: Wireless LAN Medium Access Control (MAC) and Physical Layer (PHY) Specifications," IEEE-Inst, Tech. Rep. IEEE Std 802.11-2012.

[9] *Dedicated short range communications (dsrc) message set dictionary*, Washington, DC: SAE, 2014.

[10] *Draft: Dedicated short range communication (dsrc) minimum performance requirements*, Washington, DC: SAE, 2014.

[11] R. Prasad, *OFDM for Wireless Communications Systems*, ser. Artech House universal personal communications series. Artech House, 2004, ISBN: 9781580537995.

[12] S. Bayless, A Guan, P. Patrick Son, S. Murphy, and A. Shaw, "Connected vehicle insights trends in roadway domain active sensing developments in radar, lidar, and other sensing technologies, and impact on vehicle crash avoidance/automation and active traffic management," ITS America, Washington, D.C., Tech. Rep., Aug. 2013.

[13] E. Ackerman, *Hyundai robocar competition: Kaist details weather problems philosophical differences*, spectrum.ieee.org, Ed., spectrum.ieee.org [Online; posted 18-November-2014], 2014.

[14] V. S. Shuqing Zeng Hariharan Krishnan, *Combined vehicle-to-vehicle communication and object detection sensing*, GM Global Technology Operations LLC, 2012.

[15] J. Wolf, *Rear collision avoidance system for vehicle*, Magna Electronics Inc., 2016.

[16] M. Obst, L. Hobert, and P. Reisdorf, "Multi-sensor data fusion for checking plausibility of v2v communications by vision-based multiple-object tracking," *Vehicular Networking Conference (VNC), 2014 IEEE*, pp. 143–150, 2014.

[17] D. Vlastaras, T. Abbas, D. Leston, and F. Tufvesson, "Vehicle Detection through Wireless Vehicular Communication," *EURASIP Journal on Wireless Communications and Networking*, pp. 146–, 2014.

[18] O. of Regulatory Analysis, E. N. C. for Statistics, and Analysis, "Preliminary cost-benefit analysis of ultrasonic and camera backup systems," National Highway Traffic Safety Administration, Tech. Rep., 2006.

[19] N. H.T. S. Administration, "Federal motor vehicle safety standards; rear visibility," United States Department of Transportation, Tech. Rep. 79 FR 19177, 2014.

[20] D. L. HARRIS, *1964 brought seat belts for every buyer*, autonews.com, Ed., autonews.com [Online; posted 26-June-1996], 1996.

[21] C.-M. Huang, S.-Y. Lin, C.-C. Yang, and C.-H. Chou, "A collision pre-warning algorithm based on v2v communication," *Ubiquitous Information Technologies Applications, 2009. ICUT '09. Proceedings of the 4th International Conference on*, pp. 1–6, 2009.

[22] J. Ahrems, "Implementation of collision warning algorithm based on v2v communications," *Radioelektronika (RADIOELEKTRONIKA), 2015 25th International Conference*, pp. 395–398, 2015.

[23] S. Biswas, R. Tatchikou, and F. Dion, "Vehicle-to-vehicle wireless communication protocols for enhancing highway traffic safety," *Communications Magazine, IEEE*, vol. 44, no. 1, pp. 74–82, 2006.

[24] K. Koscher, A Czeskis, F. Roesner, S. Patel, T. Kohno, S. Checkoway, D. McCoy, B. Kantor, D. Anderson, H. Shacham, and S. Savage, "Experimental security analysis of a modern automobile," in *Security and Privacy (SP), 2010 IEEE Symposium on*, 2010, pp. 447–462.

[25] A. Jafarnia-Jahromi, A. Broumandan, J. Nielsen, and G. Lachapelle, *Gps vulnerability to spoofing threats and a review of antispoofing techniques*, 2012.

[26] M. Zhao, J. Walker, and C.-C. Wang, "Challenges and opportunities for securing intelligent transportation system," *Emerging and Selected Topics in Circuits and Systems, IEEE Journal on*, vol. 3, no. 1, pp. 96–105, 2013.

[27] W. Jian, L. Yanheng, and D. Kevin, "Modelling and simulating worm propagation in static and dynamic traffic.," *IET Intelligent Transport Systems*, vol. 8, no. 2, pp. 155 –163, 2014.

[28] G. Yan, W. Yang, J. Li, and V. Ashok, "Active position security through dynamically tunable radar," in *Mobile Adhoc and Sensor Systems (MASS), 2010 IEEE 7th International Conference on*, 2010, pp. 733–738.

[29] M. Erritali and B. El Ouahidi, "A review and classification of various vanet intrusion detection systems," in *Security Days (JNS3), 2013 National*, 2013, pp. 1–6.

[30] R. P. Barnwal and S. K. Ghosh, "Heartbeat message based misbehavior detection scheme for vehicular ad-hoc networks," in *Connected Vehicles and Expo (ICCVE), 2012 International Conference on*, 2012, pp. 29–34.

[31] A. Boukerche, H. A.B. F. Oliveira, E. F. Nakamura, and A. A. F. Loureiro, "Vehicular ad hoc networks: A new challenge for localization-based systems," *Comput. Commun.*, vol. 31, no. 12, pp. 2838–2849, Jul. 2008.

[32] L. Sun, Y. Wu, J. Xu, and Y. Xu, "An rsu-assisted localization method in non-gps highway traffic with dead reckoning and v2r communications.," in *2012 2nd International Conference on Consumer Electronics, Communications and Networks, CECNet 2012 - Proceedings*, College of Information Technical Science, Nankai University, 2012, pp. 149–152.

[33] N. Alam and A. Dempster, "Cooperative positioning for vehicular networks: Facts and future," *Intelligent Transportation Systems, IEEE Transactions on*, vol. 14, no. 4, pp. 1708–1717, 2013.

[34] V. Ashok, S. Olariu, A. Gupta, and Y. Gongjun, "Privacy aware localization in vanet.," in *2010 IEEE 7th International Conference on Mobile Adhoc and Sensor Systems, MASS 2010*, Department of Computer Science, Old Dominion University, 2010, pp. 739–744.

[35] "2009 bottleneck analysis of 100 freight significant highway locations," American Transportation Research Institute and Federal Highway Administration, Tech. Rep., 2010.

[36] Y. Zou, J. Zhu, X. Wang, and L. Hanzo, "A survey on wireless security: Technical challenges, recent advances, and future trends," *Proceedings of the IEEE*, vol. 104, no. 9, pp. 1727–1765, 2016.

[37] A. Serageldin, H. Alturkostani, and A. Krings, "On the reliability of dsrc safety applications: A case of jamming," in *2013 International Conference on Connected Vehicles and Expo (ICCVE)*, 2013, pp. 501–506.

[38] I. K. Azogu, M. T. Ferreira, J. A. Larcom, and H. Liu, "A new anti-jamming strategy for vanet metrics-directed security defense," in *2013 IEEE Globecom Workshops (GC Wkshps)*, 2013, pp. 1344–1349.

[39] B. Kihei, J. A. Copeland, and Y. Chang, "Improved 5.9ghz v2v short range path loss model," in *2015 IEEE 12th International Conference on Mobile Ad Hoc and Sensor Systems*, 2015, pp. 244–252.

[40] T. S. Rappaport, *Mobile Radio Propagation: Large-Scale Path Loss*. Upper Saddle River, N.J. : Prentice Hall PTR [1995] c1996., 1995, ISBN: 0133755363.

[41] J. Karedal, N. Czink, A. Paier, F. Tufvesson, and A. Molisch, "Path loss modeling for vehicle-to-vehicle communications," *Vehicular Technology, IEEE Transactions on*, vol. 60, no. 1, pp. 323–328, 2011.

[42] L. Cheng, B. Henty, D. Stancil, F. Bai, and P. Mudalige, "Mobile vehicle-to-vehicle narrow-band channel measurement and characterization of the 5.9 ghz dedicated short range communication (dsrc) frequency band," *Selected Areas in Communications, IEEE Journal on*, vol. 25, no. 8, pp. 1501–1516, 2007.

[43] J. Kunisch and J. Pamp, "Wideband car-to-car radio channel measurements and model at 5.9 ghz," in *Vehicular Technology Conference, 2008. VTC 2008-Fall. IEEE 68th*, 2008, pp. 1–5.

[44] H. Fernandez, V. Rodrigo-Penarrocha, L. Rubio, and J. Reig, "Path loss characterization in vehicular environments under los and nlos conditions at 5.9 ghz," in *Antennas and Propagation (EuCAP), 2014 8th European Conference on*, 2014, pp. 3044–3048.

[45] H. Fernandez, L. Rubio, V. Rodrigo-Penarrocha, and J. Reig, "Path loss characterization for vehicular communications at 700 mhz and 5.9 ghz under los and nlos conditions," *Antennas and Wireless Propagation Letters, IEEE*, vol. 13, pp. 931–934, 2014.

[46] Y. Ito, T. Taga, J. Muramatsu, and N. Suzuki, "Prediction of line-of-sight propagation loss in inter-vehicle communication environments," in *Personal, Indoor and Mobile Radio Communications, 2007. PIMRC 2007. IEEE 18th International Symposium on*, 2007, pp. 1–5.

[47] O. Shagdar, A. Daniel, and S. Primak, "Beacon delivery over practical v2x channels," in *ITS Telecommunications (ITST), 2013 13th International Conference on*, 2013, pp. 68–73.

[48] R. Miucic, Z. Popovic, and S. Mahmud, "Experimental characterization of dsrc signal strength drops," in *Intelligent Transportation Systems, 2009. ITSC '09. 12th International IEEE Conference on*, 2009, pp. 1–5.

[49] M. Boban, J. Barros, and O. K. Tonguz, "Geometry-based vehicle-to-vehicle channel modeling for large-scale simulation," *IEEE Transactions on Vehicular Technology*, vol. 63, no. 9, pp. 4146–4164, 2014.

[50] A. Kavak, W. Vogel, and G. Xu, "Using gps to measure ground complex permittivity," *Electronics Letters*, vol. 34, no. 3, pp. 254–255, 1998.

[51] J. Shang and J. Umana, "Dielectric constant and relaxation time of asphalt pavement materials.," *Journal of Infrastructure Systems*, vol. 5, no. 4, pp. 135–142, 1999.

[52] B. Kihei, J. A. Copeland, and Y. Chang, "Predicting car collisions using rssi," in *2015 IEEE Global Communications Conference (GLOBECOM)*, 2015, pp. 1–7.

[53] S. Sen, B. Radunovic, R. R. Choudhury, and T. Minka, "You are facing the mona lisa: Spot localization using phy layer information," in *Proceedings of the 10th International Conference on Mobile Systems, Applications, and Services*, ser. MobiSys '12, Low Wood Bay, Lake District, UK: ACM, 2012, pp. 183–196, ISBN: 978-1-4503-1301-8.

[54] P. Gimnez, B. Molina, J. Calvo-Gallego, M. Esteve, and C. E. Palau, "I3wsn: Industrial intelligent wireless sensor networks for indoor environments," *Computers in Industry*, vol. 65, no. 1, pp. 187 –199, 2014.

[55] M. Altini, D. Brunelli, E. Farella, and L. Benini, "Bluetooth indoor localization with multiple neural networks," in *IEEE 5th International Symposium on Wireless Pervasive Computing 2010*, 2010, pp. 295–300.

[56] S. Hisaka and S. Kamijo, "Road user positioning by rssi combinations with pavement reflection at real intersection," in *2012 12th International Conference on ITS Telecommunications*, 2012, pp. 29–34.

[57] S. A. Zekavat and M. Buehrer, *Handbook of position location [electronic resource] : theory, practice and advances / by Reza Zekavat, Michael Buehrer.* Ser. IEEE series on digital & mobile communication. Oxford: Wiley-Blackwell, 2011, pp. 31–33, ISBN: 9781118104750.

[58] R. B. Chiaramonte and K. R.L.J. C. Branco, "Collision detection using received signal strength in fanets," in *Unmanned Aircraft Systems (ICUAS), 2014 International Conference on*, 2014, pp. 1274–1283.

[59] A. Boukerche, H. Oliveira, E. Nakamura, and A. Loureiro, "Vehicular ad hoc networks: A new challenge for localization-based systems.," *Computer Communications*, vol. 31, no. 12, pp. 2838–2849, 2008.

[60] R. Parker and S. Valaee, "Vehicular node localization using received-signal-strength indicator," *Vehicular Technology, IEEE Transactions on*, vol. 56, no. 6, pp. 3371–3380, 2007.

[61] N. Alam, A. T. Balaei, and A. G. Dempster, "Range and range-rate measurements using dsrc: Facts and challenges," in *IGNSS Symposium 2009, Surfers Paradise,Australia*, 2009.

[62] W. Najm, S. Toma, and J. Harding, "Pre-crash scenario framework for crash avoidance systems based on vehicle-to-vehicle communications.," in *Proceedings of the 22nd International Technical Conference on the Enhanced Safety of Vehicles (ESV)*, Washington, DC : U.S. Dept. of Transportation, National Highway Traffic Safety Administration, 2011.

[63] J. Kenney, "Dedicated short-range communications (dsrc) standards in the united states.," *Proceedings of the IEEE*, vol. 99, no. 7, pp. 1162 –1182, 2011.

[64] F. Ahmed-Zaid, F. Bai, S. Bai, C. Basnayake, B. Bellur, S. Brovold, G. Brown, L. Caminiti, D. Cunningham, H. Elzein, K. Hong, J. Ivan, D. Jiang, J. Kenney, H. Krishnan, J. Lovell, M. Maile, D. Masselink, E. McGlohon, P. Mudalige, Z. Popovic, V. Rai, J. Stinnett, L. Tellis, K. Tirey, and S. VanSickle, "Vehicle safety communications applications (vsc-a) final report: Appendix volume 2 communications and positioning," Washington, DC : U.S. Dept. of Transportation, National Highway Traffic Safety Administration, Tech. Rep. DOT HS 811 492C, 2011, D–1–18, Figure 19.

[65] H. Schumacher, H. Tchouankem, J. Nuckelt, T. Kurner, T. Zinchenko, A. Leschke, and L. Wolf, "Vehicle-to-vehicle ieee 802.11p performance measurements at urban intersections," in *Communications (ICC), 2012 IEEE International Conference on*, 2012, 7131–7135, Figure 5.

[66] R. Meireles, M. Boban, P. Steenkiste, O. Tonguz, and J. Barros, "Experimental study on the impact of vehicular obstructions in vanets," in *Vehicular Networking Conference (VNC), 2010 IEEE*, 2010, pp. 338–345.

[67] S. C. on Highways, "A policy on geometric design of highways and streets," in. Washington, D.C. : American Association of State Highway and Transportation Officials, c2001., 2001, p. 113, ISBN: 1560511567.

[68] V. Inman and G. Davis, "The effects of in-vehicle and infrastructure-based collision warnings at signalized intersections," Washington, DC : U.S. Dept. of Transportation, National Highway Traffic Safety Administration, Tech. Rep. FHWA-HRT-09-049, 2009, p. 19.

[69] P. Greibe, "Braking distance, friction and behaviour. findings, analyses and recommendations based on braking trials," Trafitec, Tech. Rep., 2007.

[70] W. Najm, R. Ranganathan, G. Srinivasan, J. Toma, E. Swanson, and A. Burgett, "Description of light-vehicle pre-crash scenarios for safety applications based on vehicle-to-vehicle communications," Washington, DC : U.S. Dept. of Transportation National Highway Traffic Safety Administration, Tech. Rep., 2013.

[71] P. Liu, B. Ai, D. W. Matolak, R. Sun, and Y. Li, "5-ghz vehicle-to-vehicle channel characterization for example overpass channels," *IEEE Transactions on Vehicular Technology*, vol. 65, no. 8, pp. 5862–5873, 2016.

[72] B. Kihei, J. A. Copeland, and Y. Chang, "Frequency injection interfacing: A novel method for delivering external information to an ofdm receiver physical layer," in *IEEE ICC 2017 Signal Processing for Communications Symposium (ICC'17 SPC)*, Paris, France, May 2017.

[73] J. Zhu and W. Lee, "Carrier frequency offset estimation for ofdm systems with null subcarriers," *IEEE Transactions on Vehicular Technology*, vol. 55, no. 5, pp. 1677–1690, 2006.

[74] B. Wang, P. H. Ho, and C. H. Lin, "Ofdm papr reduction by shifting null subcarriers among data subcarriers," *IEEE Communications Letters*, vol. 16, no. 9, pp. 1377–1379, 2012.

[75] Y. Chen, J. Yin, L. Zou, D. Yang, and Y. Cao, "Null subcarriers based doppler scale estimation with polynomial interpolation for multicarrier communication over ultrawideband underwater acoustic channels," *Journal of Systems Engineering and Electronics*, vol. 26, no. 6, pp. 1177–1183, 2015.

[76] J. Kim, S. Nam, D. S. Kwon, and D. Hong, "Time-varying channel estimation in ofdm systems with null subcarriers," in *Vehicular Technology Conference, 2008. VTC Spring 2008. IEEE*, 2008, pp. 1409–1412.

[77] V. Rabinovich and N. Alexandrov, *Antenna Arrays and Automotive Applications*. Springer Publishing Company, Incorporated, 2014, ISBN: 148999775X, 9781489997753.

[78] T. E. Tuncer and B. Friedlander, *Classical and Modern Direction-of-Arrival Estimation*. Academic Press, 2009, ISBN: 0123745241, 9780123745248.

[79] C. Warty, R. Yu, and K. ElMahgoub, "Collaborative warning system for dense vehicular networks using music algorithm doa," *Advances in Computing and Communications (ICACC), 2013 Third International Conference on*, pp. 228–232, 2013.

[80] A. Attia, A. ElMoslimany, A. El-Keyi, T. ElBatt, B. Fan, and C. Saraydar, "Mimo vehicular networks: Research challenges and opportunities.," *Journal of Communications*, vol. 7, no. 7, pp. 500 –513, 2012.

[81] A. Gurbuz, J. McClellan, and V. Cevher, "A compressive beamforming method," *Acoustics, Speech and Signal Processing, 2008. ICASSP 2008. IEEE International Conference on*, pp. 2617–2620, 2008.

[82] A. Badawy, T. Khattab, D. Trinchero, T. M. Elfouly, and A. Mohamed, "A simple aoa estimation scheme," *Computing Research Repository (CoRR)*, vol. abs/1409.5744, 2014.

[83] Y. Ozaki, J. Ozawa, E. Taillefer, J. Cheng, and Y. Watanabe, "A simple doa estimator using adjacent pattern power ratio with switched beam antenna," in *Wireless Communications and Signal Processing (WCSP), 2010 International Conference on*, 2010, pp. 1–6.

[84] A. Gorcin and H. Arslan, "A two-antenna single rf front-end doa estimation system for wireless communications signals," *Antennas and Propagation, IEEE Transactions on*, vol. 62, no. 10, pp. 5321–5333, 2014.

[85] D. Peavey and T. Ogumfunmi, "The single channel interferometer using a pseudo-doppler direction finding system," in *Acoustics, Speech, and Signal Processing, 1997. ICASSP-97., 1997 IEEE International Conference on*, vol. 5, 1997, 4129–4132 vol.5.

[86] N. Harter, J. Keaveny, S. Venkatesh, and R. Buehrer, "Analysis and implementation of a novel single-channel direction-finding method," in *Wireless Communications and Networking Conference, 2005 IEEE*, vol. 4, 2005, 2530–2533 Vol. 4.

[87] N. Harter, J. J. Keaveny, S. Venkatesh, and R. M. Buehrer, "Development of a novel single-channel direction-finding method," in *MILCOM 2005 - 2005 IEEE Military Communications Conference*, 2005, 2720–2725 Vol. 5.

[88] T. Pollet, M. V. Bladel, and M. Moeneclaey, "Ber sensitivity of ofdm systems to carrier frequency offset and wiener phase noise," *IEEE Transactions on Communications*, vol. 43, no. 2/3/4, pp. 191–193, 1995.

[89] B. Bloessl, M. Segata, C. Sommer, and F. Dressler, "An ieee 802.11a/g/p ofdm receiver for gnu radio," in *Proceedings of the Second Workshop on Software Radio Implementation Forum*, ser. SRIF '13, Hong Kong, China: ACM, 2013, pp. 9–16, ISBN: 978-1-4503-2181-5.

[90] R. Knight, *Physics for scientists and engineers : A strategic approach*. Boston: Pearson, 2013.

[91] B. Kihei, J. A. Copeland, and Y. Chang, "Doppler domain localization for collision avoidance in vanets by using omnidirectional antennas," in *2014 International Conference on Connected Vehicles and Expo (ICCVE)*, 2014, pp. 331–337.

[92] A. Goldsmith, *Wireless Communications*. New York, NY: Cambridge University Press, 2005.

[93] P. Moose, "A technique for orthogonal frequency division multiplexing frequency offset correction.," *IEEE Transactions on Communications*, vol. 42, no. 10, pp. 2908 –2914, 1994.

[94] Q. Pu, S. Gupta, S. Gollakota, and S. Patel, "Whole-home gesture recognition using wireless signals," in *Proceedings of the 19th Annual International Conference on Mobile Computing & Networking*, ser. MobiCom '13, Miami, Florida, USA: ACM, 2013, pp. 27–38, ISBN: 978-1-4503-1999-7.

[95] N. Alam, A. Tabatabaei Balaei, and A. G. Dempster, "A dsrc doppler-based cooperative positioning enhancement for vehicular networks with gps availability.," *IEEE Transactions on Vehicular Technology*, vol. 60, no. 9, pp. 4462 –4470, 2011.

[96] L. Bernad, T. Zemen, F. Tufvesson, A. F. Molisch, and C. F. Mecklenbruker, "Delay and doppler spreads of nonstationary vehicular channels for safety-relevant scenarios," *IEEE Transactions on Vehicular Technology*, vol. 63, no. 1, pp. 82–93, 2014.

[97] M. Anderson, T. U. of Texas at Austin. Electrical, and C. Engineering, *Design of Multiple Frequency Continuous Wave Radar Hardware and Micro-Doppler Based Detection and Classification Algorithms*. University of Texas at Austin, 2008, ISBN: 9780549609476.

[98] T. Hastie, R. Tibshirani, J. Friedman, and J. Friedman, *The elements of statistical learning data mining, inference, and prediction*. New York: Springer, 2009.

[99] M. Andric, Z. Durovic, and B. Zrnic, "Ground surveillance radar target classification based on fuzzy logic approach," in *EUROCON 2005 - The International Conference on "Computer as a Tool"*, vol. 2, 2005, pp. 1390–1392.

[100] L. Du, Y. Ma, B. Wang, and H. Liu, "Noise-robust classification of ground moving targets based on time-frequency feature from micro-doppler signature," *IEEE Sensors Journal*, vol. 14, no. 8, pp. 2672–2682, 2014.

[101] "Ieee draft standard for information technology–telecommunications and information exchange between systems local and metropolitan area networks–specific requirements part 11: Wireless lan medium access control (mac) and physical layer (phy) specification," pp. 1–3701, 2014.

[102] B. Kihei, J. A. Copeland, and Y. Chang, "Automotive doppler sensing: The doppler profile with machine learning in Vehicle-to-Vehicle networks for road safety," in *2017 IEEE 18th International Workshop on Signal Processing Advances in Wireless Communications (SPAWC) (IEEE SPAWC 2017)*, Sapporo, Japan, Jul. 2017.

[103] A. Theodorakopoulos, P. Papaioannou, T. Abbas, and F. Tufvesson, "A geometry based stochastic model for mimo v2v channel simulation in cross-junction scenario," in *ITS Telecommunications (ITST), 2013 13th International Conference on*, 2013, pp. 290–295.

[104] A. Zajic, *Mobile-to-Mobile Wireless Channels*. Norwood, MA, USA: Artech House, Inc., 2013, ISBN: 1608074951, 9781608074952.

[105] B. Kihei, J. A. Copeland, and Y. Chang, "Design considerations for vehicle-to-vehicle ieee 802.11p radar in collision avoidance," in *2015 IEEE Global Communications Conference (GLOBECOM)*, 2015, pp. 1–7.

[106] H. Tchouankem, T. Zinchenko, H. Schumacher, and L. Wolf, "Effects of vegetation on vehicle-to-vehicle communication performance at intersections," in *2013 IEEE 78th Vehicular Technology Conference (VTC Fall)*, 2013, pp. 1–6.

[107] L. Cheng, B. Henty, R. Cooper, D. D. Stancil, and F. Bai, "Multi-path propagation measurements for vehicular networks at 5.9 ghz," in *2008 IEEE Wireless Communications and Networking Conference*, 2008, pp. 1239–1244.

[108] A. Papoulis, *Probability, random variables, and stochastic processes*, ser. McGraw-Hill series in electrical engineering. New York: McGraw-Hill, 1991, ISBN: 0-07-100870-5.

[109] M. S. Andri, D. M. Bujakovi, B. P. Bonduli, and B. M. Zrni, "Cepstrum-based analysis of radar doppler signals," in *2011 10th International Conference on Telecommunication in Modern Satellite Cable and Broadcasting Services (TELSIKS)*, vol. 2, 2011, pp. 575–578.

[110] I. Kononenko, E. Šimec, and M. Robnik-Šikonja, "Overcoming the myopia of inductive learning algorithms with relieff," *Applied Intelligence*, vol. 7, no. 1, pp. 39–55, 1997.

[111] MATLAB, *MATLAB Statistics and Machine Learning Toolbox*. Natick, Massachusetts: The MathWorks Inc., 2016.

[112] P. Alexander, D. Haley, and A Grant, "Cooperative intelligent transport systems: 5.9-ghz field trials," *Proceedings of the IEEE*, vol. 99, no. 7, pp. 1213–1235, 2011.

[113] "Distracted driving 2011," Department of Transportation National Highway Traffic Safety Administration, Tech. Rep. DOT HS 811 737, 2013.

[114] C. Yager, S. T. Chrysler, and S. T. Cooper, "An investigation of the effects of reading and writing text-based messages while driving," Southwest Region University Transportation Center, Tech. Rep. SWUTC/11/476660-00024-1, 2011.

[115] F. Adib and D. Katabi, "See through walls with wifi!" *SIGCOMM Comput. Commun. Rev.*, vol. 43, no. 4, pp. 75–86, Aug. 2013.

[116] S. Gollakota and D. Katabi, "Zigzag decoding: Combating hidden terminals in wireless networks," in *Proceedings of the ACM SIGCOMM 2008 Conference on Data Communication*, ser. SIGCOMM '08, Seattle, WA, USA: ACM, 2008, pp. 159–170, ISBN: 978-1-60558-175-0.

[117] P. Tyagi and D. Dembla, "Investigating the security threats in vehicular ad hoc networks (vanets): Towards security engineering for safer on-road transportation," in *2014 International Conference on Advances in Computing, Communications and Informatics (ICACCI)*, 2014, pp. 2084–2090.

[118] T. D. Vo-Huu, T. D. Vo-Huu, and G. Noubir, "Fingerprinting wi-fi devices using software defined radios," in *Proceedings of the 9th ACM Conference on Security & Privacy in Wireless and Mobile Networks*, ser. WiSec '16, Darmstadt, Germany: ACM, 2016, pp. 3–14, ISBN: 978-1-4503-4270-4.

VITA

Billy Kihei was born in Miami, FL in 1986 and relocated to Atlanta, GA in 2004. He received the Bachelor of Science in Electrical and Computer Engineering from the Georgia Institute of Technology in 2009. During his degree, he worked as a co-op student for the National Security Agency in Maryland. Upon conferring his degree, he entered graduate school at his alma mater.

In 2010 he completed a Masters of Science in Electrical and Computer Engineering where he was a teaching assistant for the undergraduate digital signal processing course. He entered the work force as a systems engineer at Lockheed Martin in Marietta, GA where he worked on avionics systems for the C-5M. In 2013 he continued his graduate work pursuing a Ph.D. in Electrical and Computer Engineering with the Vehicle Ad Hoc Networking Research Group @ Georgia Tech under the Communication Systems Center.

During his Ph.D. degree, he led three undergraduate teams through the Opportunity Research Scholars program in the School of ECE, participated in the TI:GER program at the Georgia Tech Scheller College of Business learning technology commercialization, and was a visiting researcher at the Korea Advanced Institute of Science and Technology (KAIST) through support from the National Science Foundation and the National Research Foundation of Korea.

His research interests are in developing novel technologies that help people (mostly in need), and teaching others to do the same while excelling past his own contributions. Cars talking to cars are also very cool to him, too. ;)